UNIVERSITY OF CALIFORNIA, SAN DIEGO

Sensorimotor Integration and Spatial Perception in the Rat Vibrissa System

A dissertation submitted in partial satisfaction of the
requirements for the degree Doctor of Philosophy
in
Neuroscience

by

Samar Bharat Mehta

Committee in charge:

Professor David Kleinfeld, Chair
Professor Dan E. Feldman
Professor Marla B. Feller
Professor William B. Kristan, Jr.
Professor Ben A. Williams

2006

The dissertation of Samar Bharat Mehta is approved, and it is acceptable in quality and form for publication on microfilm:

_____

_____

_____

_____

_____

Chair

University of California, San Diego

2006

DEDICATION

This work is dedicated to my family, Bharat, Pallavi, Ami and Amar, for their unceasing support and friendship across tens of years and thousands of miles.

TABLE OF CONTENTS

LIST OF FIGURES

ACKNOWLEDGEMENTS

First and foremost, this dissertation exists due to the confidence and patience of my family. I know few groups of people who have gone through so many transitions and who are so different but still hold a common stake in the world. My mom, dad, sister and brother are a constant inspiration for me to look through different eyes and a constant comfort in their readiness to look through mine. They have each taken my concerns to be their own over the past seven years, and I owe them a debt I gladly carry but can never repay.

My gratitude also goes to many friends for their kindness, wisdom and support in times of doubt. I want to specially thank Sunil Gandhi and Emily Stoddard for keeping me grounded through professional and personal ups and downs. In addition, my peers in the Neurosciences program have been remarkable in their insights and readiness to talk about new ideas. Mike Baca, Kevin Briggman, Monica Brown, Kate Denning and Eric Thompson, among others, have been sounding boards and the source of many sanity breaks over the years.

Beyond my program, the Kleinfeld lab has been an tremendous source of education and dialog. The list of labmates who have been instrumental to my work and well-being is almost too long to include here. But given that I have gone to each of these people for ideas or help and consider them friends, I am unwilling to single out only a few. My thanks go to: R. Berg, O. Clay, J. Curtis, E. Dolnick, R. Figueroa, K. Ganguly, J. Groisman, D. Hill, O. Kuti, Q. Nguyen, N. Nishimura, L. Pockros, C. Schaffer, L. Schroeder, N. Steinmetz, P. Tsai, A. White, and D. Whitmer.

My committee, and the faculty at UCSD in general, have been encouraging, curious and insightful as scientific role-models. Among them, Bill Kristan in particular has been a thoughtful confidant and source of advice ever since my first months in the Neurosciences program.

Finally, the cornerstone of my experience at UCSD has been my advisor, David Kleinfeld. The appeal of neuroscience for me has always been the breadth and creativity of the thinking needed to study the brain. After several years spent in that study, I can not imagine a place where I would have been more exposed to interdisciplinary, creative thinking than under David's tutelage. David is beyond rare; he is unique in his ability to simultaneously work through multiple perspectives and speak the languages of different scientific disciplines. Inside the lab, he has pushed me to think off the beaten path while being a supportive and, in spite of my tendency to get distracted, patient mentor. Outside of the lab, the welcome and warmth shown to me by David, his gracious family and many of his similarly talented colleagues have made him a friend. For his role in all these capacities — scientist, mentor and friend — he has my sincere appreciation.

This dissertation is derived in large part from work that has been or will be published, with the kind consent of coauthors and publishers as follows. The text of Chapter II is a reprint of an article that appeared in the journal Neuron, Vol. 41, pages 191-194 (2004) by S.B. Mehta (the dissertation author) and D. Kleinfeld. The text of Chapter III is a reprint, with minor modifications, of an article that appeared in the journal Progress in Theoretical Physics Supplement, No. 161, pages 86-98 (2004) by D. Kleinfeld and S.B. Mehta (the dissertation author). The text of Chapter IV is based on a manuscript in preparation by S.B. Mehta (the dissertation author), D. Whitmer, R. Figueroa, B.A. Williams and D. Kleinfeld.

Funding for my graduate work came from the Howard Hughes Medical Institute Predoctoral Fellowship.

All procedures involving animals conformed to NIH guidelines and were approved by the IACUC at UC San Diego.

VITA

Oct 1976	Born, Belleville, Ontario, Canada
Aug 1997 - Jun 1999	Research Assistant, Dr. Stephen Smith, Department of Molecular and Cellular Physiology, Stanford University
Jun 1998 - May 1999	Teaching Assistant, Departments of Computer Science and Biology, Stanford University
Jun 1999	B.S., Biology, Stanford University
Jun 1999	M.S., Computer Science, Stanford University
Sep 1999 - Sep 2005	Howard Hughes Medical Institute Predoctoral Fellow
Apr 2001 - Jun 2001	Teaching Assistant, Department of Biology, University of California, San Diego
Feb 2001 - Jun 2006	Research Assistant, Dr. David Kleinfeld, Department of Physics, University of California, San Diego
Aug 2002 - 2005	Lecturer, Neuroinformatics, Marine Biological Laboratories, Woods Hole, MA
Jun 2006	Ph.D., Neuroscience, University of California, San Diego

PUBLICATIONS

Hopf, F.W., J. Waters, S. Mehta and S.J. Smith. (2002) Stability and plasticity of developing synapses in hippocampal neuronal cultures. Journal of Neuroscience 22(3): 775-781.

Kleinfeld, D. and S.B. Mehta. (2006) Spectral mixing in nervous systems: experimental evidence and biologically plausible circuits. Proceedings of Theoretical Physics Supplement 161: 86-98.

Lev-Ram, V., S.B. Mehta, D. Kleinfeld and R.Y. Tsien. (2003) Reversing cerebellar long-term depression. Proceedings of the National Academy of Sciences 100(26): 15989-15993.

Mehta, S.B. and D. Kleinfeld. (2004) Frisking the whiskers: patterned sensory input in the rat vibrissa system. Neuron 41: 181-184.

Young, J.J., S. Mehta, M. Israelsson, J. Godoski, E. Grill and J.I. Schroeder. (2006) CO_2 signaling in guard cells: Calcium sensitivity response modulation, a Ca^{2+}-independent phase, and CO_2 insensitivity of the *gca2* mutant. Proceedings of the National Academy of Sciences 103(19): 7506-7511.

CONFERENCE ABSTRACTS AND PRESENTATIONS

Mehta, S.B., D.J. Whitmer and D. Kleinfeld. (2004) Spatial localization in the rat vibrissa system: behavioral discrimination. Society for Neuroscience Annual Meeting, San Diego, CA.

Kleinfeld, D. and S.B. Mehta. (2005) Phase Oscillators in Sensory Systems. SIAM Conference on Applications of Dynamical Systems, Snowbird, UT.

Mehta, S.B., D. Whitmer, R. Figueroa, B.A. Williams and D. Kleinfeld. (2006) Behavioral evidence for sensorimotor integration in the rat vibrissa system. Society for Neuroscience Annual Meeting, Atlanta, GA. (submitted)

ABSTRACT OF THE DISSERTATION

Sensorimotor Integration and Spatial Perception
in the Rat Vibrissa System

by

Samar Bharat Mehta
Doctor of Philosophy in Neuroscience
University of California, San Diego, 2006
Professor David Kleinfeld, Chair

Animals perceive their surroundings both through sensory systems that transduce environmental features and through motor systems that control how those features are received. This perception, distinct from its building blocks of sensation and motion, is constructed in the nervous system by the integration of modalities. While the neural substrates of this construct are often studied by reducing perceptual systems into more simple sensory and motor components, this dissertation takes the complementary approach of studying such active sensory processes by considering the simple rat vibrissa model system in which these components are integrated to create spatial perception. We develop a conceptual and behavioral framework for the study of these integration processes in three main parts.

Chapter II introduces the rat vibrissae and divides earlier behavioral experiments in the system into two categories of environmental features, texture

and location. After brief observations on texture processing, we focus on the question of spatial perception and build on previous work demonstrating that sensory and motor streams are intermixed in the vibrissa system. We then develop a quantitative approximation of vibrissa motion to categorize potential algorithms for decoding the position of environmental objects.

Chapter III presents an aside in which we consider evidence for frequency mixing in the rat and other nervous systems. We describe an algorithm that can isolate particular components from the mixing that results from neuronal thresholds. This mixing computation is offered as a potential substrate for the phase difference algorithms described in Chapter II.

Chapter IV develops the main experimental work of the dissertation. Rats are challenged with a psychophysical test of their ability to discriminate object location using only vibrissa tactile cues through a single vibrissa. The ability of animals to perform this task with this restricted sensory apparatus constrains the algorithms discussed in Chapter II and argues that the rat brain in fact integrates sensory and motor streams to inform perception.

Chapter V concludes the dissertation with a brief demonstration of electrophysiological techniques that characterize neural activity over cortical large areas. Through experiments such as these, our single vibrissa results can be related to the function of the complete vibrissa array.

Chapter I

Introduction

The five basic senses taught to school children are sight, hearing, smell, taste and touch. These modalities, with the occasional addition of proprioception, describe the information gathering abilities of the mammalian organism as a division of labor rooted in the anatomical specializations of our external anatomy. The neurophysiologist's textbook description of the nervous system mirrors this picture, where chapters on sensation are often divided into distinct information pathways that connect neuronal receptor types to corresponding brain regions. This subdivision serves the field well, guiding microelectrodes and brain scans, and it organizes the feed-forward processing of each sense into general principles such as topographic mapping and feature-selective receptive fields.

The litany of the basic senses is restrictive, however, when it comes to the study of many natural perceptual processes. While the visual system certainly does find oriented edges in an image projected onto the retina, top-down attentional processes and bottom-up vestibular signals drive ongoing eye movements that constantly change the interpretation of the brain's retinotopic map in terms of the external world. Posture and balance rely on intrinsically sensorimotor loops that find equilibrium from muscles, muscle spindles and the inner ear, but the simple experiment of standing on one leg with eyes closed eloquently

argues that the sense of balance involves more than mechanoreceptors. These types of perceptual systems are variously called "sensorimotor" or "active sensory" processes, depending on the point-of-view, and share the unifying feature that they depend on the reciprocal interconnectivity of sensory and motor systems to inform behavior. This dissertation is inspired by the remarkable successes of biophysics, neurophysiology and psychology in explaining the foundations of the senses. It aspires, without claim to any similar level completeness, to frame a similarly interdisciplinary approach for the study of sensorimotor perception in a model mammalian system.

The sensorimotor system that we choose as this model is the vibrissa, or whisker, system of the rat (Figure I.1A). Despite their absence in humans, facial vibrissae are a common feature in most mammalian species (Ling, 1966) and are unusual amongst vertebrate systems for their highly discrete and reproducible anatomy (Rice and Arvidsson, 1991; Brecht et al., 1997). The main external sensory apparatus in the rat consists of five rows of richly innervated, thick hairs on each side of the face, extending from a few millimeters to several centimeters in a stereotyped pattern of lengths. The sensory path from each vibrissa follicle enters the central nervous system via the fifth cranial nerve and then the thalamus, clustering together to preserve a topographic map of the vibrissae at each station. It finally enters the primary somatosensory cortex in the prominent columnar pattern known as the barrels. On the motor side, the vibrissae of the rat (and related rodent species) are unlike most other mammals, as they are connected to a set of facial muscles that specifically tune their position. This set of muscles typically operates as a bilateral unit with a single degree of freedom, and the normal motion of the vibrissae is almost entirely along the azimuthal, or rostrocaudal, direction. The most common motor pattern, known as exploratory whisking, sweeps the vibrissae through this plane with a regular 5 to 15 Hz rhythm.

The functional simplicity of this discrete sensory array and the single

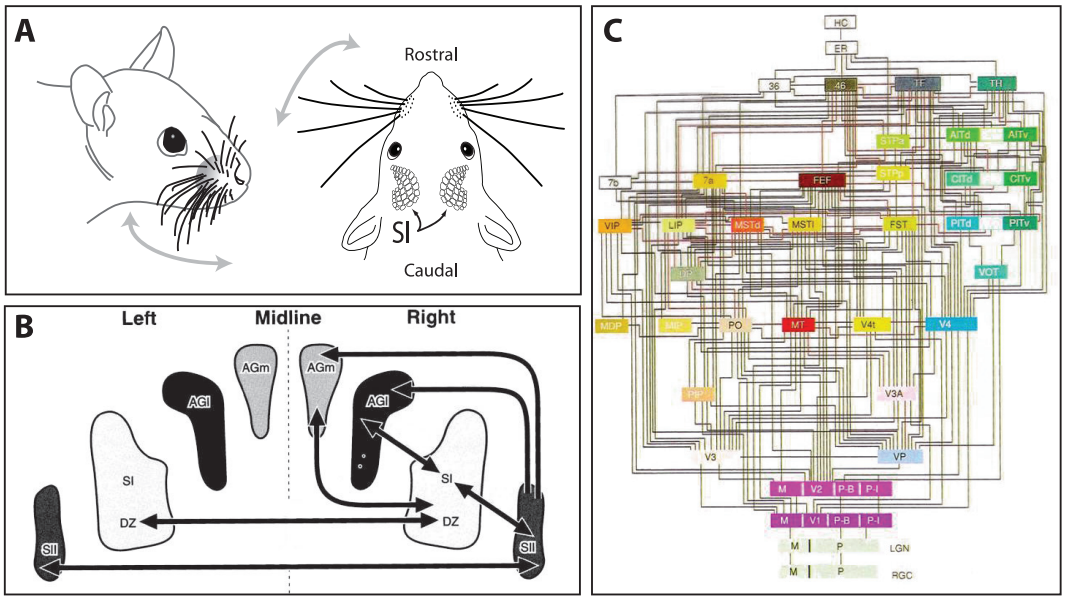

Figure I.1 **Advantages of the vibrissa system.** **(A)** Cartoon showing two views of the rat vibrissae. The view on the left shows the full complement of the large mystacial vibrissae on one side of the face; there are five rows with 4 to 6 tactile hairs per row in a stereotyped pattern. The view on the right shows only one row on each side for clarity. The arrays of circles on the head labeled SI represent the barrels of the vibrissa areas of the primary somatosensory (SI) cortex (not to scale). In both cases, the gray arrows represent the rostrocaudal direction of vibrissa motion. **(B)** Hierarchy of vibrissa-related areas in the rat cerebral cortex. The cortical areas shown here are: primary somatosensory (SI), secondary somatosensory (SII) and motor (agranular medial/lateral, AGm/AGl). DZ stands for dysgranular zone. Adapted from Paxinos (1995). **(C)** Hierarchy of vision-related areas in the primate cerebral cortex. Note that this diagram does not include oculomotor areas. Taken from Felleman and Van Essen (1991).

motor degree of freedom, along with the anatomical and behavioral importance of the system in the rat, makes an ethological argument for its use as a model of sensorimotor processes. The appeal of the system to researchers (and with luck, the NIH) is not due to any direct similarity to human touch, but rather because the vibrissae provide a relatively simple active sense with interacting afferent and efferent neural streams. The neural loops that integrate these modalities are subject to general brain functions such as plasticity and top-down modulation, but involve a smaller number of core interactions than systems in higher mammals (Figures I.1B and I.1C). These factors have made vibrissa system and associated barrel cortex into a popular testing ground for work on general cortical function. Unfortunately, the lack of direct analogy to a human modality creates a difficulty in extending this to the specific study of the vibrissae as a perceptual system, as we do not yet have a complete understanding of the functions they serve in the behaving animal.

This dissertation thus builds a framework for the study of the functional role of the vibrissae as it relates to sensorimotor perception. The approach is multidisciplinary and draws mainly from three scientific traditions: a reductionist quantitative calculation that highlights the types of neural computations needed to decode sensory signals, an engineering model that demonstrates how computations on rhythmic sensory signals might proceed, and a explicitly sensorimotor psychophysical experiment that constrains the algorithms that are actually used during behavior.

Chapter II opens this discussion with a brief review of relevant past behavioral studies. Those studies that quantified environmental parameters transduced by the vibrissae fit loosely into two categories: the quality of contacted objects and their locations. This notion matches in spirit the idea of what and where pathways in the visual system and serves as a convenient division of recent work in the field. The most mature exemplar of the "what" category is the ro-

dent ability discriminate small differences in object texture. Recent work on the biomechanical properties of the vibrissae has renewed interest in the coding of the vibrations resulting from textures, and we present a back-of-the-envelope calculation that considers the different potential sources of these vibrations. However, texture discrimination is not known to be an explicitly sensorimotor behavior, and the second half of the chapter thus focuses on the question of object location along the rostrocaudal direction of vibrissa motion. We approximate the motion as sinusoidal and describe the requirements of any algorithm that deduces spatial position from vibrissa contact. Finally, we draw on earlier physiological findings that describe touch- and motion-sensitive signals in the neurons of the vibrissae system and discuss how these signals could be used by decoding algorithms.

Chapter III detours to consider an engineering model, inspired by data from the vibrissa system and others, for computing the difference in frequency between two periodic signals in the nervous system. We rely on analytical work that demonstrates that the threshold property of a spiking neuron can produce this difference frequency and describe two circuits that could be used by the nervous system to isolate this result from side effects of the threshold. This somewhat abstruse demonstration is related to the earlier description of the algorithms needed for sensorimotor localization by two observations. First, rhythmic whisking against an external object would produce a periodic contact signal in addition to the already periodic motion signals discussed in Chapter II. Second, when two signals are at the same frequency, the circuits described here isolate a new signal proportional to the difference in phase between them. This model then provides a mechanistic description of how the brain might derive position from the lag between touch and motion signals.

Chapter IV constitutes the main experimental work of the dissertation. We isolated the sensorimotor aspect of vibrissa sensation by challenging animals to discriminate between objects whose position varies in the plane of vibrissa mo-

tion. We find that rats are able to perform this task when restricted to a single vibrissa and show that this ability rules out a class of localization algorithms that does not depend on vibrissa motion. The scanning behavior measured for the animals in this study places further constraints on the algorithms, and we analyze the vibrissa motion in the context of the possibilities described in Chapters II and III. We argue from these data that rats are able to combine touch and motion information streams to compute object position in head-centered coordinates even while their tactile sensors are in motion. While future physiological experiments are required to fully characterize the underlying neural computations, these experiments demonstrate that motion-sensitive signals can actually be used to construct an integrated picture of space.

Chapter V shows basic results from a system designed to measure the spatial and temporal patterns of activity in the vibrissa somatosensory cortex. The work from earlier chapters demonstrates the fact of angular discrimination with a single vibrissa and suggests algorithms for this computation. If a single detector is sufficient for many behavioral tasks, however, then it remains to be seen why the vibrissae in their natural state form a sensory array, with multiple detectors along the rostrocaudal axis. We believe that a satisfactory exploration of this question will require the measurement of activity across the cortical vibrissa field, ultimately from behaving animals. The data considered here from anesthetized animals briefly show how a multielectrode array might be used to characterize such activity in simple cases. This approach, adapted from other researchers, offers the possibility of identifying single neurons, and is thus complementary to similar work using optical techniques.

Chapter II

A Quantitative Framework

How are two prominent environmental features, surface texture and object location, transduced and encoded as rats whisk? Recent papers show that textures may excite intrinsic mechanical vibrations of the vibrissae. Although these vibrations are too fast to be directly followed by cortical neurons, there is evidence that the speed of the vibrations is encoded by contact-dependent sensory signals. In addition to contact, sensory signals exist that report the angular position of the vibrissae. The combination of contact and reference signals may be used to decode spatial variations in the environment, particularly the location of objects in head-centered coordinates.

II.A Introduction

The remarkable organization of vibrissa areas in the rodent nervous system has made it a popular test-bed for neurobiological study. In particular, the large, discrete representation of the vibrissa sensorimotor organs in cortex emphasizes the ethological weight carried by the vibrissae on a rodent's cheeks. Schiffman et al. (1970) asked if the tactile perceptions carried by these long hairs can, in fact, dominate the world view of the rat. They made use of a visual cliff, constructed with a platform raised a variable height above a sheet of glass, to give conflicting

visual and tactile information about the depth of the underlying floor. On one side of the platform, a checkerboard patterned floor lay immediately underneath the glass, while on the opposite side the same floor pattern was approximately half a meter below the glass and gave the visual impression of a drop. When the platform is raised so that rats cannot touch the glass without jumping, they show a strong preference to descend to the seemingly shallower side. However, when the platform is low enough for the rats to touch the glass with their vibrissae, the preference is lost and the rats readily descend to the seemingly deep side. Thus vibrissa cues can dominate visual input in rat.

Unfortunately, most early efforts to characterize the function of the vibrissae did not yield results as unequivocal as those of Schiffman et al. (1970). Vincent (1912) used animals that lacked either eyesight, vibrissa somatosensation or both and examined their performance on tests of locomotion and the use of tactile cues in maze running. Vincent found that only when deprived of both vibrissae and eyesight do rats show severe deficiencies, suggesting that the animals normally use both senses to navigate. In a review of behavioral research performed up to the mid 1970s, Gustafson and Felbain-Keramidas (1977) summarized a variety of complex behaviors, ranging from aggression to swimming, that are affected by the loss of the vibrissae. However, as they point out, behavioral plasticity in the use of other senses can obscure an understanding of precisely which environmental variables are encoded by the vibrissae.

Hutson and Masterton (1986) answered the need for sensory tests designed to isolate perceptual functions of the vibrissae and found that blind rats with intact vibrissae will leap across wider gaps than those without vibrissae. Thus the vibrissae allow animals to make a binary determination of the existence of the far side of a gap. A similar binary role for the vibrissae, but not the short hairs, follows from studies on the detection of differently shaped objects (Brecht et al., 1997). Other experiments revealed that, far from simply serving as contact

detectors, the vibrissae can be used to discriminate between spatially extended objects. Guic-Robles et al. (1989) and Carvell and Simons (1990) used a variant of the gap-crossing task to assess the ability of rats to discriminate differences in surface roughness with their vibrissae. Their data revealed that rats discriminate with an acuity that rivals that of the human fingertip.

Texture is not the only fine sense transduced by the vibrissae. Recent experiments suggest that the vibrissae convey sufficient spatial information to allow rats to distinguish between barriers whose distance from the head varies by less than five percent (Krupa et al., 2001) and to distinguish between objects of different shape and texture (Harvey et al., 2001). It remains unclear, however, if rats can decode the location of objects relative to their head as they explore their environment with synchronous, large amplitude whisks of their vibrissae.

II.B Texture

The essential result from texture discrimination is that rats can distinguish between cylinders with different pitches of corrugations machined across their surface (Carvell and Simons, 1990; Guic-Robles et al., 1989). How does this occur? One possibility, bolstered by recent results from Fend et al. (2003), Hartmann et al. (2003), and Neimark et al. (2003)), is that the mechanical properties of the vibrissae act to translate surface roughness into a spike rate. Vibrissae are slender, tapered beams and, like all beams, their transient mechanical response may be expressed in terms of intrinsic vibration modes. Each mode is described by a pattern of bending of the vibrissa and has a characteristic vibration frequency.

As a vibrissa drags across a surface, we posit that it alternately sticks and slips across rough features, whether the surface is corrugated or irregular. This leads to bending and release of the vibrissa (Figure II.1A). As the vibrissa snaps back and subsequently vibrates, the resultant motion of the shaft is a superposition of vibrations at the intrinsic modes of the vibrissa. Differences between surfaces

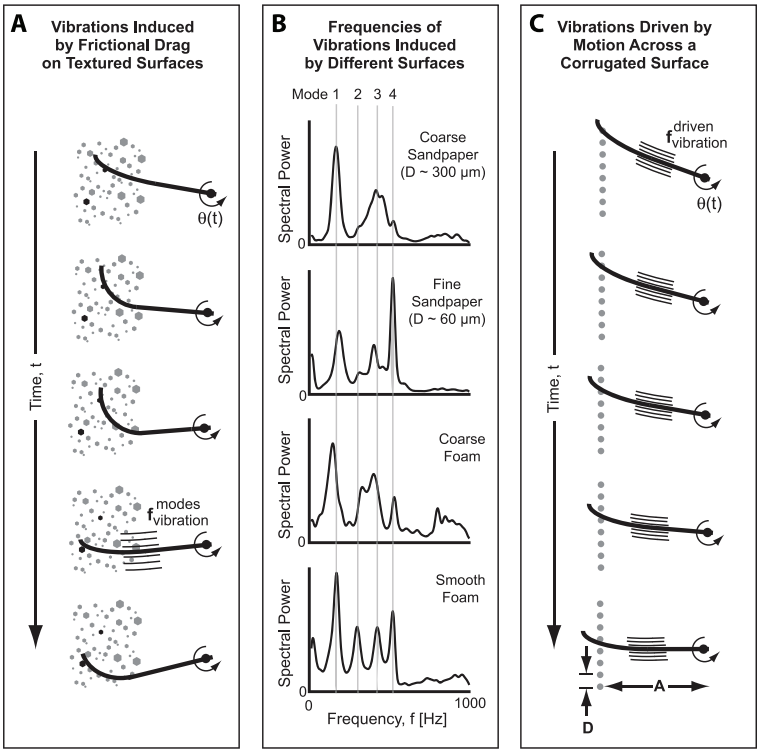

Figure II.1 **Encoding texture by contact of a vibrissa with a rough surface.** **(A)** Cartoon that shows how the drag on a vibrissa can couple to the intrinsic mechanical vibrations (modes) of the vibrissa. **(B)** Spectral power of the vibrations measured at the base of a vibrissa artificially whisked across different textures. Adapted from Fend et al. (2003). **(C)** Cartoon that shows how the sweeping motion of a vibrissa across corrugations might induce vibrations in the vibrissa shaft.

are expressed by the extent to which different modes are favored. This situation is conceptually the same as exciting different modes in a bowed string and was recently demonstrated for the vibrissae (Fend et al., 2003; Neimark et al., 2003). In particular, Fend et al. (2003) attached the base of a plucked vibrissa to a force transducer and moved the tip of the vibrissa across surfaces of differing roughness. They found that the set of frequencies of the vibration was essentially the same for all surfaces they considered. We associate these frequencies with the intrinsic vibration modes (1 through 4 in Figure II.1B; slight shifts in frequency are presumably due to loading) and denote them by $f_{vibration}^{mode}$. The relative amplitudes of each mode, $\delta\theta^{mode}$ mode, depended on the detailed properties of the surface (Figure II.1B). Thus the angular vibrissa motion, $\delta\theta(t)$, induced by drag across a texture is given by

$$\begin{aligned}\delta\theta(t) \approx \delta\theta^{(mode1)} \sin(2\pi f_{vibration}^{(mode1)} t) + \\ \delta\theta^{(mode2)} \sin(2\pi f_{vibration}^{(mode2)} t) + \cdots ,\end{aligned} \tag{II.1}$$

and encoding of different textures is transformed to encoding the amplitude of motion at the intrinsic frequencies. What evidence supports this encoding by sensory neurons?

The Merkel sensory terminals in vibrissa follicles are capable of tracking vibrations well above 1 kHz (Gottschaldt and Vahle-Hinz, 1981), which encompasses the range of intrinsic frequencies (Figure II.1B). Thus, the spiking output of primary sensory neurons in the trigeminal ganglion should be able to lock to the oscillatory motion of the vibrissa. Locking still occurs at the level of the secondary sensory neurons in nucleus principalis, albeit up to slightly lower frequencies (Deschenes et al., 2003). In contrast, the phase-locked response of neurons in vibrissa areas of ventral posterior medial thalamus (Castro-Alamancos, 2002) and primary sensory (S1) cortex (Ahissar et al., 2000; Simons, 1978) are limited to tens of hertz, although it appears that neurons in vibrissa S1 cortex can fire up to hundreds of hertz (Barth, 2003). It is of interest that Arabzadeh

et al. (2003) observed that the spike rate of neurons in S1 cortex does not lock to the high frequency movements of the vibrissae. Rather, the spike rate is of the form $Rate \propto \log(\delta\theta^{mode} f^{mode}_{vibration})$, where $\delta\theta^{mode} f^{mode}_{vibration}$ mode corresponds to the maximum speed of vibrissa deflection.

We consider how the observed dependence of the spike rate in cortex may allow the rat to encode texture in terms of the natural frequencies of the vibrissae. Two assumptions are required. First, primary neurons must respond to the velocity of deflection, consistent with observations (Gottschaldt and Vahle-Hinz, 1981). For simplicity, we calculate the velocity for the case of only a single vibration mode, in which the angular velocity induced by drag across a texture is given by

$$\frac{\mathrm{d}\{\delta\theta(t)\}}{\mathrm{d}t} \approx \delta\theta^{(mode1)} f^{(mode1)}_{vibration} \cos(2\pi f^{(mode1)}_{vibration} t). \tag{II.2}$$

Second, spiking locked to this fast signal must be demodulated and low-pass filtered along the trigeminal-to-cortical pathway, i.e., the spike rate should depend only on the magnitude of the velocity. For the particular case of demodulation by the threshold nonlinearity common to neurons, the spike rate is proportional to

$$\begin{aligned} SpikeRate &\propto function\left(\int_{\substack{multiple\\cycles}} dt \left[\frac{\mathrm{d}}{\mathrm{d}t}\delta\theta(t)\right]_+\right) \\ &\propto function(\delta\theta^{(mode1)} f^{(mode1)}_{vibration}). \end{aligned} \tag{II.3}$$

Thus, the spike rate here, as well as for other demodulation schemes, depends directly on the coupling of the vibrissae to the surface. The function that relates the spike rate to the input can be approximately logarithmic (Engel et al., 1999). This interpretation provides the basis for discrimination with only one vibrissa (Fend et al., 2003). In fact, the data confirm that discrimination between pairs of substantially differing textures is not blocked in rats shaved down to a single vibrissa; the case for closely related textures is ambiguous (Carvell and Simons, 1995). It remains an open issue if discrimination across a larger set of textures requires the presence of multiple vibrissae with distinct intrinsic

frequencies (Neimark et al., 2003). Further, it is unknown how the spike rate scales for concurrent vibrations at multiple frequencies.

An alternative hypothesis that is applicable to the discrimination of corrugated surfaces is that the frequency of vibrations in the vibrissae is directly induced by surface texture (Figure II.1C). To assess this possibility, we estimate the frequency of vibrations in the shaft of a vibrissa from the spacing of the surface features and the parameters of rhythmically driven motion. The angular position of the shaft is described by a single variable, θ. We express the time dependence of θ as a sinusoid with amplitude θ_0 and a center position θ_{set}. Thus,

$$\theta(t) = \theta_{set} + \theta_0 \sin(2\pi f_{whisk} t + \phi), \tag{II.4}$$

where f_{whisk} is the ∼9 Hz frequency of exploratory whisking (Berg and Kleinfeld, 2003) and, in anticipation of the discussion on contact angle, ϕ is a phase that specifies the origin of time. The frequency of contact of the vibrissa with successive corrugations is greatest, and most stable, near the midpoint of the sweep of vibrissa. Its value, denoted by $f^{driven}_{vibration}$, is estimated as

$$f^{driven}_{vibration} \approx \frac{A}{D} \cdot \left|\frac{\mathrm{d}\theta}{\mathrm{d}t}\right|_{maximum} = 2\pi \cdot \frac{A}{D} \cdot \theta_0 f_{whisk}, \tag{II.5}$$

where the pitch of the corrugations is given by D, the typical distance from the base of the vibrissa to the contact point is denoted by A, and θ_0 is in units of radians. Using values taken from texture discrimination experiments, e.g., $A \approx 25$ mm, $D \approx 15$–1000 μ m, and $\theta_0 \approx 10°$–$15°$(0.17–0.26 radians) (Carvell and Simons, 1995), we find $f^{driven}_{vibration} \approx 300$–$20{,}000$ Hz. The upper frequencies are too high for even primary sensory neurons to follow. Furthermore, high frequencies preferentially excite only the tip, and not the base, of a tapered beam (Cranch and Adler, 1956). Thus, except for the lowest frequencies, which correspond to coarse corrugations, the directly induced vibrations are unlikely to account for the texture discrimination described in the literature.

II.C Location

We now turn to the determination of the position of an external object. The behavioral evidence for involvement of the vibrissae in this task is incomplete, although the studies of Vincent (1912) suggest that rats use their vibrissae to orient toward a point of contact. How could a rat determine where an object is in head-centered coordinates? For the rostral-caudal angle, the issue is that the rat needs to deduce vibrissa position at the time of contact, which is equivalent to determining the phase variable ϕ in Equation II.2.

From the perspective of spatial encoding, there are three signals that can be produced in the sensory fibers that innervate the follicle of each vibrissa (Figure II.1A): (1) A reference signal that reports angular position of the vibrissae independent of contact. Neurons that encode position will preferentially spike at a preferred angle, denoted θ_{Ref}, during the whisking cycle. (2) A contact-based signal that is generated when a vibrissa first touches an object during protraction. We refer to this as the ON-contact signal for a given vibrissa. (3) A contact-based signal that is generated when a vibrissa detaches from an object during retraction. We refer to this as the OFF-contact signal.

Any two of the above three sensory signals could be used to determine vibrissa angle upon contact. Although there is a lack of evidence for spindle fibers in the facial musculature (Rice et al., 1994), recent results from Szwed et al. (2003) show that reference signals are present in a subset of primary sensory neurons located in the trigeminal nucleus (left panel, Figure II.2B). Furthermore, different neurons preferentially spike at different angles during either the protraction or retraction phase of the whisk cycle (right panel, Figure II.2B), with a bias toward protraction from the retracted position. These observations made use of a form of fictive whisking, in which motion of the vibrissae was induced by rhythmic electrical stimulation of the facial motor nerve (Zucker and Welker, 1969).

Figure II.2 **Encoding of object location based on reference and contact spike signals.** **(A)** Cartoon of a single row of vibrissae at various times relative to their contact with an object. **(B)** Spiking output from primary sensory neurons of the trigeminal ganglion (TG) was recorded during vibrissa motion induced by 5 Hz electrical stimulation of the facial motor nerve (FN). The left panel shows the trial-averaged response of the reference signal for one neuron; the spiking of this cell was not affected by contact (not shown). The angle $\Delta\theta_{Ref}$ is the extent of protraction, relative to the initial retracted position, at the peak of the neuronal response. The right panel summarizes the data for all cells with reference responses (Szwed et al., 2003). The radial coordinate is the logarithm of the peak spike rate and the angular coordinate, θ_{Ref}, is found by $\theta_{Ref} = \Delta\theta_{Ref} - (\theta_{set} - \theta_0)$, where $2\theta_0$ is the maximum defection of the vibrissa, e.g., 14°for the data on the left. **(C)** Responses in vibrissa S1 cortex measured as animals whisked without contact. The data on the left shows an example of the correlation between spiking and the peak of the electromyogram (EMG). The scale on top accounts for the 25 ms lag between vibrissa position and the EMG (Berg and Kleinfeld, 2003) and the half-period, i.e., 58 ms for this data, between protraction and retraction. The time t_{Ref} is the peak of cortical spiking relative to the fully retracted position. The panel on the right summarizes the data for all cells (Fee et al., 1997); note that the summary plot in the original paper was inadvertently inverted ($\theta \leftarrow -\theta$). The radial coordinate is the percent depth of modulation of the spike-EMG correlation and the angular coordinate, θ_{Ref}, is found by $\theta_{Ref} = \theta_{set} - \theta_0 \cos(2\pi f_{whisk} t_{Ref})$.

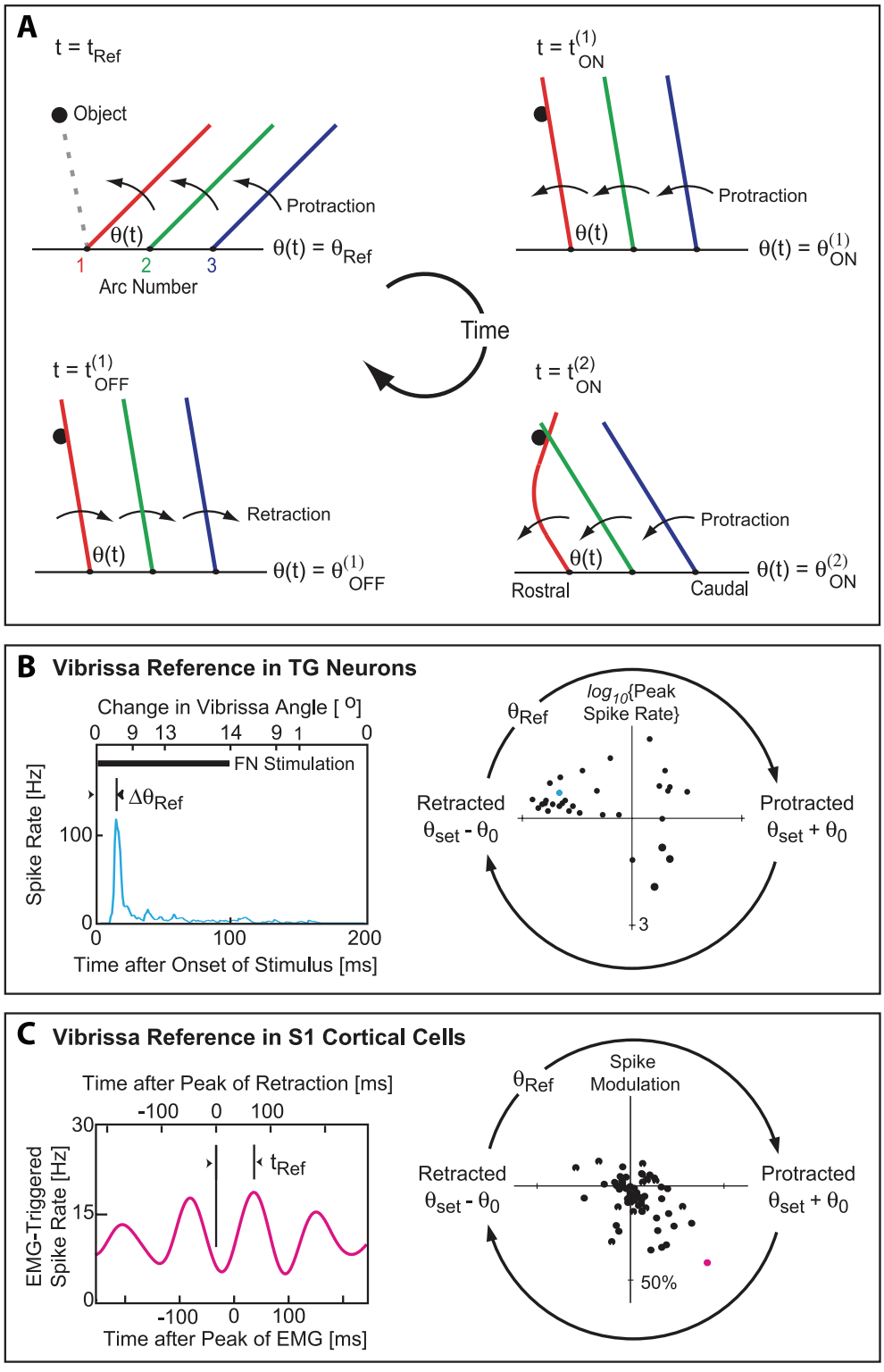

Figure II.2 (see facing page)

The recent results provide a substrate for the observation of a reference signal at the level of vibrissa S1 cortex (Fee et al., 1997). In the latter study, rats were trained to whisk in air and the reference signal appeared as spikes locked to the rhythmic motion of the vibrissae, as measured via the mystacial electromyogram (left panel, Figure II.2C). As in the case of primary sensory cells, different neurons were found to have different preferred angles along the whisk cycle (right panel, Figure II.2C) and were observed to spike over the full whisking cycle. However, the distribution of spiking for cells in S1 cortex was biased toward retraction from the protracted position, as opposed to protraction from the retracted position for the case of primary sensory neurons activated by fictive whisking (cf. right panels in Figures II.2C and II.2D). This difference may result in part from the active nature of retraction in normal whisking (Berg and Kleinfeld, 2003).

The experimental data from primary sensory neurons (Szwed et al., 2003) shows that both reference and ON- and OFF-contact signals are available to deduce contact angle in head-centered coordinates. We consider the simplest decoding scheme, which uses reference and ON-contact signals. The probability of a reference signal is maximum when the vibrissa angle $\theta(t) = \theta_{Ref}$; we identify the associated neuronal spike time as t_{Ref}. Similarly, the probability of an ON-contact signal is maximum when $\theta(t) = \theta_{ON}$, with associated spike time t_{ON}. We use these two constraints to eliminate the unknown phase ϕ from Equation II.4 and obtain a relation for the contact angle. Near the center of the whisk cycle, this reduces to

$$\theta_(ON) = \theta_{Ref} + 2\pi \cdot \theta_0 f_{whisk} \cdot (t_{Ref} - t_{ON}), \tag{II.6}$$

which shows that decoding of the contact angle depends on the difference in timing between reference- and contact-based spikes. We recall that reference signals, either from primary sensory or cortical neurons, span a range of preferred angles in the whisk cycle. In this population, there will always be reference neurons that spike close to the time of contact. The coincident detection of a contact

spike and a reference spike for a neuron with preferred angle θ_{Ref} identifies the contact angle as $\theta_{ON} = \theta_{Ref}$. Similar solutions could be accomplished with ON- and OFF-contact signals, or contact signals from separate vibrissae (Figure II.2), although these schemes involve increased complexity due to their inability to use coincidence.

II.D Next Steps

The suggestion that mechanical resonances of the vibrissae contribute to neuronal encoding of surface texture is intriguing. An obvious test of this idea is to alter the vibrissae on an experienced rat to see if this impairs discrimination. Furthermore, there is a distinct lack of data on the nature of the transformation from high frequency motion to firing rate. Electrophysiological recordings along the trigeminal-thalamocortical pathway are necessary to elucidate the nature of this code. Beyond texture discriminations, vibrations of the vibrissa may play a role in encoding contact with edges (Hartmann et al., 2003). The corresponding prediction is that contact will excite intrinsic vibrations and lead to a sensory spiking response that extends well beyond the time of contact.

While behavioral evidence for texture discrimination is strong, the corresponding evidence for object location is still developing. An essential missing experiment is to determine if rats can use their vibrissae to discriminate between similar objects positioned at different angles relative to the head. Assuming that rats succeed at this task, the question remains as to how reference and contact signals are combined. One scheme involves coincidence of spiking (Szwed et al., 2003). An alternative approach is based on the demodulation of rhythmically varying reference and contact signals (Ahrens et al., 2002). Lastly, texture discrimination and object location may well be interrelated. Experimentally, this may be revealed if rats decode spatial variations in texture.

Acknowledgement

The text of this chapter is a reprint of an article that appeared in the journal Neuron, Volume 41, pages 191-194 (2004) by S.B. Mehta (the dissertation author) and D. Kleinfeld.

Chapter III

A Model for an Underlying Neuronal Algorithm

The ability to compute the difference frequency for two periodic signals depends on a nonlinear operation that mixes those signals. Behavioral and psychophysical evidence suggest that such mixing is likely to occur in the vertebrate nervous system as a means to compare rhythmic sensory signals, such as occurs in human audition, and as a means to lock an intrinsic rhythm to a sensory input. Electrophysiological data from electroreceptors in the immobilized electric fish and somatosensory cortex in the anesthetized rat yield direct evidence for such mixing, providing a neurological substrate for the modulation and demodulation of rhythmic neuronal signals. We consider an analytical model of spectral mixing that makes use of the threshold characteristics of neuronal firing and which has features consistent with the experimental observations. This model serves as a guide for constructing circuits that isolate given mixture components. In particular, such circuits can generate nearly pure difference tones from sinusoidal inputs without the use of band-pass filters, in analogy to an image-reject mixer in communications engineering. We speculate that such computations may play a role in the coding of sensory input and feedback stabilization of motor output

in nervous systems.

III.A Introduction

Oscillations are a hallmark of neuronal activity. When two neuronal oscillators interact through synaptic connections, their respective spike patterns often synchronize or lock with a non-zero phase shift. A dramatic example concerns two cortical neurons that interact via reciprocal inhibitory connections and spike in anti-phase at low firing rate but synchronize at high firing rate (Gibson et al., 2005). This remarkable shift in behavior was predicted (Hansel et al., 1993; von der Vreeswijk et al., 1994) using the theory of weakly coupled oscillators that was pioneered by Prof. Kuramoto and elucidated so clearly in *Chemical Oscillations, Waves and Turbulence* 1984. This theory has provided further insight through its application to the dynamics of networks of neurons (Ermentrout and Kleinfeld, 2001), where collective behavior can lead to linear waves of electrical activity in a central olfactory organ (Delaney et al., 1994; Ermentrout et al., 1998; Friedrich et al., 2004) and rotating waves of electrical activity in visual cortex (Prechtl et al., 1997) and in neocortical slices under epileptic-like states (Huang et al., 2004). At a still higher level, the Kuramoto model has been used to study neuronal synchronization in stimulus coding, (Schuster and Wagner, 1990a; Schuster and Wagner, 1990b; Sompolinsky et al., 1991; Grannan et al., 1993) as appears to occur in the processing of multiple stimuli by visual cortex (Gray et al., 1989).

It is our belief that the application of Prof. Kuramoto's ideas to coupled neurons represents one of the only two intellectual threads that systematically connects single-cell behavior to network behavior. For weakly coupled neuronal oscillators, this is achieved by the reduction of the full dynamics of each cell to dynamics of a single phase variable that describes the state of a neuron along its limit cycle. The phase variables for different cells are cou-

pled through a sensitivity function, which corresponds to Kuramoto's Z-function, and an interaction function, each of which is described in terms of phase variables so that the output of one cell affects the phase of other cells (Ermentrout and Kleinfeld, 2001). For completeness, the second intellectual thread is the strong coupling of neurons with independent Poisson-spike statistics, either in the limit of large networks (Shriki et al., 2003) or slow synapses (Ermentrout, 1994); both cases result in a firing rate description that is the key ingredient of attractor neural networks (Wilson and Cowan, 1973; Hopfield, 1982; Amit, 1989).

Here we turn our attention to a functional consequence of interactions between oscillators in pursuit of the computational role they may play in sensorimotor systems. Motivated by experimental findings, we consider the spectral mixing that can occur between two periodic signals. Mixing provides a mechanism for computing the differences and sums of the frequency content of two signals. This can easily be seen when mixing is accomplished by the multiplication of two sinusoids, $\cos(2\pi f_a t) \times \cos(2\pi f_b t) = \frac{1}{2}\cos[2\pi(f_a - f_b)t] + \frac{1}{2}\cos[2\pi(f_a + f_b)t]$. When combined with a means for isolating the difference term, spectral mixing allows the comparison of even small differences in the frequency content between two signals. This phenomenon is commonly witnessed in audition, where human subjects are sensitive to the beat, or difference, frequency between two simultaneous pure tones (Oster, 1973). The perception persists when the frequencies are presented to different ears, indicating a neural rather than a biomechanical substrate for the mixing. Similar computations may be performed in various ethological tasks, including: (*i*) Electroreception, where animals sense the difference in frequency between their own rhythmic electrical discharge and that of a neighboring fish;(Bullock and Heiligenberg, 1987; Heiligenberg and Rose, 1985) (*ii*) Echolocation, where the relative speed of flight between a bat and its prey is encoded in the difference in frequency between

outgoing and reflected acoustic waves (Suga et al., 1997); and (*iii*) Pitch determination, where animals recognize the fundamental frequency of a sound based on a harmonic stack, even when the stack is missing the fundamental (Levitin and Rogers, 2005).

If we extend the example to the case in which the two sinusoids are at the same frequency but have a phase difference, we obtain, $\cos(2\pi ft)\times\cos(2\pi ft-\phi) = \frac{1}{2}\cos(\phi) + \frac{1}{2}\cos(4\pi ft - \phi)$. Here, isolating the DC term allows measurement of the relative phase between two signals. Such a function can also be relevant for sensory processing, as in (*i*) Audition, where the phase difference that results from the time it takes for a sound to reach the two ears serves as a measure of source angle (Pena and Konishi, 2001; Pena and Konishi, 2004); and (*ii*) Vibrissa somatosensation in rats, where the relative phase between a rhythmic motor signal and a touch signal may be used to decode the position of an object relative to the head (Ahissar and Kleinfeld, 2003).

III.B Electrophysiological Evidence for Spectral Mixing

While spectral mixing would appear to be a useful computation in several systems, we only know of three neurophysiological studies that have observed this phenomenon. We first review these experimental findings and use the data as motivation for a minimal model of spectral mixing by neurons. We then raise a conjecture about circuits that make use of phase shifts, rather than filtering, to isolate desired frequency components after the mixing has occurred.

III.B.1 Human Vision

An experiment by Regan and Regan (Regan and Regan, 1987) recorded electroencephalograms (EEGs) across visual cortical areas in human subjects as they attended to two superimposed, modulated visual gratings. An analysis of the EEG signals showed that the spectrum contained a term at a frequency of

$2f_1 + 2f_2$, where f_1 and f_2 were the temporal modulation frequencies of the two gratings and the factor of 2 is due to the presence of both light-to-dark and dark-to-light transitions.

III.B.2 Fish Electroreception

The sense organ of the paddlefish *Polyodon Spathula*, a species of electric fish, consists of electroreceptors that cover the animal's rostrum, a flat structure that projects from the head (Figure III.1A). Neiman and Russell 2004 demonstrate that this electroreceptor system contains two distinct oscillators. One oscillator exists within a cluster of canals in the epithelia of the sensor and produces oscillations in the range of 10 to 30 Hz. The second oscillator arises from the axon terminals and produces an oscillation in the range of 30 to 70 Hz.

The authors made extracellular recordings from the anterior lateral line nerve (ALLn) (Figure III.1A), reporting spiking from a single sensory cell. Their recordings contained rhythmic contributions from both the epithelium, with frequency f_e, and from the afferents, with frequency f_a (Figure III.1B). Critically, the authors found mixture terms at frequencies $f_a + f_e$, $f_a - f_e$, and $2f_a - f_e$. Introduction of a sinusoidal external stimulus, with frequency f_s, led to mixing among all three oscillators (Figure III.1C). The authors note that this behavior is consistent with mixing of the oscillators, although they prefer an explanation based on synaptic modulation of one oscillator by the other.

III.B.3 Rat Somatosensation

The somatosensory cortex in rat has a prominent region, known as the vibrissa primary somatosensory (S1) cortex, that is devoted to the processing of tactile stimuli from the animal's large facial whiskers, or vibrissae (Figure I.1A). Rats move their vibrissae in 5 to 15 Hz exploratory movements and such moving sensors pose a sensory challenge: the spatial meaning of a con-

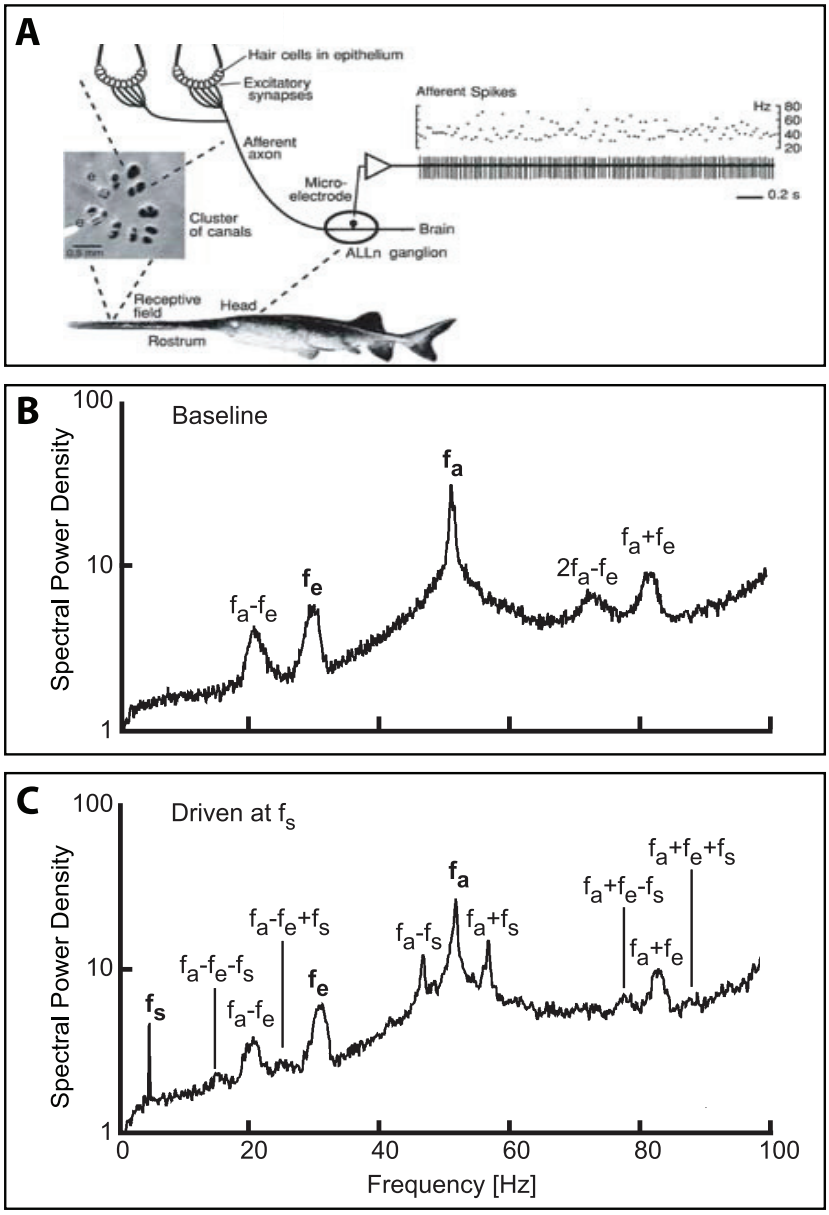

Figure III.1 **Mixing in the anterior lateral line afferents in the paddlefish.** **(A)** Diagram of the electroreceptor. Recordings are made from afferents in the afferent lateral line nerve (ALLn) ganglion. The example time series shows an extracellular recording and the corresponding instantaneous frequency. **(B)** The spectral power of the ALLn signal in the absence of stimulation. Note contributions of the afferent and epithelial oscillators, with frequencies f_a and f_e respectively, as well as the mixture terms. **(C)** The spectral power during stimulation of the epithelium at frequency f_s. Panels adapted from Neiman and Russell (2004).

tact event depends on its phase relative to the oscillating vibrissa position. A plausible model, discussed in Chapter II, for this problem approximates the position and touch signals as sinusoids, *i.e.*, Motion $\propto 1 + \cos(2\pi f_{motion} t - \phi_{motion})$, where ϕ_{motion} is the preferred phase of a given neuron (Fee et al., 1997) and Contact $\propto 1 + \cos[2\pi f_{motion}(t - t_{contact})]$ + higher-order terms[1], where $t_{contact}$ is the time of contact. Spectral mixing of these two signals leads to an output that contains the phase difference term $\cos(2\pi f_{motion} t_{contact} - \phi_{motion})$, as discussed in the introduction above. If this term is isolated, the resulting spike rate will be highest when contact occurs at particular phase relative to vibrissa motion; preliminary data provides evidence for such a signal in behaving animals (Curtis and Kleinfeld, 2005).

In our laboratory, Ahrens et al. 2002 studied the underlying computation by introducing two incommensurate frequencies into the cortex of an anesthetized rat. An intrinsic oscillation (centered at frequencies f_i from 2 to 5 Hz) was introduced to cortex through the application of the anesthetic ketamine, and a second oscillation was added using mechanical stimulation of the vibrissae at frequencies f_s in the range 5 to 15 Hz (Figure III.2B). The authors observed only intrinsic oscillations in the absence of a mechanical stimulus. During stimulation, however, they found the addition of both the stimulus frequency and the mixture frequencies $f_s \pm f_i$ (Figure III.2B and III.2C). Higher-order mixture terms, such as $2f_s - f_i$, here likely result from harmonics in the punctate shape of the stimulus rather than from the nonlinearity responsible for mixing. The authors found similar results when the two frequencies were separately applied to the two sides of the head in a procedure reminiscent of binaural mixing in audition, rather than using the anesthesia induced oscillations.

[1]Higher order terms are needed here to enforce causality as a periodic touch signal can not be symmetric about $t_{contact}$.

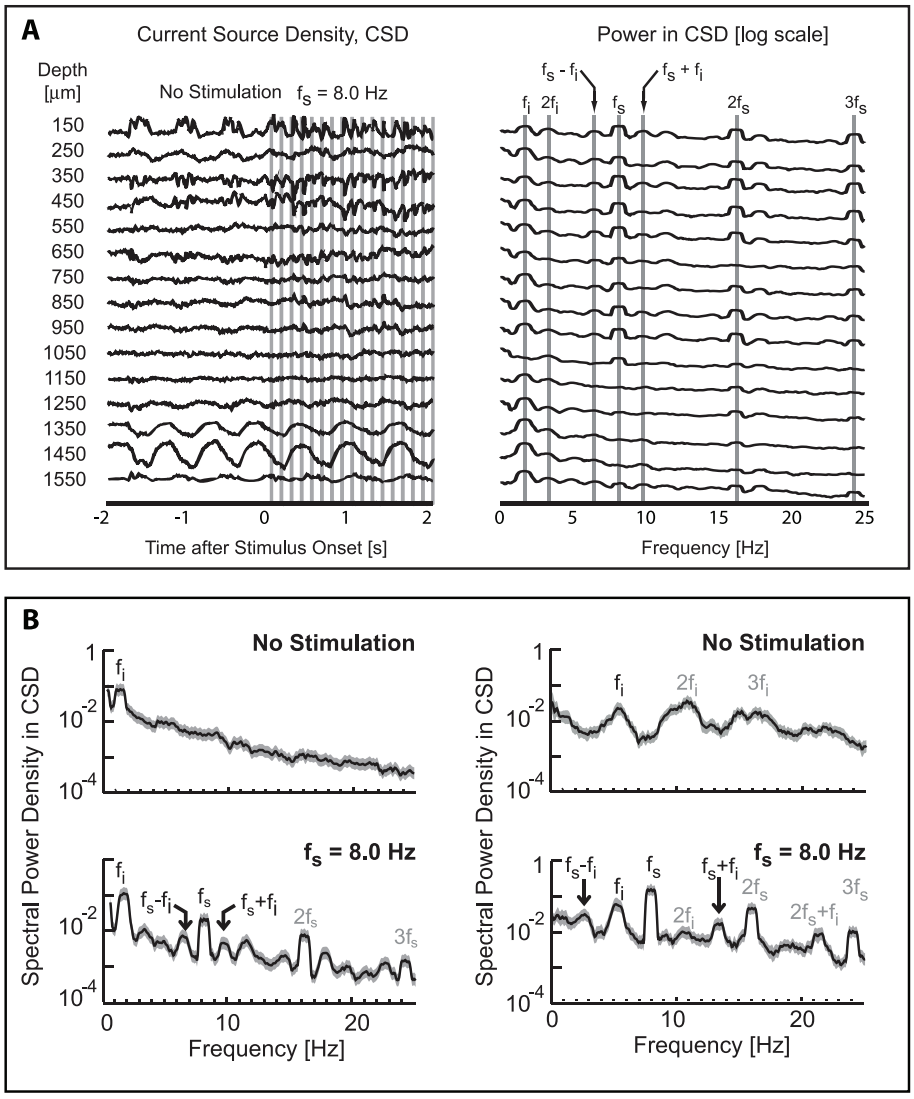

Figure III.2 **Mixing in the vibrissa primary sensory cortex from rat. (A)** Example recordings from different depths in vibrissa S1 cortex. The data on the left are time series of the the current source density (CSD), which is the discrete second derivative of the measured voltage and approximates the divergence of current flow (scale bar 10 mV/mm^2). An external stimulus with frequency f_s was turned on at time zero. The panel on the right shows the spectral power for the same depth during stimulation. Note the presence of mixture frequencies $f_s \pm f_i$. **(B)** The spectral power before (top panels) and after (bottom panels) stimulation at a depth of 450 μm. Higher order mixture terms and harmonics due to the non-sinusoidal nature of both intrinsic and stimulus-induced oscillations give rise to the peaks indicated by gray text. Gray bands correspond to 95% confidence intervals. Adapted from Ahrens et al. (2002).

III.C Threshold Model for Mixing

We now turn our attention to a phenomenological model of the experimental findings. The results for the paddlefish electroreceptive organ and the rat vibrissa S1 cortex have a number of common features: (*i*) The "input" frequencies, *e.g.*, f_s and f_i in Figure III.2, are present in the output; (*ii*) Primary mixing terms, *e.g.*, $f_a + f_e$ and $f_a - f_e$ in Figure III.2, are present in roughly equal proportion; and (*iii*) Higher-order terms, such as harmonics of the inputs, are present at the output. Any of a number of cellular nonlinearities (Koch and Poggio, 1992; Gabbiani et al., 2004) may account for these observations. We focus on the consequences of the threshold firing properties of a neuron and consider a simple but analytically tractable model.

We describe a rhythmic post-synaptic input to a neuron as

$$x(t) = \cos(2\pi f_a t + \phi_a) + \rho \cos(2\pi f_b t + \phi_b), \tag{III.1}$$

with $0 < \rho \leq 1$, and consider the threshold relation given by

$$y(t) = [x(t) - \theta_0]_+, \tag{III.2}$$

where θ_0 is the value of the threshold and $[f(t)]_+$ is the Heaviside function, *i.e.*, $y(t) = 0$ when $x(t) < \theta_0$ and $y(t) = 1$ when $x(t) \geq \theta_0$. The output can be expressed in terms of closed integrals (Ahrens et al., 2002) to yield

$$y(t) = \frac{1}{2\pi i} \sum_{n=-\infty}^{\infty} \sum_{m=-\infty}^{\infty} \mathrm{I}_{n,m}\big(\theta_0, \rho\big)\, e^{i[n(\phi_a + \pi/2) + m(\phi_b + \pi/2)]}\, e^{2\pi i (n f_a + m f_b) t}, \tag{III.3}$$

for integer mixture coefficients m and n. The first factor,

$$\mathrm{I}_{n,m}\big(\theta_0, \rho\big) \triangleq \lim_{\epsilon \to 0} \int_{-\infty}^{\infty} \frac{\mathrm{d}\Omega}{\Omega - i\epsilon}\, e^{-i\theta_0 \Omega}\, \mathrm{J}_n(\Omega)\, \mathrm{J}_m(\rho\Omega), \tag{III.4}$$

is an integral over Bessel functions that sets the magnitude of each mixture term, and must, in general, be evaluated numerically. The second factor sets the phase of each term in the sum and the final factor represents a sinusoid at one of the

mixing frequencies, $|mf_a \pm nf_b|$. We recall that $\mathrm{J}_k(\Omega) = (-1)^k \mathrm{J}_{-k}(\Omega)$, so that $\mathrm{I}_{n,-m}\big(\theta_0, \rho\big) = (-1)^m \mathrm{I}_{n,m}\big(\theta_0, \rho\big)$ and sum and difference terms of the same order have equivalent magnitudes. The spectral representation for the output of the model is given by

$$\begin{aligned}\tilde{y}(f) &\triangleq \int_{-\infty}^{\infty} e^{2\pi i f t} y(t)\, \mathrm{d}t \\ &= \frac{1}{2\pi i} \sum_{n=-\infty}^{\infty} \sum_{m=-\infty}^{\infty} \mathrm{I}_{n,m}\big(\theta_0, \rho\big)\, e^{i[n(\phi_a+\pi/2)+m(\phi_b+\pi/2)]}\, \delta[f - (nf_a + mf_b)],\end{aligned} \tag{III.5}$$

where $\delta()$ is the Dirac delta function. We see that $\tilde{y}(f)$ has contributions at all possible mixture frequencies. Numerical calculations show that the magnitude of the $\mathrm{I}_{1,\pm 1}\big(\theta_0, \rho\big)$ terms, and thus the spectral power in the sum and difference modes, is maximized for $\rho = 1.0$ and $\theta_0 = 0.8$ (Ahrens et al., 2002). An example of the threshold process and resulting power spectrum is shown for these parameters in Figure III.3.

III.D Multi-stage Mixers for Isolation of Spectral Components

The output from the threshold-based mixer contains components at the fundamental frequencies, their harmonics, the sum and difference mixture terms, and higher order mixtures. In principle, a band-pass filter could be used to isolate one of these components. This method is limited, however, as the frequencies of neighboring components may be close to each other in value. An alternative method uses interference effects in a manner analogous to the structure of image-reject mixers in communications engineering (Horowitz and Hill, 1989). The inputs to two or more threshold units are phase-shifted and the outputs summed, in such a way that undesired components cancel. This requires that we introduce additional circuit elements that can shift the phase of each of the two inputs. Al-

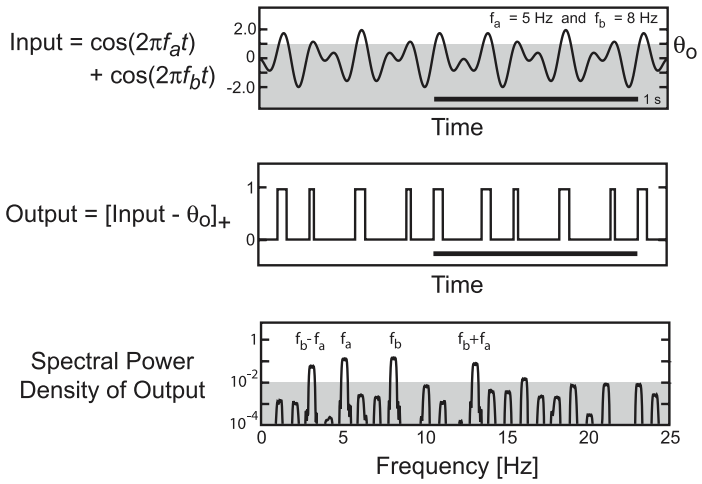

Figure III.3 **Threshold mixer example.** The top panel shows the summed input signals and threshold level θ_0 (gray band). The middle panel shows the result of applying the transformation in Equation III.2 to the input. The bottom panel shows the power spectrum computed from a 10 sec output time series. The gray band here indicates approximately one decade below the power of the fundamentals. Parameters were set to $\rho = 1.0$, $f_a = 5$ Hz, $f_b = 8$ Hz, and $\theta_0 = 0.8$. Panels adapted from Ahrens et al. (2002).

though a simple delay line could accomplish this for a fixed frequency, we describe next a solution that works over a range of frequencies.

III.D.1 Phase Shifters

We first consider the special but useful cases of shifts of $\phi = \pi$ radians, $\phi = \pi/2$ radians, and $\phi = -\pi/2$ radians.

Phase shifting by a factor of π radians can be accomplished with a fast inhibitory synapse, so that the corresponding post-synaptic input to the threshold unit is negative going rather than positive going (Figure III.4A). Then,

$$\phi_{output} = \phi_{input} + \pi, \tag{III.6}$$

corresponding to inversion of the signal.

A phase shift of $\pi/2$ radians arises naturally in the neuronal implementation of a phase-locked loop (PLL) (Ahissar and Vaadia, 1990; Ahissar, 1998;

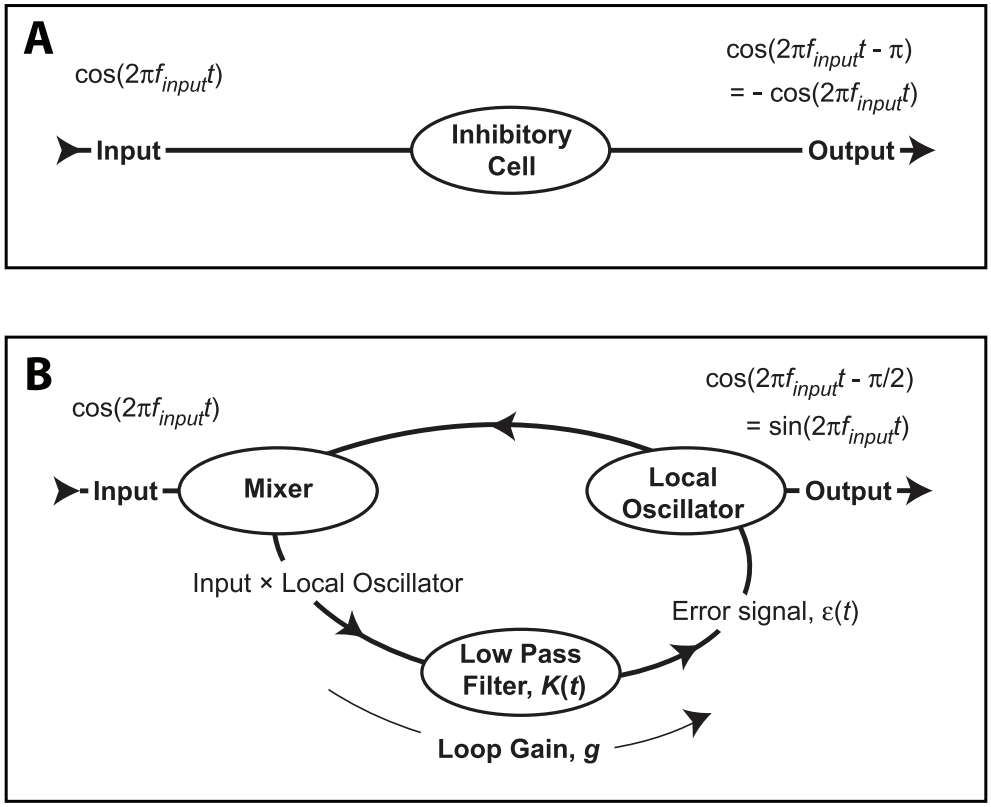

Figure III.4 **Phase shifter circuits.** **(A)** Shift of π radians via an inhibitory interneuron that functions as an inverting but otherwise linear input-output device. **(B)** Shift of $\pi/2$ radians with a phase-lock loop that consists of 3 neurons: one operating as a mixer, one acting as a low-pass filter, and an oscillator whose frequency is a monotonically increasing function of its input.

Hoppensteadt, 1997; Kleinfeld et al., 2002), which is a feedback circuit that adjusts the frequency of a local oscillator to match that of an input signal (Best, 1984). A generic analog PLL consists of three components. First, a mixer multiplies the input oscillator by the output of a local oscillator. Second, a low-pass filter $K(t)$ isolates the error term, $\epsilon(t)$, where

$$\epsilon(t) \propto \int_{-\infty}^{t} \mathrm{d}\tau \; K(t-\tau) \cos(2\pi f_{input}\tau + \phi_{input}) \cos(2\pi f_{local}\tau + \phi_{local} - \pi/2).$$

Third, the frequency of the local oscillator is shifted so that $f_{local} = f_0 + g\epsilon(t)$, where f_0 is a center frequency and g is a gain factor. When the PLL locks, $f_{local} \approx f_{input}$ and $\epsilon(t) \propto \sin(\phi_{input} - \phi_{local})$.

Self-consistency requires that the measured phase, ϕ_{out}, at the output of a locked PLL is of the approximate form

$$\phi_{out} \approx \phi_{input} + \frac{\pi}{2} + \sin^{-1}\Big(\frac{f_{input} - f_0}{G}\Big), \tag{III.7}$$

where the constant G is proportional to the gain factor g. [2] The local oscillator and the input will tend to be $\pi/2$ radians out of phase when either the gain g, and thus the constant G, is large or the input frequency f_{input} is close to the intrinsic frequency f_0. Intuitively, the shift of $\pi/2$ radians occurs because for a PLL at steady-state, the product of the input sinusoid and the local oscillator must average to zero when the PLL is at steady-state.

With the above results, we note that a phase shift of $-\pi/2$ is readily achieved by following a phase shift of $\pi/2$ (Equation III.7) with an inversion (Equation III.6).

[2] The factor of $\pi/2$ is commonly implicit in textbook formulas, as the local oscillator is described by a sine function while the external input is given as a cosine. This factor was inadvertently dropped in Equation 10 from Kleinfeld et al. (2002).

III.D.2 A Circuit to Isolate the Difference Frequency

We use a mixer in combination with phase shifters of π and $\pm\pi/2$ radians to construct outputs that differ only in the phase term

$$exp\{i[n(\phi_a + \pi/2) + m(\phi_b + \pi/2)]\} \tag{III.8}$$

from Equations III.3 and III.5. The phase shifts are chosen so that summation of the outputs leads to a cancellation of the input sinusoids, their harmonics, and the sum frequency, as in an image-reject mixer (Horowitz and Hill, 1989).

As a step toward the design of the difference circuit, we first consider the cancellation of the fundamental frequencies. We start with two inputs of equal amplitude, labeled a and b, and two threshold units, labeled 1 and 2. We then define $\cos(2\pi f_a + \phi_{a,1})$, as the input a, phase-shifted by $\phi_{a,1}$, to threshold unit 1; analogous expressions apply for all combinations of inputs and outputs. From the phase term above, we find that the output at each input frequency, corresponding to mixture terms $(n = 1, m = 0)$ and $(n = 0, m = 1)$, is simply phase-shifted by $\pi/2$ relative to the input. We thus choose, e.g.,

$$\begin{aligned} \phi_{a,1} &= 0 \quad \text{and} \quad \phi_{b,1} = \pi \\ \phi_{a,2} &= \pi \quad \text{and} \quad \phi_{b,2} = 0, \end{aligned}$$

with the result that the output terms for the fundamentals cancel when summed. The summed output, $Y(t) = y_1(t) + y_2(t)$, is given by

$$\begin{aligned} Y(t) = \frac{i}{\pi}\, \mathrm{I}_{0,0}\big(\theta_0, 1\big) - \frac{i}{\pi}\big\{\, \cos[2\pi(f_a + f_b)t] + \cos[2\pi(f_a - f_b)t]\big\}\, \mathrm{I}_{1,1}\big(\theta_0, 1\big) \\ + O(|n| + |m| > 2). \end{aligned} \tag{III.9}$$

Apart from the constant term, the output is similar to that for multiplication.

We now move to the case of maintaining only the primary difference term. In principle, this can be done with three mixers and phase shifts of $\phi = 0, +2\pi/3$

and $-2\pi/3$ radians, but such shifts are difficult to generate. We consider an alternative scheme with four threshold units, where the phase of the input to each unit is given by

$$\begin{aligned}
\phi_{a,1} &= 0 \qquad\quad \text{and} \quad \phi_{b,1} = \pi \\
\phi_{a,2} &= \pi \qquad\quad \text{and} \quad \phi_{b,2} = 0, \\
\phi_{a,3} &= +\pi/2 \quad \text{and} \quad \phi_{b,3} = -\pi/2 \\
\phi_{a,4} &= -\pi/2 \quad \text{and} \quad \phi_{b,4} = +\pi/2.
\end{aligned}$$

The summed output, $Y(t) = y_1(t) + y_2(t) + y_3(t) + y_4(t)$, is then

$$Y(t) = \frac{2i}{\pi}\mathrm{I}_{0,0}\big(\theta_0, 1\big) + \frac{4i}{\pi}\cos[2\pi(f_a - f_b)t]\ \mathrm{I}_{1,1}\big(\theta_0, 1\big) + O(|n| + |m|) > 2). \quad \text{(III.10)}$$

The difference circuit is illustrated schematically in Figure III.5A, together with the calculated results for the spectral power density for the choices $f_a = 8$ Hz and $f_b = 5$ Hz (Figure III.5B), demonstrating that the fundamentals are almost entirely suppressed.

We note that a straightforward modification of this circuit will preserve the sum rather than the difference terms.

III.E Discussion

Spectral mixing is an integral aspect of electronic communication, as it provides a means to detect and isolate specific frequency components. Certain designs, such as double-balanced mixers and image-reject mixers, exploit the summation of phase-shifted replicas to cancel out designated terms, much as interference effects are used to direct radio signals from antenna arrays and to produce patterned illumination in optics. It is of interest that despite the central role played by oscillators in nervous systems, analogies to these spectral mixers have not been identified *in vivo*. Given the presence of mixing terms in the experiments cited above, it is tempting to conjecture that spectral mixing plays a

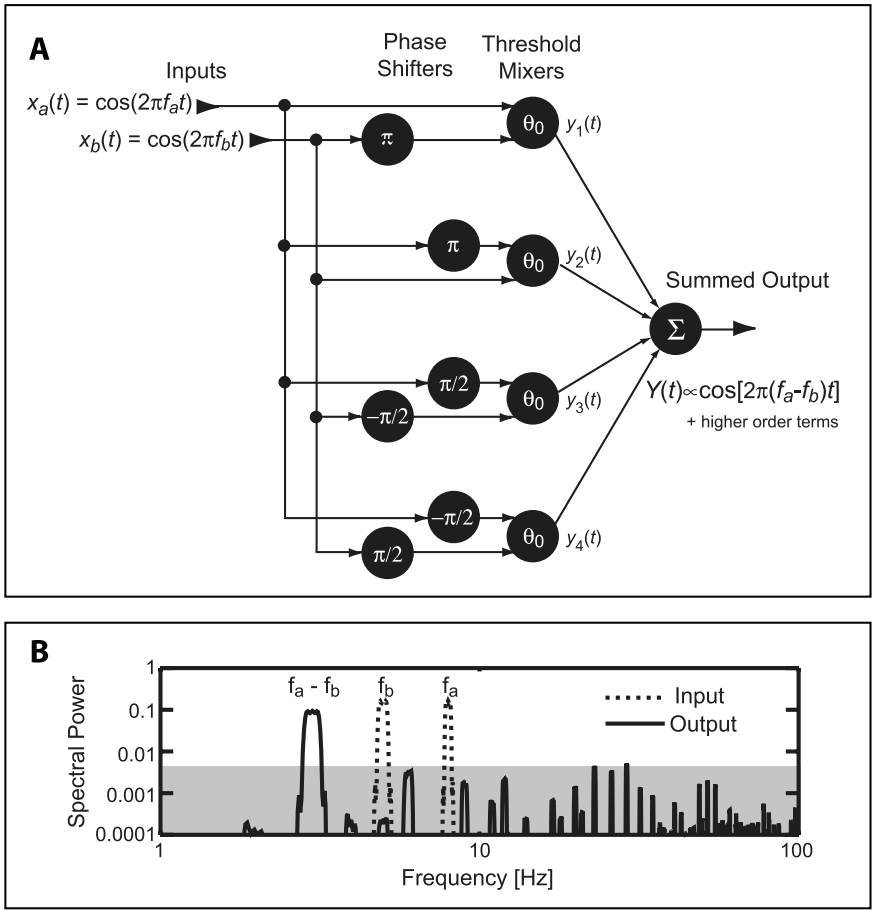

Figure III.5 **Neuronal image-reject mixer circuit. (A)** Schematic of the circuit, which consists of phase-shifters of π, $\pi/2$ and $-\pi/2$ radians (Equations III.6 and III.7), threshold units that act as mixers (Equation III.5), and a linear summation element. **(B)** Spectral analysis of the output of the mixer circuit in Equation III.10 for input sinusoids with $f_a = 8$ Hz and $f_b = 5$ Hz, and where $\theta_0 = 0$. The gray band indicates the power in the largest of the higher-order components.

role in neuronal computations. We thus attempted here to demonstrate an implementation that is biologically plausible, although experimental evidence for a neuronal implementation of a PLL is admittedly weak.

As a technical issue, one weakness of our scheme is the need for constant phase shifts over a broad range of frequencies. We choose to use phase-locked loops, a common element in communication and control circuits (Best, 1984), but even these engineering implementations have limitations. Locking will not occur if the loop gain is too small, while a PLL will lock to a harmonic if the loop gain is too large. In engineering applications, the latter issue typically limits the useful frequency range of a PLL in the absence of additional circuitry. For example, initial locking may require that the intrinsic frequency be swept, starting near $f_0 = 0$, so that locking occurs at the fundamental.

Our focus has been on mixing to form the difference and sum terms $f_a \pm f_b$, which are prevalent in the experimental data summarized here. Other mixing terms are also of potential interest, however, such as a $2f_a - f_b$ term that arises in psychoacoustics (Hartmann, 1997). Although these terms can be generated by spectral mixing, alternative formulations are possible. For example, mixing terms can also arise if one oscillator directly provides synaptic modulation to another (Neiman and Russell, 2004), rather than two oscillators summing in a third threshold unit. As an example of such a system, and as a closing nod to the Kuramoto model, we consider a system of two phase oscillators with unidirectional coupling[3]:

$$\frac{\mathrm{d}\phi}{\mathrm{d}t} = 2\pi\big[f_0 + K\sin(2\pi f_d t - \phi)\big], \tag{III.11}$$

where $\phi(t)$ is the phase of the driven oscillator, f_0 is its intrinsic frequency, f_d is the frequency of the driving oscillator, and K is the coupling strength.

The dimensionless ratio $K/|f_0 - f_d|$ determines the behavior of this system. If this ratio is smaller than one, the driven oscillator will not entrain to the

[3]See Appendix A for an expanded analysis of this system.

drive and instead undergoes phase walk-through (Ermentrout and Rinzel, 1984). In this case, we obtain an explicit solution[4] for $\phi(t)$ as

$$\phi(t) = 2\pi f_d t - 2\tan^{-1}\left\{\frac{K+\sqrt{(f_0-f_d)^2-K^2}\,\tan\left[\pi\sqrt{(f_0-f_d)^2-K^2}\,(t+C)\right]}{f_0-f_d}\right\}, \tag{III.12}$$

where C is a constant. A sinusoidal oscillator with this phase can be shown to contain spectral components at frequencies given by $f_d \pm m\sqrt{(f_0-f_d)^2-K^2}$, for integer m. In the limit that $K << |f_0-f_d|$, the driven oscillator has power at frequencies $\{f_d, f_0, 2f_0-f_d, f_0-2f_d, ...\}$, demonstrating another plausible route to generating nonlinear mixing terms from the interaction of neuronal oscillators.

Acknowledgement

The text of this chapter is a reprint, with minor modifications, of an article that appeared in the journal Progress in Theoretical Physics Supplement, No 161, pages 86-98 (2004) by D. Kleinfeld and S.B. Mehta (the dissertation author).

[4]This equation was incorrect in the published version of this manuscript and is corrected here.

Chapter IV

Haptic Perception, Sensorimotor Integration and Behavior

Haptic perception is an active process that provides an awareness of objects encountered as an organism scans its environment. In contrast to the sensation of touch produced by contact with an object, perception of the location of an object arises from the integration of tactile signals with the configuration of the body as it moves. A discrete sensory representation and a low number of motor degrees of freedom make the ethologically prominent rat vibrissa system an ideal model for the study of the neuronal computations that underlie this integration. We find that rats with only a single vibrissa can combine touch and movement to distinguish the location of objects that vary in angle along the sweep of vibrissa motion. The patterns of this motion and of the corresponding behavioral responses show that rats can scan potential locations and decide which location contains a stimulus within 150 ms. This interval is consistent with just one to two whisk cycles and provides constraints on the underlying perceptual computation. These data argue against strategies that do not require the integration of sensory and motor modalities. Rather, the ability to judge spatial angle with a single vibrissa connects previously described, motion-sensitive neurophysiological

signals to perception in the behaving animal.

IV.A Introduction

> Neurophysiologists ... have been reluctant to face up to [changes in anatomy from moment to moment] in explaining perception, for they know more about the anatomy of the eyes, ears, and skin than they do about the physiology of looking, listening, and touching (Gibson, 1966, pp. 4).

Forty years ago, the noted psychologist J.J. Gibson argued that the sensations produced by feed-forward transformation of inputs from neuronal exteroreceptors are distinct from the dynamic perception of the environment derived from the "neural loops of an active perceptual system" (Gibson, 1966, pp. 5). Gibson's thesis was that perception of the location of a contacted object, for example, was fundamentally different from the sense impressions that arise from skin mechanotransduction. Perception requires an integration of information across sensory and motor modalities that can be not be derived from successive transformations of the touch data alone. Studies in systems from posture control (Peterka, 2002; Deliagina et al., 2006) to eye movement (van Beers et al., 2001) have elucidated principles of such "neural loops" when used for feedback in motor systems with explicit sensory dependence. The work described here addresses a complementary case of positional context in a sensory system with explicit motor drive (Moss et al., 2006; Cullen and Roy, 2004).

The rat vibrissa system provides our prototype for this sensorimotor model. For over a century, researchers inspired by the prominence of these tactile hairs and their associated neural architecture, have compiled behavioral evidence of the use of the vibrissae as a complex sensory system able to identify and locate objects (Gustafson and Felbain-Keramidas, 1977). While intriguing recent insights into the mechanical properties of the vibrissae (Neimark et al., 2003; Hartmann et al., 2003) may explain the processing of qualities such

as texture (Andermann et al., 2004; Arabzadeh et al., 2005; Hipp et al., 2006; Moore and Andermann, 2005), few experiments have quantitatively characterized the spatial information available from the vibrissae. Early work indicated that rats use this system for detection of surfaces during navigation (Vincent, 1912), and more recent studies have shown that the vibrissae provide information about object distance (Shuler et al., 2001), shape (Harvey et al., 2001) and orientation (Polley et al., 2005; Benison et al., 2006). Few of these behaviors appeared to be inherently sensorimotor, and rats are known to perform some tasks, such as vibration (Hutson and Masterton, 1986) and bilateral distance (Krupa et al., 2001) discrimination, with only passive vibrissa contacts. The system as a whole, in contrast, is fundamentally active. While nearly all mammalian species have vibrissae (Ling, 1966), rats and related rodent species have specifically evolved the ability to move their vibrissae for dynamic exploration of the environment (Rice and Arvidsson, 1991). This adaptation begs the question of whether touch and motion are used in concert, in the spirit of Gibson, to form an "active perceptual system."

Neurophysiologically, the sensory and motor processes are tightly interwoven. A nested series of loops, at levels from brainstem to cortex, connect the vibrissa sensory stream to a hierarchical motor drive that ordinarily produces a rhythmic rostrocaudal movement known as whisking (Kleinfeld et al., 1999). Sensory inputs feed back to motor areas at all levels and can alter motor output at even the lowest-order loop (Nguyen and Kleinfeld, 2005). The information flow is bidirectional, however, and electrophysiological recordings have found neurons, again at levels from the brainstem to cortex, that encode the real-time position of the vibrissae even in the absence of contact with an external object (Fee et al., 1997; Szwed et al., 2003). These cells complement somatosensory neurons that encode the qualities of contact and could allow the brain to maintain a reference as self-generated motion modulates the external location corresponding to that contact.

The existence of position sensitive signals does not prove that they are actually used for spatial perception. What has been lacking in the study of the neural computations underlying the fusion of these touch and motion signals is a vibrissa-mediated behavior that requires sensorimotor integration. One such task would ask if a rat can use its vibrissae to differentiate between objects that differ only in rostrocaudal angle. However, the nervous system could in principle ignore motor information and solve this problem using the topography of the vibrissa array. When the motion of the vibrissae is comparable to their separation, the rostrocaudal position of an object can be judged from the peripheral origin of the touch signal (Figure IV.1A), in an encoding known as a labeled-line (Perkel and Bullock, 1968). In this scheme, the topographic identity of the cortical region activated by contact corresponds to object location because each region of space is only scanned by a single sensor. An animal could then succeed in such a discrimination task if it used large amplitude, exploratory motion to detect an object and switch to smaller motion for localization.

In the more typical exploratory whisking motion (Carvell and Simons, 1990; Bermejo and Zeigler, 2000), vibrissa sweeps overlap and the angular location corresponding to contact requires information beyond the identity of the contacting vibrissa (Figure IV.1B). In this case, the presence of position-sensitive neurons suggests that the position of the vibrissae at the time of contact could provide context to disambiguate the contact event. This approach falls under the rubric of haptic perception, as it is based on an animal determining the position of "an object relative to the body and the body relative to an object" (Gibson, 1966, pp. 97). Other algorithms based on the touch sensation, such as duration of contact (discussed in Szwed et al. (2003) and Chapter II), are possible if different object positions result in reproducible differences in the structure of the contact event. These approaches share the common feature that they do not depend on vibrissa identity and therefore, unlike the humble labeled-line, can be performed

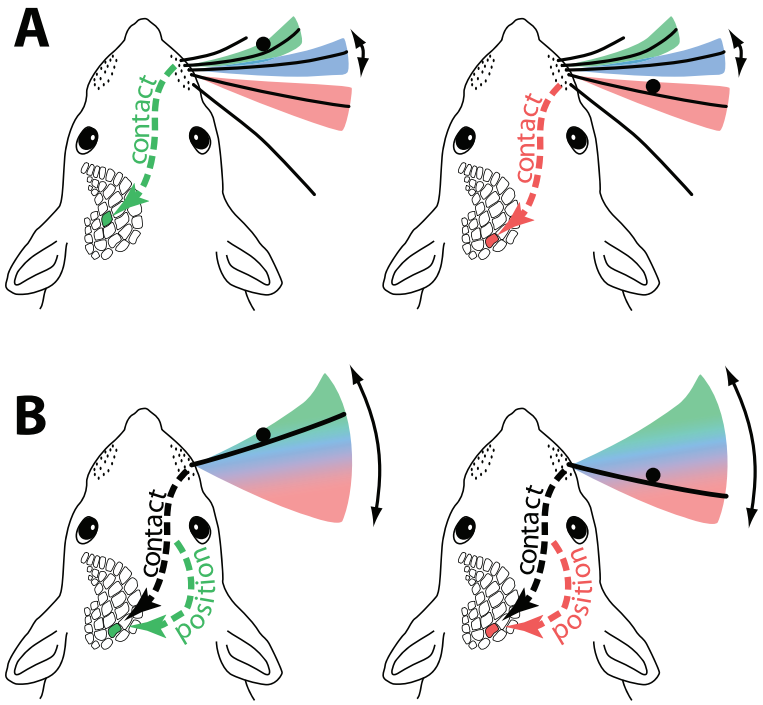

Figure IV.1 **Two localization algorithms: topographic labeled-line and haptic sensing.** Each cartoon depicts an animal contacting a small object (black circle) near its head and an idealization of the resulting neural streams (dashed arrows) afferent to the vibrissa region of the primary somatosensory cortex. **(A)** A labeled-line strategy. During small motion, the location of an object is encoded in the identity of the vibrissa it contacts. For clarity, only one row of vibrissae is shown; additional rows do not directly aid localization. **(B)** A sensorimotor strategy. During large motion, contact on a given vibrissa leaves object position ambiguous. Information about the position of the vibrissae at the time of contact resolves the confound. This scheme only requires a single vibrissa.

with a single vibrissa. To differentiate between these classes of spatial encoding and relate known sensorimotor physiological signals to a sensorimotor behavior, we thus ask if behaving rats are able to discriminate between objects at different rostrocaudal angles when restricted to the use of a single vibrissa.

IV.B Results

We tested fourteen rats in a spatial angle discrimination task using an apparatus designed for high-throughput, semi-automated training (Figure IV.2). Briefly, each animal was assigned two stimulus positions whose rostrocaudal angles differed by 15°. One of these positions was designated the rewarded, or ***S+***, stimulus and the contrasting position was designated unrewarded, or ***S-***. The animal performed a series of trials in which it maintained a fixed head position while challenged with a thin rod at one of these two positions. Under a go/no-go paradigm, the animal was required to respond to the ***S+*** position with at least L lever presses (L ranged from 1 to 6) in return for a fluid reward (Figure IV.7D). Lever presses in the ***S-*** condition were ignored. An animal was considered to discriminate the two positions when multiple consecutive sessions showed a statistically significant difference between ***S+*** and ***S-*** trials in the latency to reach this response requirement. Animals who learned this discrimination using all of their vibrissae were tested next with only one row of vibrissae intact, and finally with only a single vibrissa.

Figure IV.2 **Apparatus for behavioral testing and training. (A)** View of training arena. Animals were placed in the vestibule at the start of a session, and their position was monitored through infrared sensors. In the tunnel, the U-shaped restraint bar allowed access to the operant response lever and nose poke. Stimulus discrimination trials were initiated when an animal interrupted the nose poke sensor, causing either the rostral or the caudal stimulus pin to descend into the vibrissa field. The stimuli were driven by air-pistons and positioned through a circular guide fixed relative to the nose poke (some supporting parts are not shown for clarity; see Figure B.1). Behavioral responses were measured with a lever, and lever presses in response to the $S+$ stimulus, designated rostral or caudal for each animal, were rewarded with a drop of water in the fluid dispenser. Any remaining fluid was withdrawn by vacuum at the end of the trial. An infrared lamp provided backlit contrast of the head and vibrissa for the camera recording the ventral view shown in (C). The entire arena was enclosed in a dark, sound-attenuated chamber (not shown). **(B)** Detail of stimulus area from (A). **(C)** View of stimulus area from (A), as reflected in the mirror and seen by the camera. The nose poke resulted in reproducible positioning of the stimuli in head-centered coordinates (see also Figures IV.6A–B, D–E).

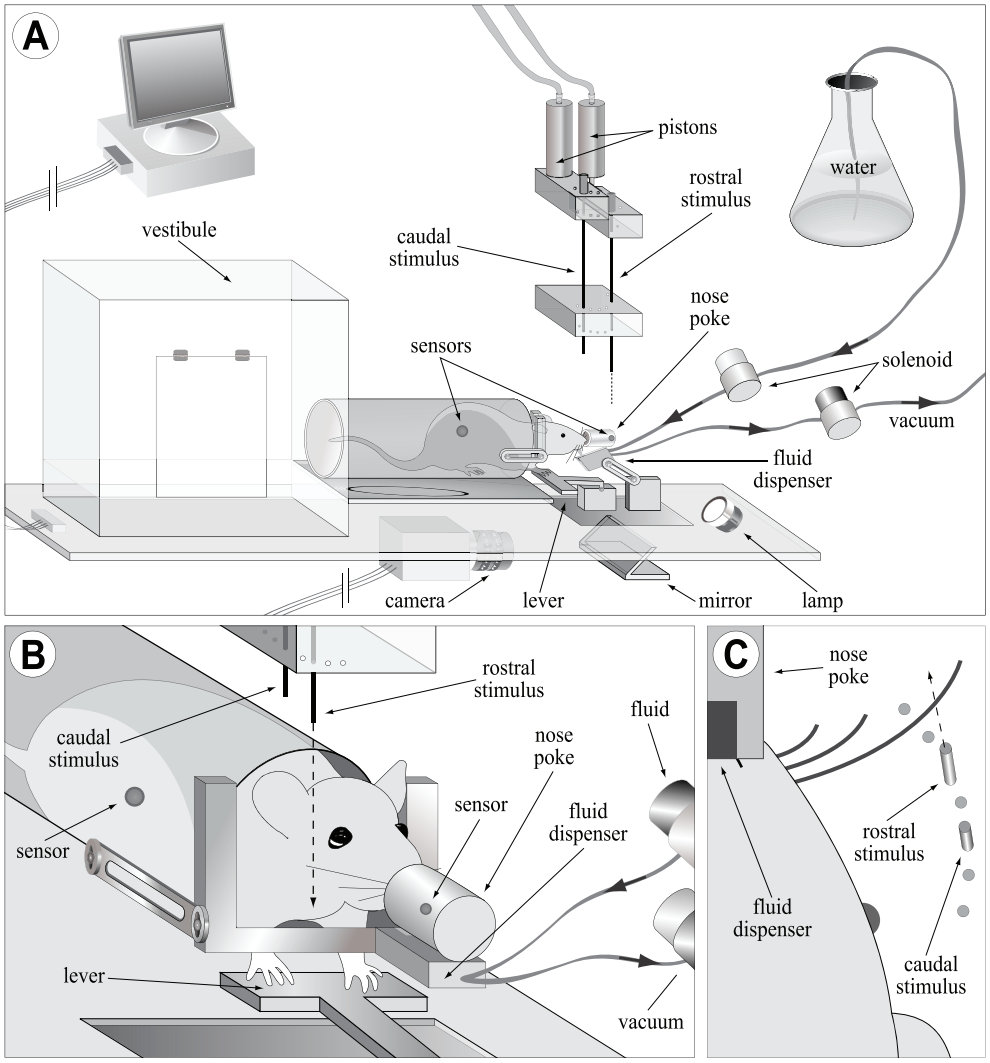

Figure IV.2 (see facing page)

We consider it likely that the typical rat has the perceptual ability needed to perform this single vibrissa discrimination, despite the fact that only five of our initial fourteen animals showed consistent differences in behavioral output between ***S+*** and ***S-*** trials (Figure IV.3). The largest contribution to this attrition was a weakness in the behavioral measure used early in the study. Over half (5 of 9) of the animals who did not succeed in the single vibrissa test were required to make only a single lever press response ($L = 1$) during ***S+*** trials (Figure IV.3, gray numbers). The majority of these animals failed to show significant differences between ***S+*** and ***S-*** trials in the latency to this single lever press even when tested with a full complement of vibrissae. As there was little penalty in this condition if an animal responded to ***S-*** trials rather than risk missing a reward, we raised the required number of lever presses L to four or more for later animals (directly adding negative reinforcement failed as it lowered the total number trials rather than selectively suppressing ***S-*** responses). This discouraged animals from responding when they could predict that no reward would be forthcoming, and we successfully measured discrimination for all animals tested on this larger value of L with all vibrissae intact. While a fraction of these animals (3 of 8), failed to perform consistently when tested with a single vibrissa row, their occasional successes suggested that further limitations in our task design rather than inability to recognize spatial differences were responsible for this failure.

IV.B.1 Analysis of Single Vibrissa Discrimination

Once a response requirement L was established for each animal, we compared the pattern of lever presses between ***S+*** and ***S-*** trials to characterize the spatial discrimination process. In our analysis, we considered only the first L responses in each trial, as the presence or absence of a reward after L lever presses could itself be used to distinguish two stimulus conditions (e.g., Figure IV.4A).

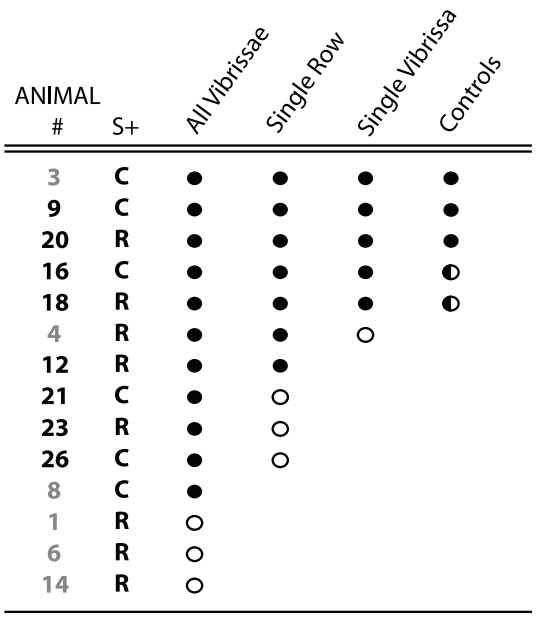

Figure IV.3 **Summary of performance levels achieved for all animals.** Each row represents one of fourteen animals tested on the spatial discrimination task. The first column gives an identifying number, and the second column gives an ***S+*** stimulus assignment (R for rostral and C for caudal). Animals with numbers in gray were required to make a single response for a reward in an ***S+*** trial, while the remaining animals were required to make four or more responses per ***S+*** trial. The next three columns summarize performance as the number of intact vibrissae decreased. Filled circles indicate stable performance at a given level and open circles indicate that an animal was tested but did not achieve stable performance. "Stable performance" here is defined as statistically significant differences in ***S+*** and ***S-*** responses over multiple sessions. In two cases (Rat #8, Rat #12), circumstances unrelated to the experiment ended testing despite success at all attempted stages. The final column describes testing under a series of control conditions. Filled circles here indicate that a given animal passed all controls. Animals who habitually sampled the stimuli with their head are shown with half-filled circles in the control column, as it was unclear if this movement provided extra spatial information.

Figure IV.4 **Temporal profile of behavioral responses for one session. (A)** Lever press responses in a session by Rat #20 restricted to the right C1 vibrissa. The trial length T was 8 sec and response requirement L was 5 lever presses (cf. Figure IV.7). Each row shows the first five lever presses in a trial (responses from ***S+*** trials are in green and those from ***S-*** trials are in red). The fifth response in an ***S+*** trial was followed by a reward, while all responses during an ***S-*** trial were ignored. The session consisted of 58 ***S+*** trials and 56 ***S-*** trials over 30 min. **(B)** Cumulative number of lever presses from (A), averaged separately over ***S+*** and ***S-*** trials. The inset illustrates this data transformation. The green line and shaded region give the mean $\pm$ 2σ (S.E.M.) cumulative lever press counts for ***S+*** trials; equivalent data for ***S-*** trials are in red. The two gray arrows at 0.5 sec mark the first time point after which the 2 σ error regions do not overlap. **(C)** Distribution of latencies from the start of a trial to the fifth lever press, for the trials shown in (A). Trials in which fewer than five responses were recorded are shown at infinite latency. The bars and left ticks show histograms of trials as a function of latency, and the lines and right ticks show the same data as cumulative distributions. The ***S+*** and ***S-*** distributions are statistically distinct ($p < 0.001$, 2-sided Kolmogorov-Smirnov (K-S) test). Green indicates ***S+*** and red indicates ***S-*** . **(D)** Receiver operating characteristic (ROC) curves summarizing differences between ***S+*** and ***S-*** latency distributions for multiple sessions. The fraction of ***S+*** trials with latencies below some threshold τ is plotted against the fraction of ***S-*** trials with latencies below τ; the curves are constructed by parametrically varying τ. The result for the data from (C) is shown by the solid black line, where the thicker portion corresponds to the threshold having traversed the thick sections in the inset data. The gray lines are from twelve subsequent single vibrissa sessions performed by the same animal (Rat #20). The orange line corresponds to the control session from Figure IV.5C. Identical ***S+*** and ***S-*** distributions would yield the diagonal dashed line.

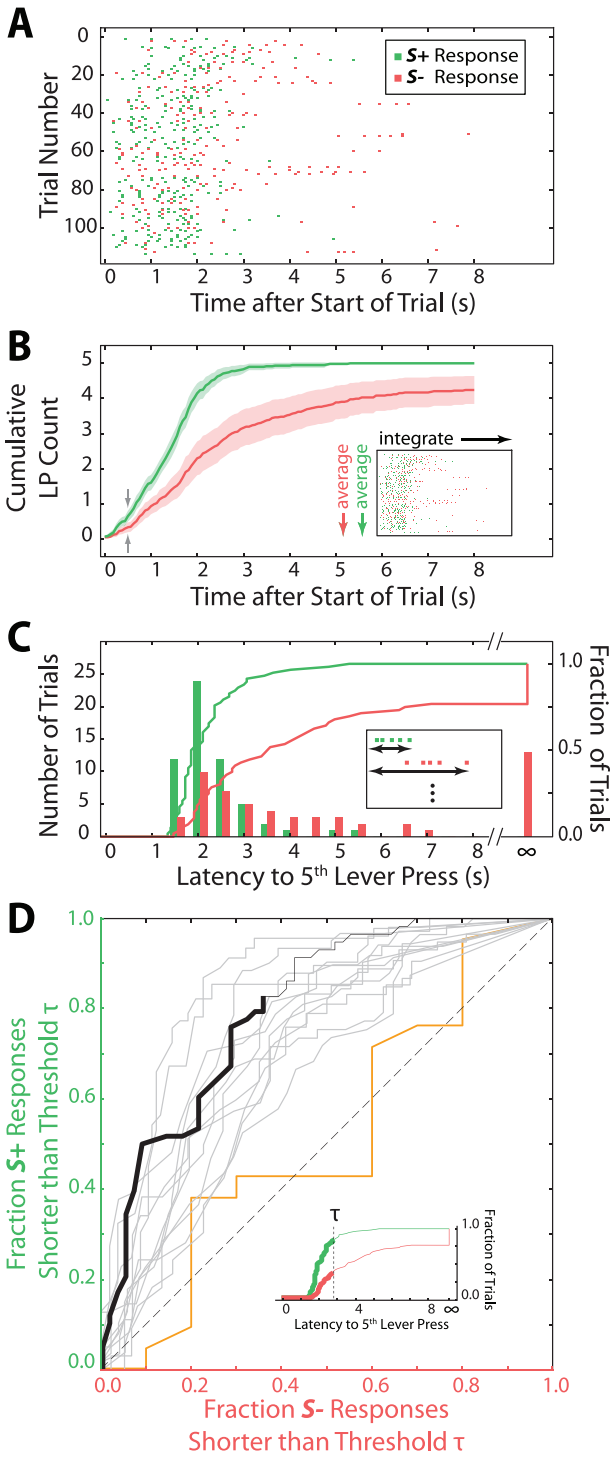

Figure IV.4 (see facing page)

The timing of the lever presses in the two conditions gave an estimate of the temporal requirements of the behavioral decision. The cumulative response count, averaged separately for all ***S+*** and ***S-*** trials, quantified this time course for a given session (Figure IV.4B). The difference between the two conditions was reflected in both a higher response rate and a lower latency to response onset in ***S+*** trials as compared to ***S-*** trials. In a typical session for the animal with the fastest responses (Rat #20), the average responses for the two conditions would begin to diverge by 250 ms after the start of a trial and the 95% confidence regions would become permanently non-overlapping after 500 ms (gray arrows in Figure IV.4B). Thus, within half a second of stimulus delivery, we could confidently measure a difference in the average response to ***S+*** and ***S-*** stimuli for this animal.

To determine the fraction of this interval used for active sensing, we estimated the time needed for the motor act of pressing the lever in two ways: (1) The maximum slope of the cumulative response gave the mean response rate during sustained responding. This rate was ∼2.5 lever presses per second, or 400 ms per lever press on average, for the ***S+*** responses measured again from the animal with the fastest responses. (2) The shortest time taken by any animal to reach $L = 5$ lever presses was ∼1.5 sec (e.g., Figure IV.4C). As few responses occurred in the first 250 ms of a trial (e.g., Figure IV.4B), this leaves 1.5 sec for five lever presses, or 250 ms per lever press in the fastest cases. We therefore estimate that this initial motor act requires 250 ms or longer. Given that a difference in the responses is evident by 500 ms, these data demonstrate that the complete sensorimotor process required to detect the stimulus and form a percept of stimulus position can be completed less than 250 ms after the start of a trial.

Beyond these individual lever press timings, the total latency to reach the required number of responses L in each trial (designated ∞ if L was never reached) served as evidence of behavioral discrimination (Figures IV.4C and IV.5A). A given session was considered to demonstrate successful stimulus discrimination

when the ***S+*** and ***S-*** latency distributions were significantly different, as measured by a 2-sided Kolmogorov-Smirnov (K-S) test. Consistent with the discussion above of the lack of a penalty for responding on ***S-*** trials, we observed many more false positive (type I) errors, in which an animal completed L lever presses during an ***S-*** trial with low latency, than false negative (type II) errors (e.g., Figures IV.4C, IV.5A–B). As the K-S statistic does not retain information about the types of errors, we confirmed consistent performance over multiple sessions by plotting receiver operating characteristic (ROC) curves (Green and Swets, 1966) for the detection of the ***S+*** stimulus (Figure IV.4D). Each ROC curve shows the dependency between false positive trials (i.e., ***S-*** trials with latencies shorter than a threshold τ) and true positive trials (i.e., ***S+*** trials with latencies shorter than τ), as the latency threshold τ is varied. Loosely, a steep slope near the left side of the graph indicates few type I errors, while a shallow slope near the right side of the graph indicates few type II errors; the integrated distance to the diagonal is a measure of the overall discriminability of the two distributions.

IV.B.2 Differences across Animals

The bimodal nature of the latencies (e.g., Figure IV.4C) was consistent for all five animals in the single vibrissa task, although several features varied from animal to animal and session to session. The numbers of type I and type II errors fluctuated but generally showed a tendency for false positive errors (e.g., Figure IV.4D for Rat #20; ROC curves not shown for the remaining animals, but all showed similar variability). The time at which ***S+*** and ***S-*** responses diverged also varied across sessions. The animal who performed the session shown in Figure IV.4 was the fastest (500 ms was typical), but each of the three animals who passed all controls (see below) performed sessions in which the average ***S+*** and ***S-*** responses diverged within 650 ms; the remaining two animals took longer ($>$ 1000 ms) due to the head-turning behavior described below. These times are

consistent with an upper bound of approximately 250 ms for the decision time, as described above.

In addition, the experimenter-defined association of stimulus position with reward condition varied across these five animals. Although all single vibrissa trials were performed at an angular separation of 15°, the animals were tested on different absolute stimulus positions and two animals had rostral ***S+*** assignments while three had caudal ***S+*** assignments. For example, Rat #20 was tested using vibrissa C1 with ***S+*** set to +15° and ***S-*** set to 0°, while Rat #9 was tested with vibrissa C2 for ***S+*** = -7.5° and ***S-*** = +7.5°. We did not find any gross differences in training time or performance correlated with these parameters, suggesting that the absolute position of the ***S+*** and ***S-*** stimuli did not play a critical role in the discrimination.

IV.B.3 Controls

For each of the five animals in our cohort who successfully performed the single vibrissa task in multiple sessions, we performed three controls to verify that this performance depended solely on vibrissa-mediated tactile cues. We first tested for visual cues. Although behavioral testing was performed in a dark, covered chamber, a high-intensity infrared lamp with a peak wavelength of 850 nm was used for videography. This lamp remained dimly visible to the human eye and we considered it possible, though unlikely (Jacobs et al., 2001), that residual light was available to the animals. We thus tested performance in control sessions for which the lamp was turned off (e.g., Figure IV.5B) and found that none of the five tested animals lost the ability to perform the task in the absence of the infrared illumination.

We next tested for a contribution from head movements. Stimuli were delivered when an animal fixed its head position in a nose poke and retracted when this fixation was broken (e.g., Figure IV.7C–D), but a mechanical lag allowed a

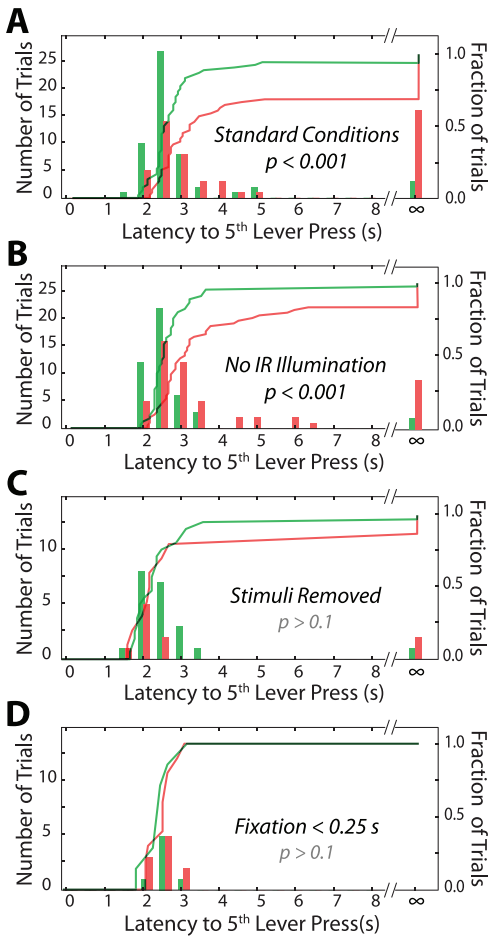

Figure IV.5 **Controls for extravibrissal cues. (A)** Latency distributions for a standard session, performed by Rat #20 and similar to Figure IV.4C. The session contained 54 ***S+*** trials and 51 ***S-*** trials and showed a significant difference in the latencies to the completion of the five lever press response requirement when comparing responses from ***S+*** and ***S-*** trials ($p < 0.001$, 2-sided K-S test). **(B)** Data from a session performed without IR illumination. The session contained 45 ***S+*** trials and 54 ***S-*** trials and showed a significant difference between ***S+*** and ***S-*** response latencies ($p < 0.001$, 2-sided K-S test). **(C)** Data from a session in which the stimulus pins were removed. The session contained 21 ***S+*** trials and 10 ***S-*** trials and showed no significant difference between ***S+*** and ***S-*** response latencies ($p > 0.1$, 2-sided K-S test). The number of trials was smaller here because the animal performed trials at a lower rate in this condition and because the session was short (15 min vs. 30 min above) to minimize extinction of the discrimination behavior. (D) Data from the session shown in (A) above, restricted to trials in which the animal broke fixation before the stimulus had fully extended. This condition included 7 ***S+*** trials and 10 ***S-*** trials and showed no significant difference between ***S+*** and ***S-*** response latencies ($p > 0.1$, 2-sided K-S test).

$\sim$150 ms window after an animal left the nose poke during which the stimulus was not fully retracted. From video observations, two of the five animals who showed single vibrissa discrimination ability habitually turned to probe the stimuli with their snouts after contacting it with their vibrissae. It was not clear whether the head movement was executed after judgment of the stimulus location or if it was used to aid localization. As we could not rule out the latter explanation, we considered these two cases ambiguous (Figure IV.3), half-shaded circles.

Our last control tested the remaining three animals for the use of auditory and vibrational cues. Stimuli were delivered by air-actuated pistons, damped to reduce vibrations, and a white noise audio mask was played in the chamber to interfere with any sound differences in ***S+*** and ***S-*** stimulus delivery. To verify that residual cues did not contribute to discrimination, each animal was tested in a session where the stimulus apparatus functioned as usual but the stimulus pins were absent. A resulting degradation in performance (e.g., Figure IV.5C and the orange line in Figure IV.4D), indicated that tactile contact with the vibrissa was required to perform the task. None of the three tested animals showed significant discrimination under these conditions.

In several sessions, we were able to perform a further control for vibration cues by considering trials in which the animal broke fixation less than 250 ms after the start of a trial. In these cases, the stimulus was retracted before it fully entered the vibrissa field, leaving the vibrissae little time to encounter the stimulus. For sessions in which we had sufficient numbers of these "jump-the-gun" trials, we confirmed that behavioral performance was degraded when the analysis was restricted to only these trials (e.g., Figure IV.5D). Using this measure, we confirmed that discrimination performance was at or near chance for trials in which the animal had decreased opportunity for vibrissa contact.

IV.B.4 Whisking Strategies

As a means to understand the perception-forming interval preceding the motor response, we obtained high-speed infrared video recordings of vibrissa motion for two of the three animals who passed all of the controls (Rat #9, Rat #20). The tracked vibrissae positions from these recordings demonstrate a typical pattern of slowly drifting vibrissa position until roughly 100 ms into the trial, followed by larger amplitude, but often non-sinusoidal, vibrissa motion on a changing baseline (e.g., Figures IV.6C and IV.6F). When we considered vibrissa motion in the interval from 0 to 250 ms after the start of a trial, we did not find any gross differences between ***S+*** and ***S-*** trials that were repeatable across sessions or animals.

Constraints on sensorimotor algorithms can be obtained from patterns in the vibrissa motion. An animal could adopt a purely motor strategy by repeatedly positioning its vibrissa in the expected location of one of the stimuli and then simply detecting whether or not contact occurs. To rule out this approach, we examined the distribution of all vibrissa positions (both ***S+*** and ***S-***) at the beginning of each trial to look for a bias toward either of the two potential stimulus locations. The distribution of positions in the first 250 ms, an interval which included few stimulus contacts, was in all cases centered between the two stimuli, indicating that vibrissa positions spanned both potential locations, rather than selecting only one (Figure IV.6G).

Figure IV.6 **Patterns of vibrissa motion during discrimination.** The data in panels (A) to (F) are from the session analyzed in Figure IV.4, with the ***S+*** stimulus (rostral for Rat #20) at +15° and the ***S-*** stimulus at 0°. The scale bar in the photographs is equal to 4 mm. **(A)** Projection of frames from a single ***S+*** trial. This image shows the range of vibrissa motion in the interval from -0.5 to +1.5 sec relative to the start of a trial. The neighborhood of the ***S+*** stimulus is indicated by a green box and the ***S-*** stimulus region is in red. The dark line in the green box is due to stimulus motion; compare to the green boxes in (B) and (E) which show fully extended and retracted positions, respectively. Stimulus displacement appears smaller than the actual 2" travel because the motion was nearly normal to the focal plane (see Figures IV.2A–C). **(B)** Single frame in which the vibrissa contacted the ***S+*** stimulus, taken from the trial in (A). The blue rectangle illustrates the region in which vibrissa position was estimated for (C). **(C)** Vibrissa position as a function of time. The green and red bands correspond to the vertical extent of the similarly colored boxes in (A). The gray lines give position traces from 58 ***S+*** trials, and the black line highlights the trial shown in (A). The presence of the stimuli is not indicated here, but both stimuli started their descent at ∼30 ms and reached full extension at ∼250 ms. The stimuli were fully withdrawn within 150 ms of the loss of nose poke fixation; this occurred at 315 ms (median value) for ***S+*** trials and 530 ms (median value) for ***S-*** trials. The green arrow marks the ***S+*** contact in (B). Breaks in the lines are due to tracking errors. **(D–E)** Video images from an ***S-*** trial, analogous to (A) and (B). **(F)** Vibrissa position traces for 56 ***S-*** trials, analogous to (C). The red arrow marks the ***S-*** contact in (E). **(G)** Summary of all tracked vibrissa positions from 0 to 0.25 sec after the start of each trial, including both ***S+*** and ***S-*** trials. The green and red bands correspond to the vertical extent of the similarly colored regions in (A) and (C) and demonstrate that the vibrissa scanned both stimulus positions. The dark line is based on the session analyzed in (A) through (F), and the light blue line shows data from another session by the same animal (Rat #20). The lavender line is from a session performed by Rat #9 (right C2 vibrissa); this line was scaled to align with the ***S+*** and ***S-*** bands drawn for Rat #20. **(H)** Vibrissa contact event durations. Bold lines show the distribution of contact durations from (C) and (F). The thin lines are taken from five more sessions by Rat #20 and four by Rat #9. The traces vary in the width of the early peak and the fraction of sustained contacts (= 300 ms), but none shows marked differences between ***S+*** and ***S-*** distributions. ***S+*** contacts are in green and ***S-*** contacts are in red.

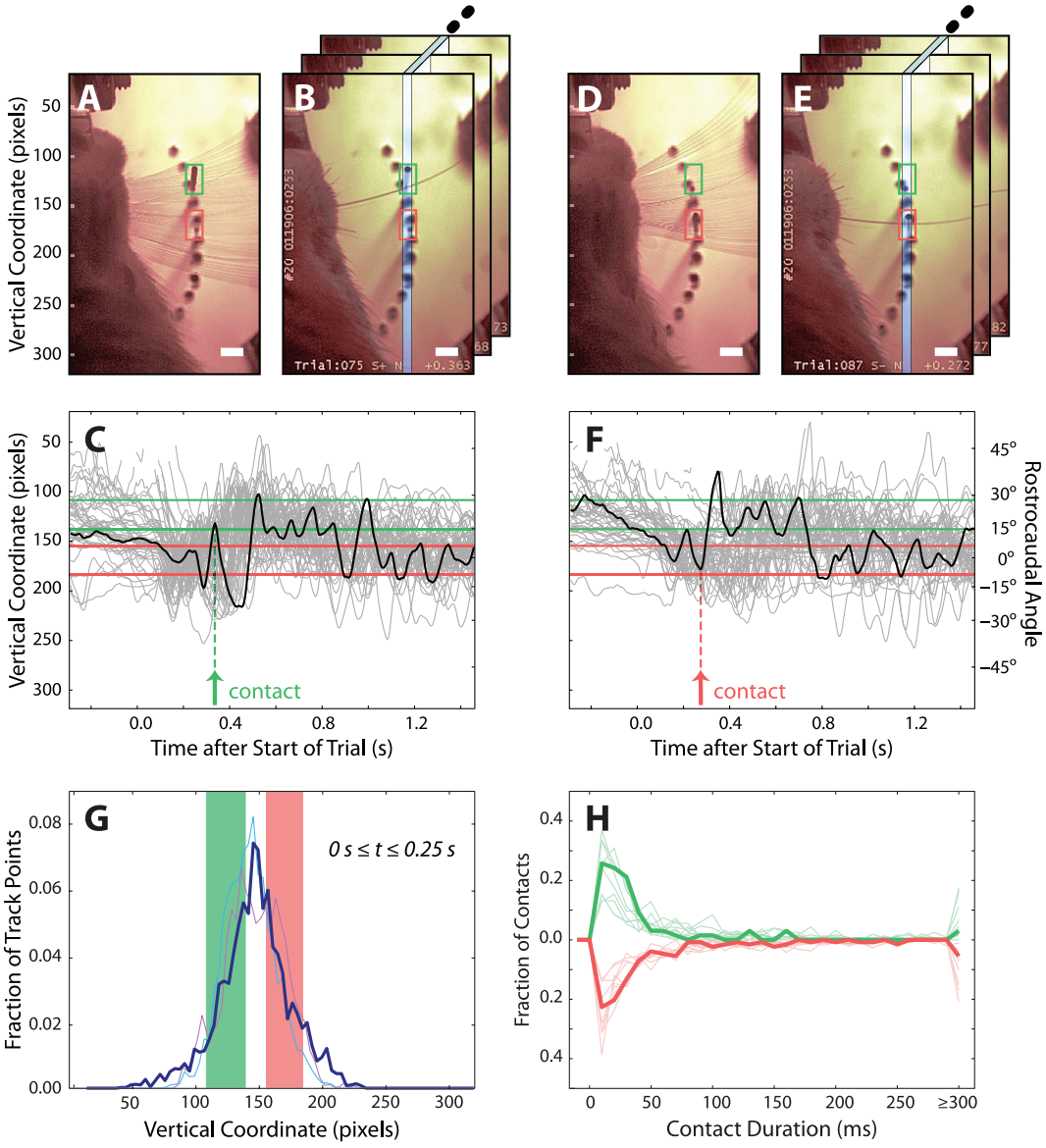

Figure IV.6 (see facing page)

Another class of algorithms, discussed in Chapter II, that does not require integration of positional and contact information depends on the duration of vibrissa contact (Derdikman et al., 2006b; Szwed et al., 2003). For periodic vibrissa motion, the time between contact onset and offset can be transformed into a surrogate for object position. Such a scheme is more difficult to implement with the irregular motion (e.g., Figures IV.6C–F), but might still be accomplished if the response of the motor circuitry depends on absolute vibrissa angle. We thus asked if the profile of contact event durations was different for ***S+*** and ***S-*** trials. These events were predominantly short (< 50 ms), although extended contacts of greater than 300 ms occasionally occurred (Figure IV.6H). In all cases, the variability of the contact durations was large compared to the separation between the peaks of the distributions for the ***S+*** and ***S-*** conditions. In light of these data, we consider an algorithm based on the duration of contact unlikely to account for the behavioral performance of these animals.

IV.C Discussion

We have demonstrated that rats with a single vibrissa can respond to differences in the position of external objects that differ only in angle along the direction of vibrissa motion. A rat with a full array of vibrissa could in principle perform this task by limiting vibrissa motion to non-overlapping fields and using the vibrissa columns, or arcs, as a spatial sensory array to test multiple locations in parallel (Figure IV.1A). The ability of animals to identify spatial angle when prevented from using this approach argues that this sensorimotor system is able to determine the position of an object contact while serially scanning a single sensor. In characterizing this scanning process, we observed that vibrissa motion spanned both stimulus locations before contact (Figure IV.6G) and then remained in contact with both ***S+*** and ***S-*** stimuli for a similar duration (Figure IV.6H).

The time scale for the tactile search can be estimated from the measured

behavioral responses. Animals could initiate a motor response within ∼250 ms after the start of a trial (Figures IV.4B–C). In this short interval, we typically observed delays on the order of ∼100 ms from the start of a trial before the vibrissa appeared to start a large amplitude scanning motion (Figures IV.6C–F). Taken together, these two intervals imply that the entire sensorimotor process of motor scanning, object detection and spatial categorization can be completed in ∼150 ms. As the typical frequency of exploratory whisking is in the range of 7 to 15 Hz (Berg and Kleinfeld, 2003), this suggests that no more than one to two whisk cycles were sufficient to judge position. Although the animals in our study often did not show the highly sinusoidal vibrissa motion found in other studies (Carvell et al., 1991; Berg and Kleinfeld, 2003), the observed motion is consistent with these frequencies (Figures IV.6C–F).

IV.C.1 Neural Algorithms

Earlier studies have suggested the calculation of dorsoventral angle from the identity of the contacting row (Brecht et al., 1997; Derdikman et al., 2006b) and demonstrated discrimination of distance from contact information from multiple vibrissae, even in the absence of active whisking (Krupa et al., 2001). We focused here on the decoding of angle along the axis of vibrissa motion because of the complication arising due to that motion; the environmental meaning of exteroceptive tactile signals changes as an animal moves its vibrissae. Given that this computation can be accomplished using the information associated with a single moving sensor, we consider what algorithms might be used to transform a contact signal into a spatial position.

A purely motor strategy was possible because of the fixed stimulus locations in our task design. Since only two positions were possible, an animal might learn to focus its now sparse sensory apparatus on one of these two positions and use the presence or absence of a contact event to detect the ***S+*** (or equivalently,

the ***S-***) condition without having to combine sensory and motor information. This is a single vibrissa approximation of a labeled-line strategy (Figure IV.1A), although it requires motor control sufficient to hold a lone sensor near an expected target. This approach was ruled out by the motion patterns of the vibrissa; in at least the two animals for which we performed vibrissa tracking, this motion was not restricted to the region of a single stimulus (Figure IV.6G). At the opposite extreme, the wealth of sensory information available from the vibrissa follicle suggests two purely sensory strategies that might arise from differences in the nature of contact as a function of position. The existence of separate on- and off-contact touch signals (Szwed et al., 2003) suggests that the nervous system might determine the duration of a contact and convert this to a spatial position, if different positions result in characteristic contact durations. This temporal delay scheme is contraindicated by the similarity of the measured contact durations (Figure IV.6H). As an alternative, the recent work on resonance vibrations (Moore and Andermann, 2005) in the vibrissae yields the possibility that animals might sense differences in the mechanical interactions between a vibrissa and stimuli at different locations. Although we cannot rule this out, as we did not sample vibrissa motion in the high frequency range at which mechanical resonances occur, the measured large variability in vibrissa motion patterns (Figures IV.6C–F) makes it unlikely that the interaction of the vibrissa with the stimulus was highly reproducible.

The most parsimonious remaining explanation for the computation needed to derive spatial position from a contact event is the integration of touch with kinesthetic information about the location of the vibrissa at the time of contact. Although there is no evidence of proprioceptive muscle spindles in the mystacial pad (Rice et al., 1994), physiological studies have shown that a reafferent motor signal from the pad is present at levels from the trigeminal ganglion (Szwed et al., 2003; Zucker and Welker, 1969) to thalamic nuclei (Yu et al., 2006) to

primary somatosensory cortex (Fee et al., 1997; Curtis and Kleinfeld, 2005). The behavioral evidence described in this work argues that information of this nature can be used behaviorally as a reference against which to interpret sensory contact, informing spatial perception of objects near the head.

Previous theoretical studies, such as the model discussed in Chapter III, have taken advantage of the rhythmic nature of exploratory whisking to suggest neuronal circuits that might compute spatial location given periodic spike trains representing both contact and vibrissa motion (see also Ahissar (1998)). The mathematical formulation of this class of algorithm, however, requires averaging over multiple rhythmic whisk cycles. In the current work, the ability of animals to form a spatial percept from oscillatory but irregular vibrissa motion, and the evidence that this percept can be formed in one to two whisk cycles, argues against these proposed mechanisms. A more direct circuit that performs the same computation would compare spiking in contact-sensitive cells and position-sensitive cells of varying preferred position. Ongoing physiological studies characterizing these neuronal interactions suggest that this comparison can in fact integrate tactile and haptic streams (Curtis and Kleinfeld, 2005). Finally, while it was not our goal here to establish the limits of spatial acuity in the system, a last constraint on any proposed neuronal implementation of a spatial decoding algorithm should predict sufficient resolution to distinguish contacts separated by 15° or less.

IV.C.2 The Vibrissa System and Sensorimotor Integration

Our behavioral task was designed to isolate a sensory process that is ordinarily used in concert with other behaviors. Earlier studies involving spatial behaviors support the notion that the vibrissae serve as binary detectors in freely exploring animals (Hutson and Masterton, 1986), and this may be the ethologically more typical usage when an animal can orient its head following contact. Indeed, upon detection of the salient and asymmetric stimulus used in this study,

some animals in our study reflexively oriented to explore the stimulus further, perhaps bringing their microvibrissae to bear. Although we could not determine whether those animals had judged stimulus position before this movement, we note that refined rostrocaudal information from the vibrissae is necessary if a rat is to orient rapidly on contact without further search. While the current study does not attempt to characterize the role of angular perception during natural activity, the vibrissae are involved in activities with complex spatial demands, such as navigation (Vincent, 1912; Brecht et al., 1997), aggression (Thor and Ghiselli, 1975) and swimming (Griffiths, 1960) (for a general review of older literature, see Gustafson and Felbain-Keramidas (1977)). This ubiquitous role suggests that these sensorimotor organs contribute a richer picture of the tactile world than binary detection alone would allow. When taken with the recent work on the role of the vibrissae in the transduction of fine texture (Andermann et al., 2004; Hipp et al., 2006; Arabzadeh et al., 2005; Moore and Andermann, 2005), the proportionally large neural territory given to vibrissae-related processing emerges as the locus of integration for multiple modalities.

A practical advantage to the study of integration processes in the vibrissa system lies in the large body of work on the plasticity, anatomy and sensory response properties (e.g., Feldman and Brecht, 2005; Kleinfeld et al., 1999; Petersen, 2003) related to the vibrissa primary somatosensory, or barrel, cortex. An array of recent studies take advantage of this growing body of literature and use the vibrissa system to develop modern experimental methodologies (e.g., Derdikman et al., 2003; Nishimura et al., 2006; Margrie et al., 2003; Brecht et al., 2004). In recognition of the requirements of these techniques, our choice of a go/no-go paradigm, rather than a two-alternative forced choice design (e.g., Shuler et al., 2002), was in part motivated by the hope of eventually measuring behavior in animals head-fixed for imaging or intracellular studies (e.g., Waters and Helmchen, 2004; Brecht et al., 2004; Holtmaat et al., 2005). Far from simply

being a test bed for these techniques, however, the system served by the barrel cortex provides an example of cortical computation that combines the simplicity of discreteness and a low number of degrees of freedom with the same type of haptic computations that must be performed by our own tactile organs. The present work demonstrates that rats can use this popular model system to integrate feedforward sensory events and motor feedback to inform their model of the external world. The elucidation of the circuitry that performs this computation will bring us a step closer to understanding how sensorimotor loops derive the perception of space from the sensation of touch.

IV.D Methods

Our initial cohort of behavioral subjects consisted of 24 female Long-Evans rats, ranging from 100 to 200 g at the start of training. We describe below the training apparatus and behavioral paradigm used to obtain measurements of spatial discrimination. All procedures involving animals conformed to NIH guidelines and were approved by the IACUC at UC San Diego.

IV.D.1 Training Apparatus

Animals were trained and tested in a custom arena (Figure IV.2A). The arena was contained in an 760 mm x 500 mm x 420 mm enclosure (not shown in Figure IV.2) made of 1/4" acrylic, painted black, and padded with skinned polyether foam (1", NRC 0.8, McMaster-Carr, 5692T49) to dampen external sound and light. The enclosure contained a speaker to deliver sound cues and a custom auditory white-noise mask, a SecuraCam (Swann) infrared camera (942 nm illumination) for experimenter monitoring and a low-flow gas line to ensure breathable air. The area available to the animal consisted of an acrylic vestibule, 200 mm on a side, and a 200 mm long x 57 mm ID tunnel, both placed on an acrylic shelf elevated 60 mm above the floor of the external enclosure. Motion through the tun-

nel was monitored with an 880 nm infrared photodiode (Photonic-Devices, PDI-E802)/phototransistor (DigiKey, QSE156-ND) pair to signal the presence of a rat. The end of the tunnel was fitted with a U-shaped restraining bar that allowed free movement of the head and paws, while preventing escape (Figure IV.2B).

Behavioral output was measured through a water-sealed lever of ∼25 g activating force (Cherry E73-series switch, DigiKey, CH566-ND), placed at the end of the tunnel with a plastic crossbar glued to the end (Figure IV.2B). Animals typically rested on the lever and activated the lever by briefly raising their paws; early in training, a small spring was often placed to aid this motion. Fluid rewards were delivered to a sip cup in a stainless steel dispenser, placed ∼60 mm from the end of the tunnel and designed with inflow and outflow ports to control the timing of fluid delivery. Fluid was delivered in 50 μL aliquots through a miniature DC solenoid valve (Parker-Hannifin, 004-0008-900) with a custom timer circuit (UCSD Physics Electronics Shop) to gate flow from a fluid reservoir and removed by a similarly controlled solenoid gating a vacuum line. A bright yellow LED (587 nm, 1900 mcd, Radio Shack 276-351) was wired in parallel with the reward timer to indicate reward availability and prevent visual dark-adaptation to any residual light in the chamber (e.g., from the camera illumination lamp; see below). This entire fluid delivery system was flushed with enzymatic detergent (MaxiZyme, Henry Schein, #10-7410) after each training session to prevent build-up of organic solids. This was particularly necessary early in the training when chocolate milk was sometimes used as a liquid reward.

Rat head position was fixed by a 13 mm OD brass nose poke cone, painted black to minimize reflections, with an analog reflective IR sensor (940 nm, DigiKey, QRD1114-ND) whose output was taken to a comparator (LM319N, DigiKey, 497-1577-5-ND). The comparator was wired as a Schmitt trigger and referenced to a potentiometer adjusted to control sensitivity. The nose poke was placed close to the water dispenser and fixed relative to the stimulus with an alu-

minum bracket (not shown in Figure IV.2). This system allowed some positional ambiguity, as an animal could roll its snout freely while maintaining fixation. However, translational position was reproducibly constrained (e.g., Figure IV.6).

Digital inputs taken from the lever, tunnel sensor and nose poke sensor were sampled at 16 Hz by a multifunction digital I/O board (National Instruments, AT-MIO-16DE) in a PC running custom LabVIEW software (National Instruments). The software logged the inputs, implemented training logic and supplied digital control signals for the reward, vacuum and stimulus valves.

IV.D.2 Tactile Stimuli

The stimuli for the spatial task were 0.86 mm steel rods translated into and out of the vibrissa field by a custom air-piston and guide assembly. Two paired guide blocks (1/2" Lexan) were aligned on Teflon-coated shafts (6" L x 0.248" D, McMaster-Carr, 7875K11). The floor of the bottom guide rested on plastic legs ∼110 mm above the floor of the tunnel (these legs, the top-guide and the alignment shafts are not shown in Figure IV.2A for clarity, but see Figure B.1). A carriage block (1/2" Lexan) with a captured linear bearing was free to slide on the two rostral shafts and a mirror-image block traveled along the two caudal shafts. Two stainless steel air cylinders (spring-return, 2" travel, McMaster-Carr, 6498K27) were fixed to the top block, each with its piston bolted to a carriage block. Air at 20 PSI was delivered to the pistons through a pair of 3-way miniature solenoid valves (Parker-Hannifin, 004-0008-900) which were placed outside of the enclosure to minimize noise. These solenoid valves were connected to 12V DC power supplies via power transistors (Mouser, 610-2N6387) to permit digital control. Inflowing air was passed through a restriction valve, common to both stimuli, which was adjusted to slow piston descent and minimize vibration during stimulus delivery. Outflowing air was similarly restricted and silicone bumpers were placed between the carriage and guide blocks to damp vibration from the sudden deceleration at

the end of travel. The resulting stimulus descent and ascent took ∼250 ms and ∼150 ms, respectively, for the full 2" travel, including a 30 ms delay in both cases for computer processing, solenoid switching and the build-up of a sufficient air pressure change. The white-noise audio mask (see above) was played continuously in the box to confound any auditory differences between the stimuli.

Both carriage blocks and the bottom guide block were drilled with matching hole patterns on a circle of 25 mm diameter with either 15° or 7.5° spacing. The nose poke was bolted to the bottom guide block and positioned such that a line connecting the caudal edges of both mystacial pads would approximately coincide with the center of this circle. Eighteen-gauge hypodermic tubing was glued to the back of 90 mm lengths of the 0.86 mm diameter stimulus rods as a backstop. The backstops rested above the stimulus carriage blocks (Figure IV.2A) and allowed the stimuli to travel with the carriage blocks, extending from 10 mm to 61 mm below the floor of the bottom guide block. This arrangement allowed the angular location of the stimuli to be rapidly adjusted for each animal and was intrinsically safer for the animals, as the stimuli dropped due to gravity rather than direct piston drive. Our typical configuration fixed potential locations for the stimuli at $3.75° + n\ 7.5°$ (where n is an integer between -5 and 5), measured relative to a line through the center of the circle described above and perpendicular to the animal's midline. In all cases, one stimulus was placed at a positive angle and another placed at a negative angle; the angular difference and offset were adjusted for each animal such that both rostral and caudal stimuli fell within the range of vibrissa motion (e.g., Figure IV.6A–B, D–E).

IV.D.3 Video Imaging

High-speed videography was used to characterize the movement of the vibrissae once discrimination was established. A IEEE-1394 monochrome CMOS camera (Basler Vision Technologies, 602f) with IR sensitivity was mounted under

the elevated shelf in the training enclosure, and focused on the plane of the nose poke using a TV lens (f/0.95, 17 mm, JML, 71932) and a 45° mirror under the stimuli (Figure IV.2A). Illumination was provided by an IR lamp (850 nm, The LED Light) filtered at 850nm to reduce leakage into the rat visible spectrum. Further, as noted above, a high-intensity LED was switched on during reward periods to interfere with potential retinal dark adaptation. The camera was interfaced to a PC running custom LabVIEW software and typically acquired 360 x 300 pixel images at 200 Hz. Images were read into a circular buffer and 600 images were saved to disk 2.5 sec after the start of each behavioral trial, with the result that 0.5 sec of pre-trial video was included in each video sequence. To reduce blurring of the vibrissae, the IR lamp was modified to double its optical power and then strobed to give an effective 1.2 ms camera exposure.

Video images were analyzed in Matlab (The Mathworks). Gross head motion was extracted from the videos to control for cases in which animals were able to break fixation and reach the stimulus before it could be fully withdrawn. Vibrissa motion was estimated from linescan data extracted from an image column over multiple time points (Figure IV.6B–E). The median column over time was subtracted from each column to remove stationary objects, and custom segmentation and tracking algorithms (Mehta, S.B., unpublished) were applied to estimate vibrissa position at each time point. This linescan analysis was performed on regions 10 pixels to the left and right of the stimulus region, to avoid contamination from the motion of the stimulus itself, and the position in the stimuli column was interpolated from a linear fit through these left and right position estimates. Over these short regions, vibrissae were well described by a linear fit; quadratic fits from three-point estimates showed negligible contributions from the second-order coefficient. For simplicity, line scans were used throughout rather than arcs, and the position of the vibrissa tracks along the vibrissa length was thus not constant (Figures IV.6C–F). In these tracks, the distance of the linescan column from

the mystacial pad at 30° is ∼15% greater than the distance at 0°. However, the placement of the stimuli was such that there was no systematic difference in the length at which a vibrissa contacted the rostral and caudal stimuli.

To identify potential contact events, the motion of the stimulus was estimated from the linescan images. Epochs were identified in which the vibrissa position track overlapped the stimulus position and showed a velocity of no more than 4 pixels per frame (Figure IV.6H). We used this approximation because we lacked a bona fide detector for stimulus contact and because image overlap of the vibrissa with the stimulus did not necessarily correspond to physical contact in three-dimensions. However, a representative sample of these contact events was verified by manual inspection of the corresponding video frames.

IV.D.4 Operant Shaping

The discrimination behavior was shaped in three stages through classical operant training techniques (Reynolds, 1968). A small number of parameters were varied in the behavioral program to increment task difficulty, and a large part of training occurred without further experimenter intervention. The parameters used in Figure IV.7 and in the description below are: T: trial length, D: delay between trials, N: duration of nose fixation, P: delay until audio prompt, and L: number of lever press responses required to elicit reward. P and L were used in rewarded stimulus trials only.

The first stage defined the lever response and brought it under experimental control (Figure IV.7A). In this stage, animals were required to be in the tunnel without emitting lever press responses for an interval of D sec to elicit an audio prompt (300 ms at 2 kHz) that indicated the start of a trial. The first lever press response within T sec following the prompt was rewarded with 50 μL of water, signaled by an LED indicator as described above. At the end of T sec, the trial ended and any water still in the dispenser was removed by vacuum. This

schedule encouraged responses soon after the audio prompt, as responses that were late but still within T sec after the prompt afforded less time to drink and responses at greater than T sec delayed the next prompt presentation. The trial length T was set to 6 sec and the delay parameter D was increased from 0.25 sec to 4 sec. Human intervention was often necessary in the first several sessions to model the lever press response, but was minimal as D increased.

Figure IV.7 **Behavioral logic for operant training and discrimination testing.** All diagrams use 0.5 second intervals for clarity; the actual sampling rate was 16 Hz. **(A)** Lever press response training. Animals who waited D sec without emitting a lever press would elicit an audio prompt that signaled the start of a trial. The first lever press response in the following $T = 6$ sec was rewarded with a drop of water. At the end of the trial, any remaining water was withdrawn. D was increased from 0.25 to 4 sec. **(B)** Nose poke training. D was first increased from 4 to 60 sec to decrease the frequency of trial initiated by waiting. Trials could alternatively be initiated if an animal placed its nose in the nose poke for N sec. As this behavior was established, N was increased from 0.063 to 1.5 sec. **(C)** Stimulus training. All trials in this stage were initiated by a 1.5-second nose poke. Each trial was randomly assigned as either ***S+*** or ***S-*** , and the start of the trial was signaled by the descent of the corresponding stimulus pin. The pin remained in the vibrissa field until nose fixation was broken or until the trial ended. In ***S+*** trials, the first lever press response after the start of the trial resulted in a reward. If no response occurred within P sec, an audio prompt sounded. P was increased from 0.125 to 6 sec. Lever presses were ignored in ***S-*** trials. **(D)** Stimulus discrimination testing. The audio prompt was eliminated from ***S+*** trials. The number of lever press responses, L, required to obtain a reward in ***S+*** trials was increased until a difference between ***S+*** and ***S-*** responses was apparent. This value was typically $L = 5$ or 6; the example here illustrates $L = 2$. The structure of ***S-*** trials was unchanged.

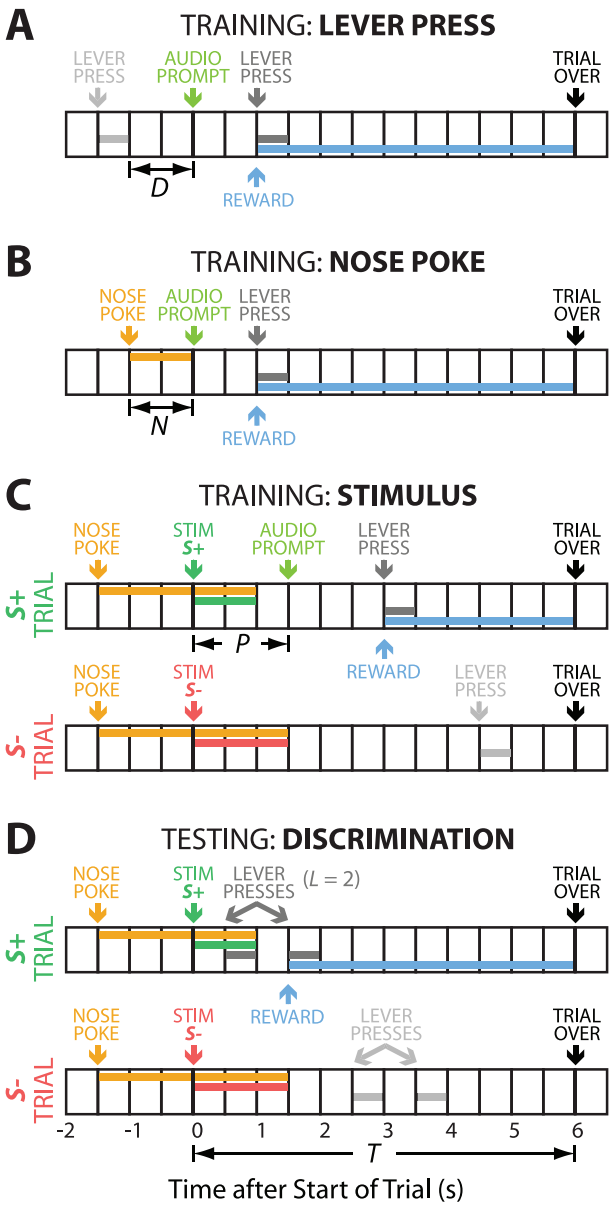

Figure IV.7 (see facing page)

The second stage shaped the nose fixation behavior (Figure IV.7B). Here, the D parameter from stage 1 was increased from 4 sec to 60 sec, so that spontaneous emission of the audio prompt was less frequent. As before, the first lever press response within T (= 6) sec of the prompt was rewarded. A nose poke response of duration N sec short-circuited this delay and immediately elicited the audio prompt that indicated the start of a trial. The nose fixation duration N was increased from 0.063 sec to 1.5 sec in increments of 0.063 sec. Acquisition of the basic nose poke behavior was assisted by increasing the sensitivity of the nose cone sensor and baiting the nose cone with water or chocolate milk; after this acquisition, little intervention was required if the fixation duration parameter N was increased.

The final training stage transferred the reward context from the audio prompt to one of the two stimuli in a go/no-go task (Figure IV.7D). Each animal was randomly assigned a relative position, more rostral or more caudal, to permanently be the rewarded condition for that animal. For each session, the two tactile stimulus that occupied this relative angular position was designated ***S+*** , as opposed to the ***S-*** stimulus at the second position. In this stage, trials could only be initiated by nose fixation. After a nose poke of N (= 1.5) sec, either the ***S+*** or the ***S-*** stimulus, chosen at random with equal probability, was delivered to indicate the start of a trial. For ***S-*** trials, lever press responses in the T (= 6) sec following stimulus delivery were unrewarded, and the audio prompt used in earlier stages was never presented. For ***S+*** trials, the first lever press in the T (= 6) sec after the start of the trial was rewarded, as before. In these trials only, if no lever press response had occurred after within P sec after stimulus delivery, an audio prompt was presented to the animal. This prompt delay P was increased from 0.125 sec to T sec and as before, any unfinished reward was removed after the trial's end at T sec. Thus, responses to the audio prompt would receive diminishing amounts of time to drink, while responses that used the ***S+*** stimulus as a

predictor would not. In both ***S+*** and ***S-*** trials, the stimulus was removed from the vibrissa field if nose poke fixation was broken or the trial ended, whichever came first.

Acquisition of stimulus discrimination was indicated when the number of lever press responses in the first P sec of a trial differed significantly between ***S+*** and ***S-*** trials. (The first P sec were used because the animal had access to additional information, in the form of the cue, after P sec.) At this point, the audio prompt was eliminated and performance was measured. For several of the animals (see Results below), a final parameter was varied during this testing stage. The number of lever press responses L required to elicit a reward increased from 1 to 5 (Figure IV.7D) and the trial length T was increased to 8 sec to allow more time for the behavioral response. This manipulation increased the effort necessary to make a positive response in the go/no-go task.

IV.D.5 Fluid Restriction and Training Sessions

Animals began training at 150 to 200 g in batches of four littermates. They were initially acclimated to handling and to chocolate milk (Yoo-Hoo, Cadbury-Schweppes) from the fluid dispenser in the behavioral chamber over a period of 2–3 weeks. Animals were housed in pairs and maintained on a standard light/dark cycle, and both morning and evening training sessions were used. We did not observe any significant effect of time of day or estrous cycle periodicity on behavioral performance. Further, although chocolate milk was used early in training, fluid deprived animals appeared to perform equally well for water rewards, which were preferred for ease of delivery.

Upon reaching ∼230 g, animals entered a fluid restriction regimen in which water was removed from their home cage 16–23 hours before training to increase motivation. Animals were allowed *ad libitum* fluid access two days a week and weights were monitored daily. We used a variable restriction schedule for two

reasons. First, the total duration of the training ranged from 6–12 months, and the long-term health of the animals was a concern. Second, longer deprivation did not correlate strongly with an increased number of trials per session. In fact, extreme deprivation at times appeared to decrease discrimination accuracy (data not shown). Restriction duration was thus tuned separately for each animal.

Daily training sessions were initially 20–30 min in duration. The physical proximity of the tactile stimulus and response apparatus allowed animals to perform a large number of trials in this amount of time; 50 trials was typical in intermediate stages of training and 100 trials (of which approx. 50 were rewarded) was typical of well trained animals on the full discrimination task. This required animals motivated to perform at high rates and five of the initial cohort of 24 rats were removed early in training (after fewer than 27 sessions) because they performed significantly fewer trials than their littermates. A further five animals were removed at intermediate stages (after approx. 100 sessions) for performing small numbers of trials after the lever and nose poke were introduced. We do not consider these ten animals in the summary analysis shown in Figure IV.3, as they were never introduced to the stimulus.

For the remaining fourteen animals, the number of sessions required to acquire the lever press response and nose fixation of 1.5 sec ranged from 225 for our earliest animals to 61 for animals who started training later in the study. This large reduction in number of sessions occurred as the training procedures described above were established and the earlier numbers reflect our adjustments to these procedures rather than the intrinsic time needed to train these behaviors. Further, we chose relatively short session durations to facilitate the concurrent training of multiple animals as we developed the procedures described above, although in many cases, animals would still be performing trials at the end of a session, albeit at a decreasing pace. It is thus likely that the use of our eventual protocol with longer sessions to obtain more trials per animal per day would have

further decreased the training time necessary to achieve this level of behavioral performance.

The number of sessions required to learn the stimulus task was more variable, ranging from 17 to 75. This number did not show the same trend of decreasing over the course of the study and did not appear correlated with eventual performance as the vibrissae were trimmed.

IV.D.6 Vibrissa Trimming

Animals who successfully discriminated their assigned ***S+*** and ***S-*** stimuli in the absence of the audio prompt (Figure IV.7D) in multiple consecutive sessions were then trained with only a single vibrissae row intact. At least once per week, animals at this stage were lightly anesthetized on isoflurane and all vibrissae on the left side and all vibrissae on the right side except for the C row were trimmed. Animals continued training with a single row until they again demonstrated successful discrimination in multiple consecutive sessions, at which point their vibrissae were further trimmed to leave only a single vibrissa intact. This vibrissa was required to be sufficiently long to reach the stimuli and was thus typically chosen to be C1. Animals who performed successfully with a single intact vibrissa were recorded on video as described above and challenged with a series of controls (e.g., Figure IV.5).

Acknowledgement

The text of this chapter is based on a manuscript in preparation by S.B. Mehta (the dissertation author), D. Whitmer, R. Figueroa, B.A. Williams and D. Kleinfeld.

Chapter V

Spatiotemporal Patterns in S1 Cortex

V.A Introduction

The ability of rats to perform spatial localization with a single vibrissa suggests that animals obtain spatial information during active movements by relying on sensorimotor integration. This ability poses the following ethological question: What is the advantage of having multiple sensors in the rostrocaudal direction? A detector array typically provides an advantage in spatial coverage or resolution when compared to a single detector. In the case of the vibrissae, however, coverage and resolution appear to depend on active motion rather than a multiplicity of sensors. When this motion causes multiple vibrissae to contact the same stimulus (e.g., Figure V.1), it is unclear if these contacts provide additional information. Yet the anatomical regularity of the vibrissae grid suggests an evolutionarily conserved feature (Brecht et al., 1997), and several researchers have speculated as to the sensory function served by this array. The best developed of these proposals relate to detection of distance (Brecht et al., 1997) and texture (Neimark et al., 2003; Hartmann et al., 2003; Moore, 2004;

Andermann et al., 2004), although recent work argues that these parameters may also be encoded in the neural input from a single vibrissa (Krupa et al., 2001; Thajchayapong and Hartmann, 2004; Arabzadeh et al., 2005; Derdikman et al., 2006a; Hipp et al., 2006; Szwed et al., 2006). Thus, in contrast to the increasingly rich story of the information conveyed by a single vibrissa, a consistent behavioral model does not yet exist for the function of the full vibrissa sensory array.

Despite the lack of quantitative behavioral evidence, physiological interactions between cortical vibrissa representations are well documented (e.g., Moore et al., 1999; Petersen and Diamond, 2000; Derdikman et al., 2003; Wirth and Luscher, 2004; Ego-Stengel et al., 2005). The use of spatial imaging technologies such as multielectrode arrays and optical techniques increasingly allow the measurement of large scale spatiotemporal dynamics in the cortex, and the relative simplicity of the vibrissa system has made it an attractive target for the study of cortical function using these approaches. The correlation of these brain dynamics with perception will require recordings from behaving animals, both to obtain measures of animal performance and to place neural activity in the context attentional and plastic changes (e.g., Ganguly and Kleinfeld, 2004; Aguilar and Castro-Alamancos, 2005; Feldman and Brecht, 2005).

As a closing nod to the need for such experiments, this chapter briefly demonstrates a technique (based on Petersen and Diamond (2000) for recording spatiotemporal activity in rat primary somatosensory cortex, in the hope that this strategy will eventually be used in behaving animals. Although the data here were taken from anesthetized rats, these experiments illustrate cortical activity patterns that result from simple stimulation protocols and provide a template for awake experiments. Recent analogous work using optical techniques in anesthetized (Petersen et al., 2003) and awake animals (Ferezou et al., 2006) have demonstrated that these spatial activity patterns are modulated by both ongoing internal activity and attention. While the multielectrode array offers decreased

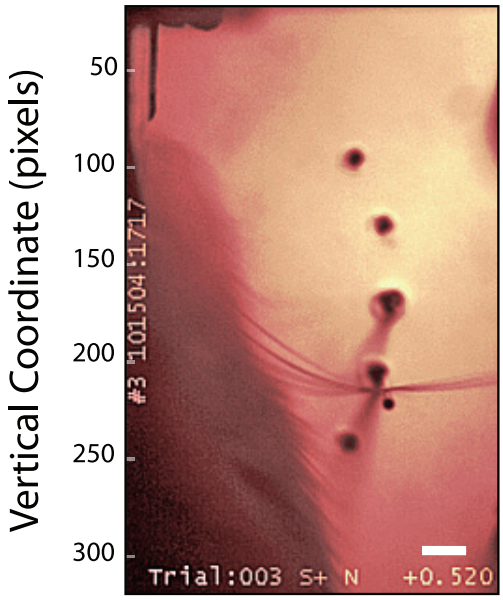

Figure V.1 **Contact with multiple vibrissae.** Multiple vibrissae contacting a stimulus in the behavioral task described in Chapter IV, for an animal with only its C row intact. Scale bar is 4 mm.

spatial resolution when compared to optical imaging, the potential for recording single neurons makes this a complementary approach.

V.B Activity from Simple Stimulation Patterns

Primary sensory cortices form extended topographic representations of an environmental feature space and are often comprised of modular units known as cortical columns (Horton and Adams, 2005). While the function of these columns is unclear in some systems, the approximately 400 μm columns (known as barrels) in the vibrissa S1 cortex form one of neuroanatomy's most recognizable signposts. To connect with previous results, a measurement of millimeter scale activity in the cortex should ideally be able to place the recorded activity in the context of these barrels. While this can be done to high precision using post-mortem immunohistological techniques, experiments with awake animals can take advantage of the ability to target external stimulation to the area being recorded (e.g., Petersen

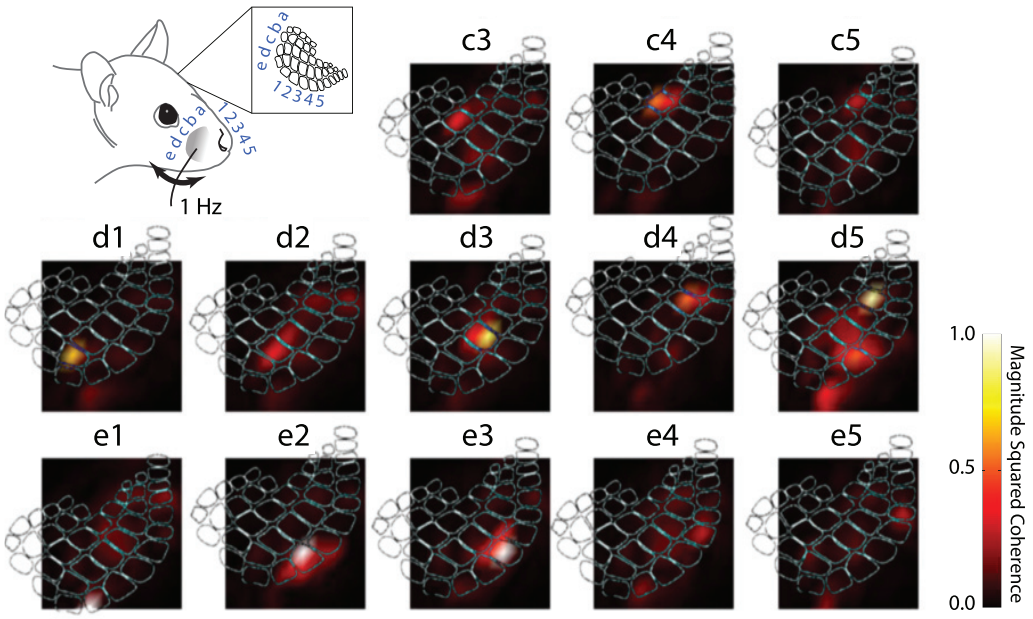

Figure V.2 **Topographic map from single vibrissa stimulation.** Responses to 1 Hz, single-vibrissa stimulation for each of thirteen vibrissae. The magnitude-squared coherence was calculated between the piezoelectric stimulus command signal and the multi-unit response on each electrode. This coherence has been interpolated here for ease of visualization. The overall orientation of the topographic vibrissa map was fit to the data from all thirteen vibrissae, and the translational position was then individually adjusted to the activity profile for each vibrissa in order to create the overlays shown here. The anatomy corresponding to these maps is given in the inset as a guide. Each black square is 3.6 mm on a side, representing data from the 10 $\times$ 10 electrode grid.

and Diamond, 2000; Curtis and Kleinfeld, 2005). To this end, a rough map of the location of an implanted multielectrode array was constructed from a series of single vibrissa stimulation trials (Figure V.2).

This topographic representation can also be used to interpret induced activity patterns in cortex. Sequential stimulation of the vibrissae causes a wave-like pattern of activity as regions corresponding to the stimulated vibrissae become active in order of stimulation (Figure V.3). Comparison of this passively driven wave to the activity generated when an whisking rat contacts a stationary post would clarify the relationship between active whisking and cross-vibrissa integration.

Figure V.3 **Cortical waves from sequential stimulation.** Responses to 8 Hz sequential stimulation of the full vibrissa field. The complex coherence was calculated between a reference signal at the stimulation frequency and the multi-unit response on each electrode. All electrodes with magnitude-squared coherence below 0.1 were removed from further consideration and colored gray. The phase values from the remaining electrodes were interpolated for ease of visualization and plotted here as temporal delays. As the precise timing of vibrissa contact was not available, the color bar gives the relative timing between electrodes; 0 ms here has no special meaning. An anatomical map for this animal, analogous to the maps in Figure V.2, is overlaid. **(A)** The stimulus passed through the vibrissa field from caudal to rostral, as indicated in the inset. **(B)** The stimulus passed through the vibrissa field from rostral to caudal, as indicated in the inset. Note the reversed pattern of delays when compared to (A).

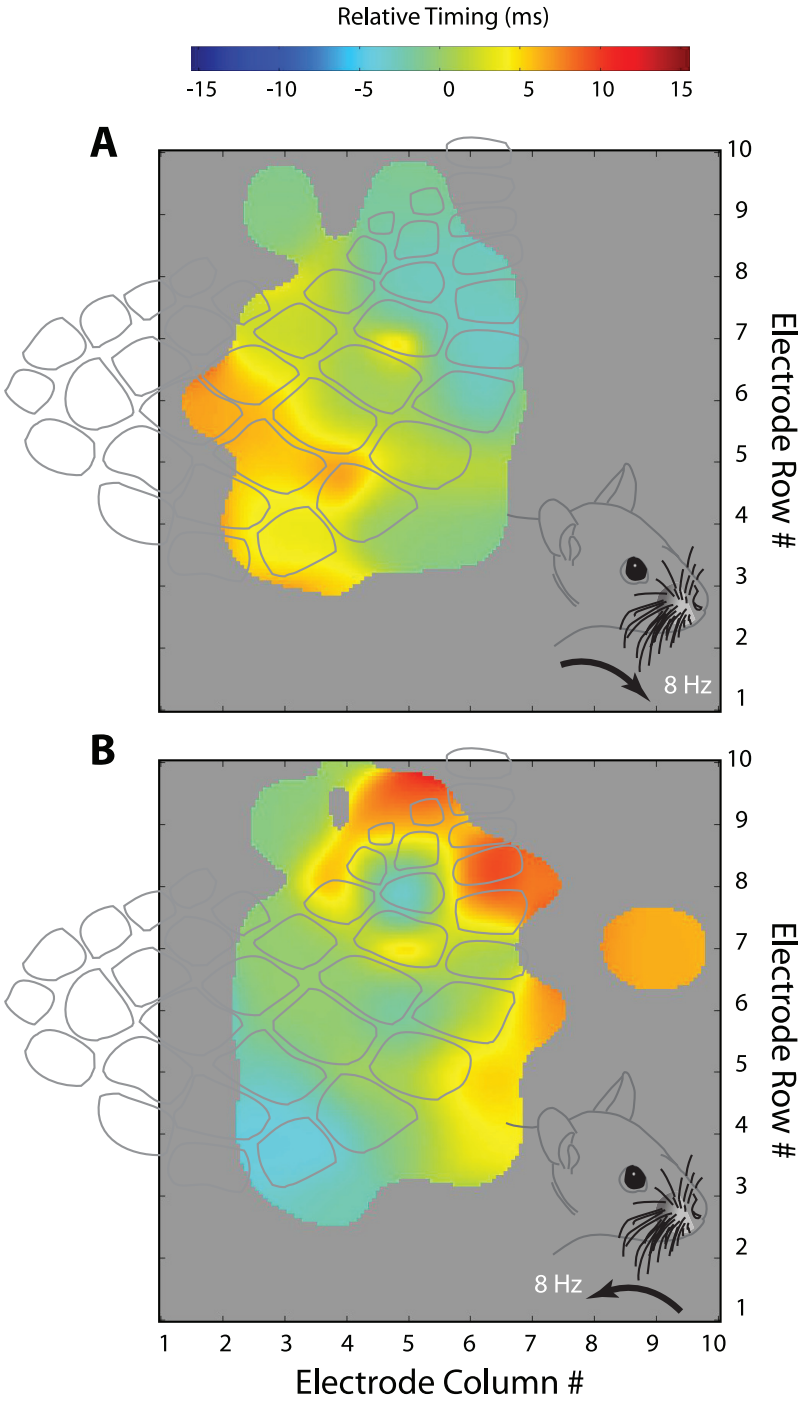

Figure V.3 (see facing page)

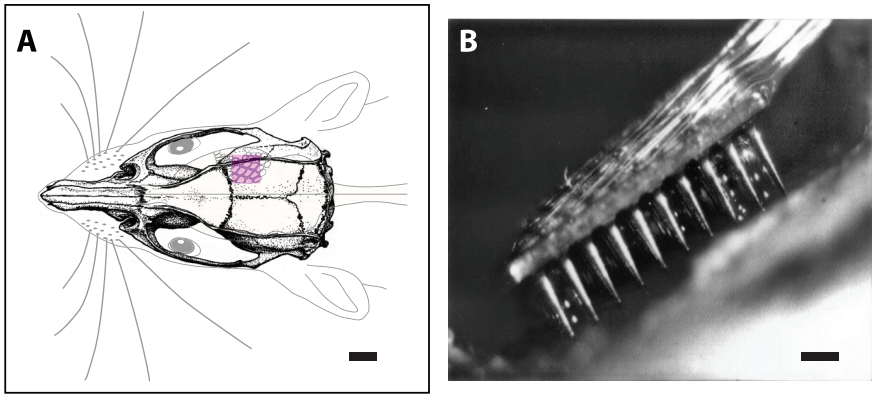

Figure V.4 **Multielectrode array implantation.** **(A)** Diagram showing the approximate target location of the craniotomy used for implantation of the multielectrode array, relative to anatomical markers. The magenta box shows the target region of the craniotomy with the estimated location of vibrissa S1 cortex visible underneath. The drawing of the skull was adapted from Paxinos and Watson (1986). Scale bar is 5 mm. **(B)** Photograph of the implanted array. The electrodes extend 1.5 mm from the base to the active tip; ∼750 μm are visible here before the electrodes enter the brain. The electrodes are laterally spaced by 400 μ on a 10 × 10 grid. Scale bar is 500 μm.

V.C Methods

The experimental subjects were female Long-Evans rats (Charles River, ME) of 250–300 g initial weight. Rats were anesthetized with urethane and maintained on humidified O_2 at 37℃. The cortex was surgically exposed with a craniotomy extending from 0.0 to 4.5 mm posterior to bregma and from 3.5 to 8.0 mm lateral to the midline (Figure V.4A). A custom headmount made from printed circuit board was cemented to the skull along the midline and secured with screws; this allowed the head to be held during acute experiments while simultaneously allowing access to the cortex and the vibrissae. All procedures conformed to NIH guidelines and were approved by the IACUC at UC San Diego.

Recordings were made with a multielectrode array (Cyberkinetics, Inc.; e.g., Figure V.4B) suitable for topographic characterization of the activity across S1 cortex (Rousche et al., 1999; Petersen and Diamond, 2000). The array consists

of a 10 × 10 grid of insulated silicon microelectrodes with Pt-Ir coated tips, spaced at 400 μm for a total cortical coverage of 3.6 mm × 3.6 mm. The array was aligned relative to cortex using a custom sterotactic holder in spherical coordinates (S.B. Mehta and D. Kleinfeld, unpublished design) and inserted into cortex using a commercial pneumatic insertion device (Cyberkinetics, Inc.). The depth of insertion was in the range 750 to 1000 μm and assumed to be cortical layer IV.

Voltage traces from all electrodes were filtered (0.3 Hz – 7.5 kHz), amplified and digitally sampled at 30 kHz, using a Cerebus module (Cyberkinetics, Inc.). Once digitized, the signals were acquired using a high-speed digital I/O board (PCI-6534, National Instruments) and further separated into a low-frequency, local field potential channel and a high-frequency channel for neuronal action potentials.

The cortical activity patterns shown here were derived from an analysis of multi-unit data from the high-frequency data channel, but similar results were obtained for field potential data (data not shown). As the ability to measure single units is the main potential advantage of this technology over current optical techniques (e.g., Ferezou et al., 2006), the action potential data was sorted into single units using an algorithm based on Fee et al. (1997)[1]. Several of the electrodes in these studies did show evidence of waveforms that appeared to be from single neurons (Figure V.5), but these results are not considered further in this chapter as they were not needed for the demonstration of large-scale activity patterns.

[1]This algorithm has been modified by D.N. Hill and S.B. Mehta. The modified algorithm has not been published, but has was used by other researchers, including Celikel et al.(2004) and K. Denning and P. Reinagel (manuscript in preparation). Versions of this software, written in Matlab, were used in Lev-Ram et al.(2002), Young et al.(2006) and in the Neuroinformatics course at the Woods Hole MBL from 2002–2005.

Figure V.5 **Isolating single neural units.** Evidence of waveforms corresponding to action potentials, or spikes, from single neurons using the multielectrode array. **(A)** Action potential waveforms. These waveforms were isolated from the raw individual electrode data streams by high-pass filtering at 250 Hz and applying a negative going threshold. This procedure was applied to a 30 min. recording of spontaneous activity in somatosensory cortex, and the resulting 4079 waveforms are shown in the left panel. The right panel shows the same data as a density histogram, where the voltages were histogrammed for each time sample. This allows better visualization of common waveforms when a outliers obscure a plot of the raw data. The right panel shows that two waveform shapes predominate in this set of spikes. **(B)** Spike waveforms for a 7×8 subset of the electrodes in the array. The row and column numbers correspond to the analogous numbers given in Figure V.3. The density histograms for the waveforms from each channel were computed as described above, and the image outlined in magenta corresponds to the right panel of (A). The channels showing cyan regions with a distinct bimodality are characteristic of recordings from single neurons. **(C)** When an electrode measures spikes from a single neuron contaminated with noise or background firing, "spike sorting" is required to identify units corresponding to the single neuron. The modified algorithm referenced in the text was used with the data from (A) to produce the sorted data shown here. Waveforms putatively derived from a single neuron are shown in blue, and background noise is shown in gray.

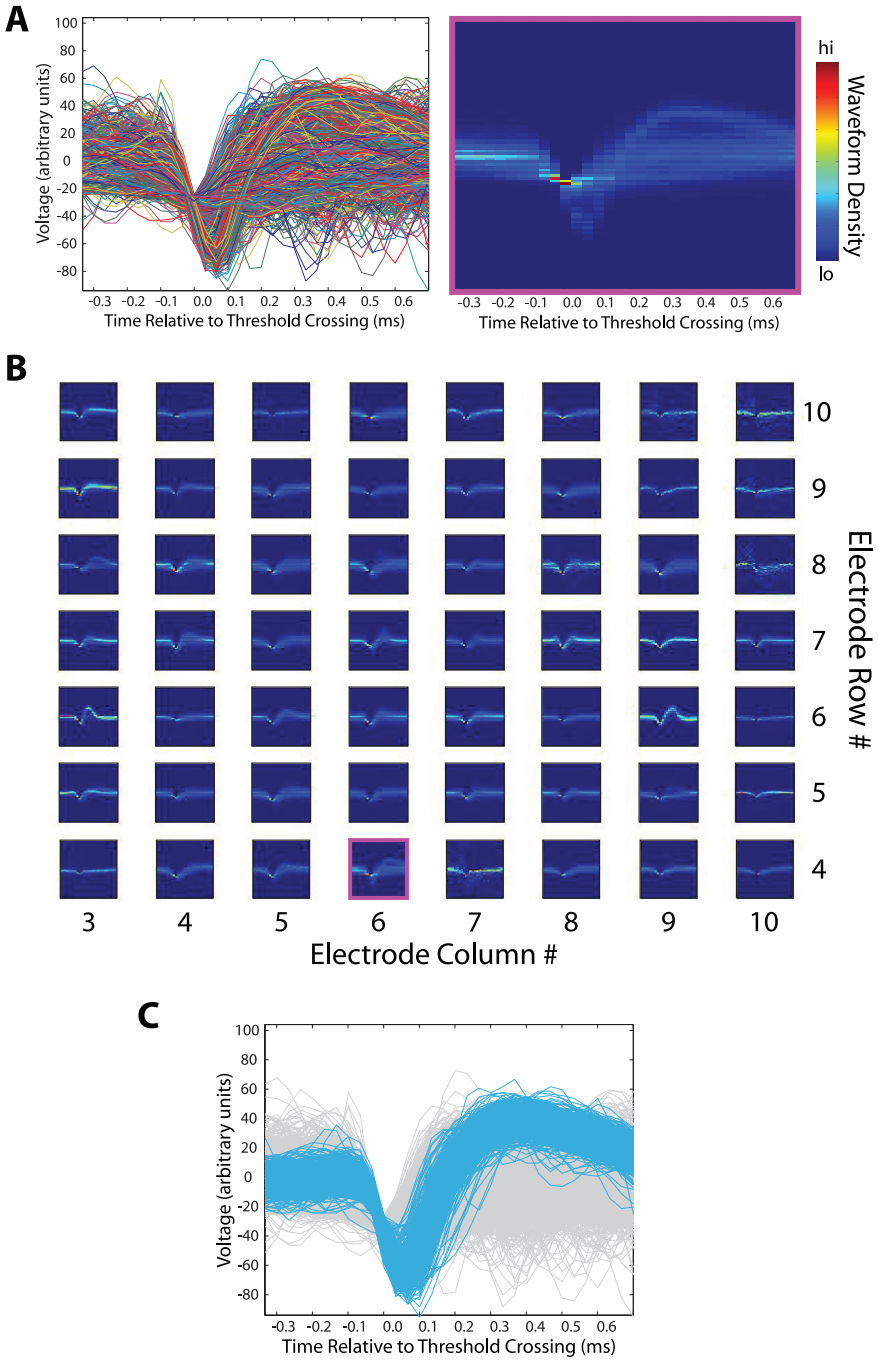

Figure V.5 (see facing page)

The analysis used for Figures V.2 and V.3 was performed on the raw multi-unit data, using a techinque designed to highlight spatiotemporal patterns which are well-localized in frequency. The approach is essentially that used in Prechtl et al. (1997) and Cacciatore et al. (1999). Briefly, the statistical estimation of linear phase predictability, known as coherence, as a function of frequency was used to measure the magnitude and phase of the coherent spiking response on each electrode at the stimulation frequency. The coherence (distinct from the "spatial coherence" described in Prechtl et al. (1997)) was robustly estimated using multi-taper techniques to minimize spectral leakage. The cortical response to single vibrissa stimulation (Figure V.2) was determined from the magnitude of the coherent response at the 1 Hz test frequency. The spatial patterns resulting from multiple vibrissa contacts (Figure V.3) were obtained by eliminating electrodes with low magnitude responses at the 8 Hz test frequency and calculating the coherence phase on the remaining electrodes.

Frequency domain techniques were used for two reasons. First, periodic stimulation avoids the nonlinearities that can arise when the cortex is not in steady state (Webber and Stanley, 2004). Second, many spontaneous activity patterns (e.g., anesthesia-induced oscillations) and noise sources (e.g., heartbeat) are well localized in the frequency domain(Mitra and Pesaran, 1999). This contamination can is then conveniently avoided when the stimulus is at a well-isolated frequency, in any system for which nonlinear interactions between frequencies are negligible.

Chapter VI

Conclusion

> [Vibrissae are] delicate tactile organs, which function in equilibrium, locomotion, and the discrimination of surfaces (Vincent, 1912, pp. 69).
>
> Of all the techniques designed to disclose the behavioral function of vibrissae, the most informative ought to be tests of sensory discrimination that have employed vibrissal cues alone. Such tests are difficult to design and they have not been employed (Gustafson and Felbain-Keramidas, 1977, pp. 478).
>
> ... the rat sweeps its vibrissae through the space around its head to find and characterize objects of interest (Fee et al., 1997, pp. 1144).
>
> ... an object's location is encoded by the time interval between receptor firing at the onset of a whisking cycle and receptor firing due to perturbation of whisker motion by an external object ... (Ahissar et al., 1997 pp. 11633).
>
> There is no direct proof that such feedback loops can decode whisker position (Diamond, 2000, pp. 247).

These words span nearly a century of work related to the perceptual function of the vibrissae, selected to frame the work discussed in this dissertation. They begin with an early observation on the sensory abilities of the vibrissae (Vincent, 1912) and a much later recognition of the need for precise, well-controlled behavioral tests (Gustafson and Felbain-Keramidas, 1977). With the demonstration of motion-selective cells in the nervous system (Fee et al., 1997), researchers

made a leap from physiology to behavior, assuming that signals they measured provided a substrate for a spatial perception (Ahissar et al., 1997). The conceptual framework and experiments described here were motivated by the recognition that this connection was incomplete without a behavioral test of that perception (Diamond, 2000).

The description offered is neither a fully consistent nor a complete picture of spatial perception and sensorimotor integration in this system. The vibrissa motion patterns measured in Chapter IV suggest that the reduced sinusoidal model of Chapter II and the frequency mixing model of Chapter III are oversimplified, as the animals in this study do not use pure sinusoidal whisking or require multiple whisk cycles to form a spatial percept. Further, no novel physiological evidence for sensorimotor or multi-vibrissa integration was presented, although the the technique presented in Chapter V suggests one way this might be done. Despite these missing pieces, this dissertation has sought to provide "direct proof that ... feedback loops can decode whisker position" through "tests of sensory discrimination that [employed] vibrissal cues alone." It is my hope that this study of active sensing in the vibrissae contributes a framework that will help to better understand these "delicate tactile organs."

Appendix A

Mixing in Coupled Phase Oscillators

We illustrate here an alternative route to frequency mixing through the dynamics of two interacting phase oscillators. These oscillators, which do not include an explicit threshold, are a reduced mathematical model for the study of neuronal dynamics (Ermentrout and Kleinfeld, 2001). As such, it is of interest that simple frequency mixing arises from a nonlinearity quite different from the threshold expansion considered in detail in Chapter III. However, the precise interactions treated here are difficult to realize biophysically, and we thus do not suggest a direct biological interpretation of these interactions.

A.1 Phase Oscillators

We begin with a single nonlinear phase oscillator with intrinsic frequency f_0 such that its free-running phase $\phi(t)$ is given by

$$\phi(t) = 2\pi f_0 t. \tag{A.1}$$

We consider the behavior of this oscillator when it is modulated by a

driving function with phase description $\Phi(t)$:

$$\Phi(t) = 2\pi f_d t, \tag{A.2}$$

where the modulation depends only on the phases $\phi(t)$ and $\Phi(t)$. We focus below on two simple forms of modulation.

A.2 Modulation Dynamics

Case I The first case occurs when the modulation is independent of the phase of the driven oscillator and depend solely on the phase of the forcing function. The modulation function must then be 2π-periodic in the phase of the modulation (since, e.g., $\Phi = \pi$ and $\Phi = 3\pi$ are equivalent), and we choose a sine finction as the simplest example:

$$\frac{\mathrm{d}\phi}{\mathrm{d}t} = 2\pi(f_0 + K\sin(\Phi)), \tag{A.3}$$

where K is a coupling constant describing the strength of the interaction.

Case II The second case occurs when the modulation depends on the relative phase of the modulated and modulating oscillators. The modulation must then be 2π-periodic in the difference $\Phi - \phi$, and we again choose the sine function:

$$\frac{\mathrm{d}\phi}{\mathrm{d}t} = 2\pi\big(f_0 + K\sin(\Phi - \phi)\big). \tag{A.4}$$

A.3 Modulated Oscillator Solutions

Case I The ODE in Equation A.3 can be directly integrated to give

$$\phi(t) = 2\pi f_0 t - \frac{K}{f_d}\cos(2\pi f_d t). \tag{A.5}$$

Case II To ease notation, we first define

$$\Delta \triangleq f_d - f_0$$
$$\psi(t) \triangleq \Phi(t) - \phi(t).$$

We next write an expression describing the evolution of the phase difference $\psi(t)$ between modulated and modulating oscillators:

$$\frac{\mathrm{d}\psi}{\mathrm{d}t} = 2\pi\big(\Delta - K\sin(\psi)\big). \tag{A.6}$$

If $|K| > |\Delta|$, $\frac{\mathrm{d}\psi}{\mathrm{d}t} = 0$ has two solutions and $\psi(t)$ thus has two fixed points. It can be shown that one of these is stable, since the system undergoes a saddle-node bifurcation at $|K| = |\Delta|$, where it has a single half-stable fixed point. When the stable fixed point exists, the phase difference ψ will converge to a constant, and the modulated oscillator is synchronized with (or equivalently, entrained by) the modulating oscillator.

When $|K| < |\Delta|$ (implying $\Delta \neq 0$), the strength of the coupling is insufficient to entrain the modulated oscillator, and the pair undergo phase walk. We can obtain an explicit solution to Equation A.6 using Equation A.9 (setting $\tau = \frac{1}{\Delta}$ and $\rho = \frac{K}{\Delta}$:

$$\psi(t) = 2\tan^{-1}\left(\frac{K}{\Delta} + \sqrt{1 - \frac{K^2}{\Delta^2}}\tan\left(\pi\Delta\sqrt{1 - \frac{K^2}{\Delta^2}}(t + C)\right)\right). \tag{A.7}$$

The driven oscillator $\phi(t) = \Phi(t) - \psi(t)$ then has solution:

$$\phi(t) = 2\pi f_d t - 2\tan^{-1}\left\{\frac{K + \sqrt{(f_d - f_0)^2 - K^2}\,\tan\left(\pi\sqrt{(f_d - f_0)^2 - K^2}\,(t + C)\right)}{f_d - f_0}\right\}. \tag{A.8}$$

A.4 Modulated Oscillator Power Spectra

We now examine the simplest periodic system with phase given by $\phi(t)$, namely $\cos(\phi(t))$. Both cases considered above can lead to spectral mixing in this system, each with a different pattern of resulting frequencies.

Case I Combining Equation A.5 with Equation A.10, we find that the power spectrum of Equation A.5 is given by the spectrum of $exp\{i(\frac{K}{f_d}\cos(2\pi f_d t))\}$ shifted by base frequencies $\pm f_0$. We note that $exp\{i(\frac{K}{f_d}\cos(2\pi f_d t)\}$ is periodic with period $1/f_d$, and its power spectrum therefore consists only of harmonics of f_d — the exact solution can be obtained by expanding the exponential expression as a sum of Bessel functions. The resulting spectrum has lines at $\{\pm f_0 + kf_d, k \in \mathbb{Z}\}$ (Figure A.1a).

Case II For Equation A.8, the expression for the Fourier transform of $exp\{i\phi(t)\}$ can be simplified somewhat using trigonometric identities. However, we can obtain the essential form of the solution by observing that Equation A.8 is a function of $\tan(\frac{1}{2}\sqrt{\Delta^2 - K^2}(t + C))$, and therefore has period $2\pi/\sqrt{\Delta^2 - K^2}$. Its power spectrum can then only contain power at the harmonics of $\tilde{\Delta} = \sqrt{\Delta^2 - K^2} \approx \Delta$ for small K. The power spectrum of Equation A.8 is then by these harmonics shifted by frequencies $\pm f_d$ to give lines at $\{\pm f_d + k\tilde{\Delta}, k \in \mathbb{Z}\}$. For small K, the positive base frequency results in lines near $\{\cdots, 2f_d - f_0, f_m, f_0, 2f_0 - f_d, \cdots\}$ (Figure A.1b).

A.5 General Driven Oscillator Solution

We derive the solution to an ODE of the form $\tau\dot{y} = 1 - \rho\sin(y)$, where $|\rho| < 1$ and $\tau \neq 0$.

We first note the following trigonometric identity:

$$\sin(2\tan^{-1} x) = 2\sin(\tan^{-1} x)\cos(\tan^{-1} x) = \frac{2x}{1 + x^2}.$$

We next define $\sigma \triangleq \sqrt{1 - \rho^2}$ and a change of variables $u = \tan\frac{y}{2}$.

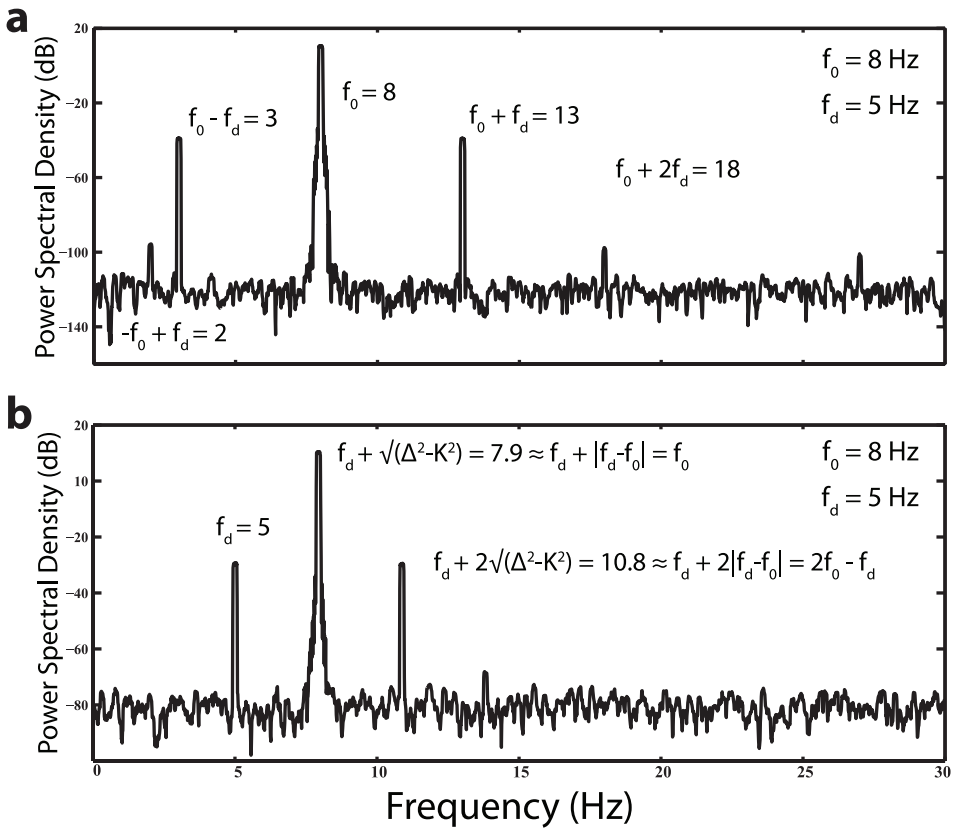

Figure A.1 **Power spectra for two types of driven oscillators.** These spectra were obtained by numerical simulation of the differential equations A.3 and A.4. In both cases, noise was added to the solution before taking the power spectrum. This visually obscured higher order mixture terms, providing visual clarity here; the methods described in Chapter III provide a more biophysically plausible approach to cancellation of undesired frequency terms. **(a)** Power spectrum of $\cos(\phi(t))$, for $\phi(t)$ defined by Equation A.3. Note the peaks at $f_0 \pm f_d$. **(b)** Power spectrum of $\cos(\phi(t))$, for $\phi(t)$ defined by Equation A.4. Note the peaks at approximately $f_d, f_0, 2f_0 - f_d$.

Then,

$$\begin{aligned}
\tau\frac{\mathrm{d}y}{\mathrm{d}t} &= 1-\rho\sin y \\
\frac{1}{\tau}\int_0^t dt' &= \int \frac{\mathrm{d}y}{1-\rho\sin y} \\
\frac{1}{\tau}t &= \int \frac{1}{1-\frac{2\rho u}{1+u^2}}\ \frac{2}{1+u^2}\mathrm{d}u \\
&= 2\int \frac{1}{1+u^2-2\rho u}\mathrm{d}u \\
&= 2\int \frac{1}{(u-\rho)^2+\sigma^2}\mathrm{d}u \\
&= \frac{2}{\sigma}\tan^{-1}\frac{u-\rho}{\sigma}+C_1 \\
t+C &= \frac{2\tau}{\sigma}\tan^{-1}\frac{\tan\frac{y}{2}-\rho}{\sigma}
\end{aligned}$$

$$\therefore y(t) = 2\tan^{-1}\left(\sigma\tan\left(\frac{\sigma}{2\tau}(t+C)\right)+\rho\right), \tag{A.9}$$

where C is a function of $y(0)$:

$$C = \frac{2\tau}{\sigma}\tan^{-1}\left(\frac{1}{\sigma}\Big(\tan(\frac{y(0)}{2}-\rho\Big)\right)$$

A.6 Derivation of General Power Spectrum

We derive the power spectrum of the function $\cos(\nu t + f(t))$, for $\nu \in \mathbb{R}^+$ and $f(t) : \mathbb{R} \to \mathbb{R}$.

We first recall the identity

$$\cos(x \pm y) = \cos x \cos y \mp \sin x \sin y,$$

and the convolution theorem

$$\mathscr{F}[f(t)g(t)](\omega) = \mathscr{F}[f(t)](\omega) \star \mathscr{F}[g(t)](\omega),$$

where $\mathscr{F}[h(t)](\omega)$ denotes the Fourier transform of $h(t)$, and $\star$ denotes convolution.

Then, for $g_\nu(t) = \cos(\nu t + f(t))$,

$$\begin{aligned}
\mathscr{F}[g_\nu(t)](\omega) &= \mathscr{F}[\cos(\nu t)\cos(f(t)) - \sin(\nu t)\sin(f(t))](\omega) \\
&= \frac{1}{2}\big[\delta(\omega'+\nu) + \delta(\omega'-\nu)\big] \star \mathscr{F}[\cos(f(t))](\omega') - \\
&\quad \frac{1}{2}i\big[\delta(\omega'+\nu) - \delta(\omega'-\nu)\big] \star \mathscr{F}[\sin(f(t))](\omega') \\
&= \frac{1}{2}\Big\{\delta(\omega'+\nu) \star \mathscr{F}[e^{-if(t)}](\omega') + \delta(\omega'-\nu) \star \mathscr{F}[e^{if(t)}](\omega')\Big\} \\
&= \frac{1}{2}\Big\{\mathscr{F}[e^{-if(t)}](\omega+\nu) + \mathscr{F}[e^{if(t)}](\omega-\nu)\Big\}
\end{aligned} \tag{A.10}$$

Defining $Z(u) \triangleq \mathscr{F}[e^{if(t)}](u)$,

$$\begin{aligned}
|\mathscr{F}[g_\nu(t)](\omega)|^2 &= \frac{1}{4}\left|\Big\{\overline{Z(-\omega-\nu)} + Z(\omega-\nu)\Big\}\right|^2 \\
&= \frac{1}{4}\Big\{|Z(-\omega-\nu)|^2 + |Z(\omega-\nu)|^2 + 2\Re\{Z(-\omega-\nu)Z(\omega-\nu)\}\Big\}
\end{aligned} \tag{A.11}$$

We observe that the expression in Equation A.10 is closely related to the modulation theorem used in FM radio, i.e., the Fourier transform of the original signal $\cos(\nu t + f(t))$ is formed from frequency shifted copies of the Fourier transform of a function of that signal ($e^{if(t)}$ in this case) We further note that the power spectrum of $g_\nu(t)$ is non-zero at angular frequency ω iff the power spectrum of $e^{if(t)}$ is non-zero for at least one of $\{\omega-\nu, -\omega-\nu\}$.

Appendix B

Design of Tactile Stimuli

This appendix provides detailed information on the stimulus delivery apparatus from the behavioral task in Chapter IV. Due to the specialized nature of the task, commercial options are not available, and we present the following as an design example for researchers who need to deliver tactile stimuli in rodent vibrissa experiments. This design emphasizes rapid, quiet movement of small stimuli over a distance equal to the span of the rat vibrissa

Figure B.1 **Complete stimulus assembly.** Overall assembly, including support structures not omitted from Figure IV.2. The rostral stimulus is shown in a position that makes it available to the vibrissae and the caudal stimulus is fully retracted. **(a)** Three-dimensional perspective. The large horizontal rectangular block is the main platform. Two air-driven pistons are held above the main platform. Each independently drives a carriage that supports a stimulus pin. The hole pattern in the carriages matches the guide pattern inset into the main platform. The teflon rods on which the carriages travel are shown in brown. The nose poke is the black cylindrical object hanging below the main platform, and it defines the position of the rat relative to the stimuli. **(b)** Front view. **(c)** Side view.

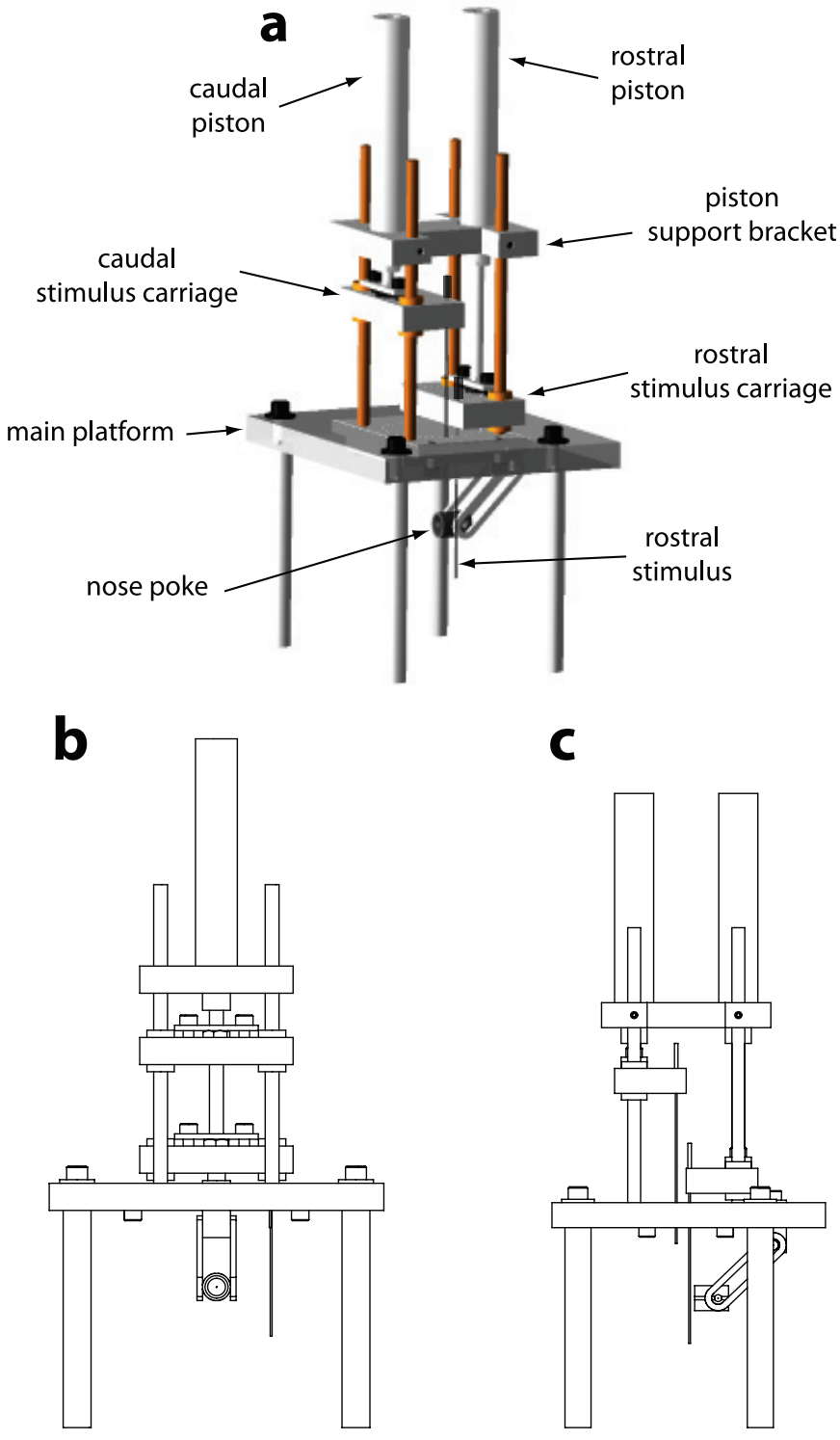

Figure B.1 (see facing page)

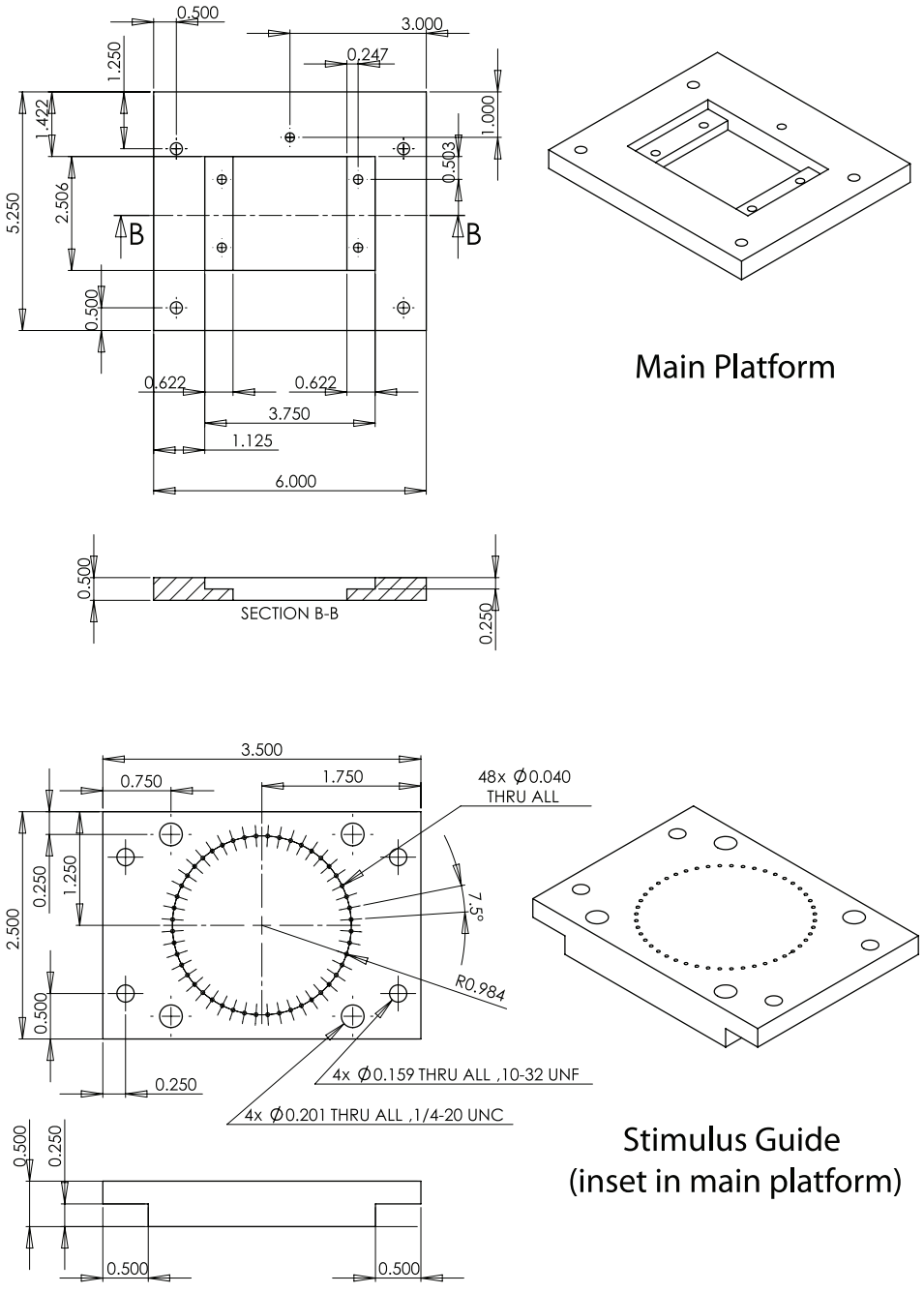

Figure B.2 **Main platform and stimulus guide pattern.**

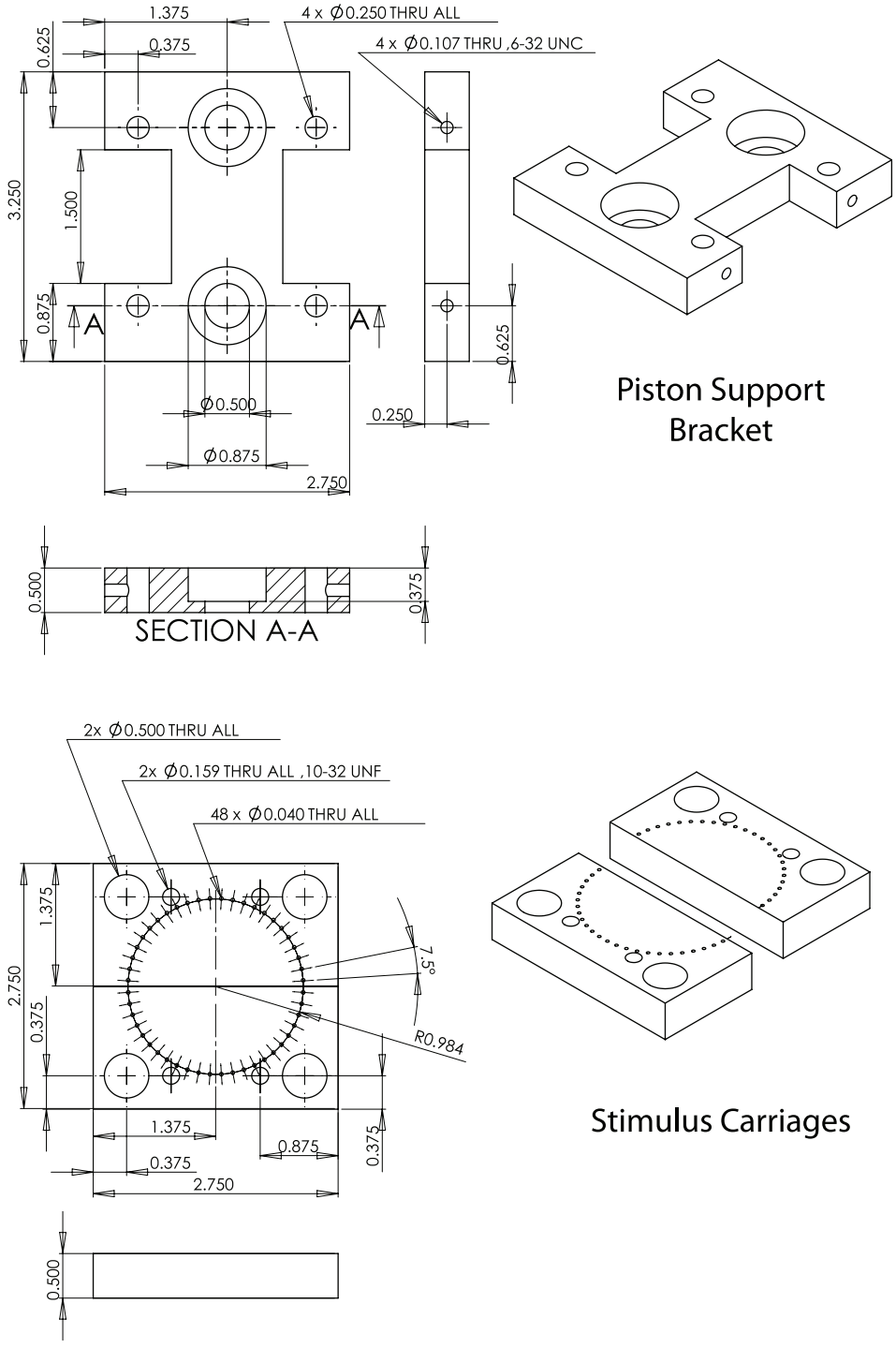

Figure B.3 **Piston support and stimulus carriage.**

Figure B.4 **Stimulus position relative the to the full vibrissa field.** Video still images of rats in the stimulus assembly nose poke (cf. figures IV.6B and IV.6E). Each of (a),(b) and (c) below shows a side view and bottom view. The two views in each panel were not taken simultaneously but show similar situations. The scale bar in all cases is 4 mm. **(a)** Rat with all vibrissae. Note the span of the vibrissae in both rostrocaudal and dorsoventral directions. **(b)** Rat with only C row. The C3 vibrissa is shown contacting the rostral stimulus. The green arrows point to the location of contact. **(c)** Rat with only C row. The γ, or C0, vibrissa is shown contacting the caudal stimulus. The red arrows point to the location of contact. This stimulus is 30° caudal to the stimulus shown in (b).

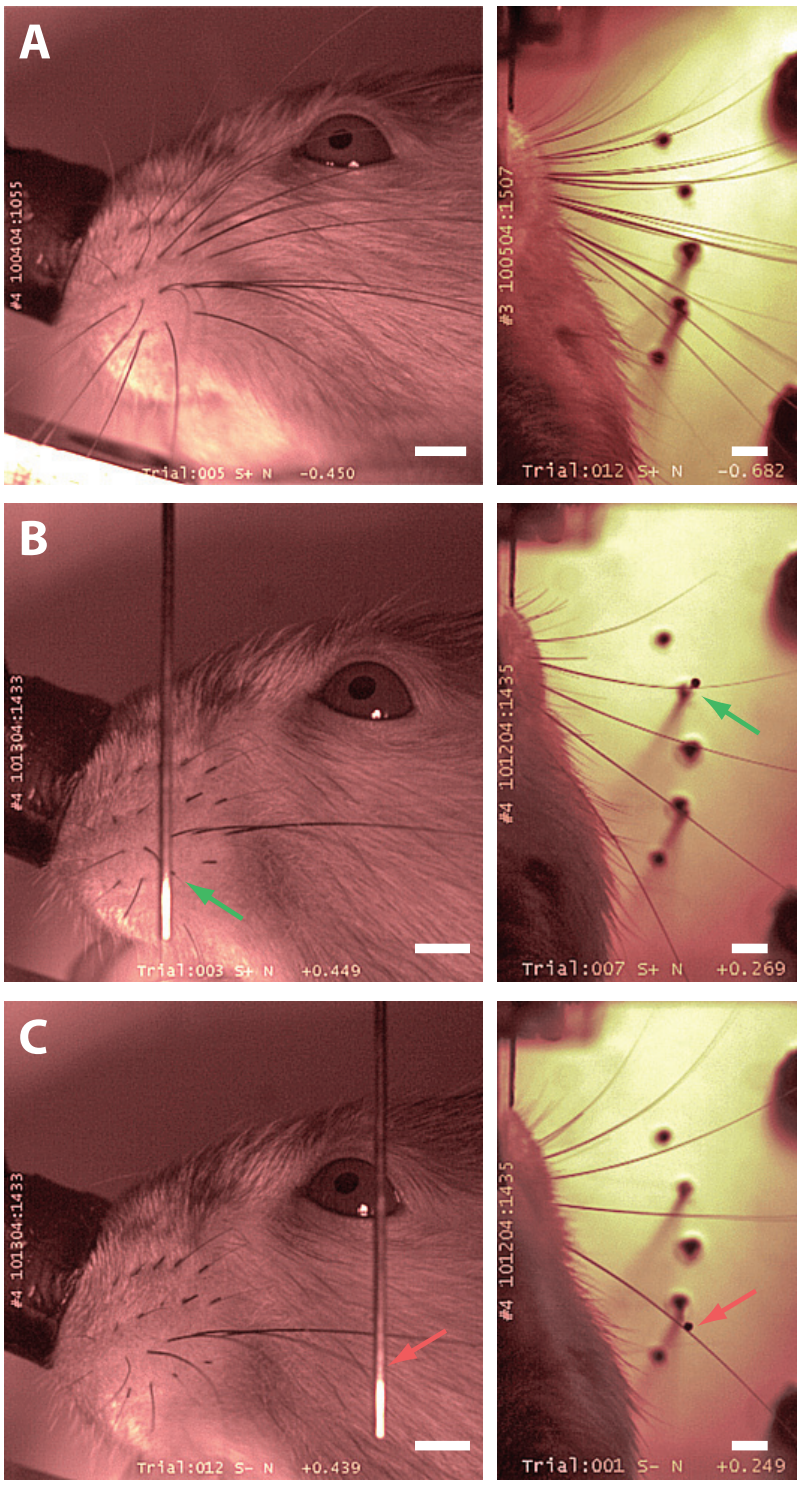

Figure B.4 (see facing page)

References

Aguilar, J. R. and M. A. Castro-Alamancos (2005). Spatiotemporal gating of sensory inputs in thalamus during quiescent and activated states. *Journal of Neuroscience* 25(47): 10990–1002.

Ahissar, E. and D. Kleinfeld (2003). Closed loop neuronal computations: Focus on vibrissa somatosensation in rat. *Cerebral Cortex* 13: 53–61.

Ahissar, E., R. Sosnik, and S. Haidarliu (2000). Transformation from temporal to rate coding in a somatosensory thalamocortical pathway. *Nature* 406: 302–306.

Ahissar, E. and E. Vaadia (1990). Oscillatory activity of single units in a somatosensory cortex of an awake monkey and their possible role in texture analysis. *Proc. of the National Academy of Sciences USA* 87: 8935–8939.

Ahissar, Ehud (1998). Temporal-code to rate-code conversion by neuronal phase-locked loops. *Neural Computation* 10: 597–650.

Ahissar, Ehud, Sebastian Haidarliu, and Miriam Zackenhouse (1997). Decoding temporally encoded sensory input by cortical oscillators and thalamic phase comparators. *Proc. of the National Academy of Sciences USA* 94: 11633–11638.

Ahrens, K. F., H. Levine, H. Suhl, and D. Kleinfeld (2002). Spectral mixing of rhythmic neuronal signals in sensory cortex. *Proc. of the National Academy of Sciences USA* 99: 15176–15181.

Amit, D. J. (1989). *Modeling Brain Function: The World of Attractor Neural*

Networks. Cambridge University Press, Cambridge.

Andermann, M. L., J. Ritt, M. A. Neimark, and C. I. Moore (2004). Neural correlates of vibrissa resonance: Band-pass and somatotopic representation of high-frequency stimuli. *Neuron* 42: 451–463.

Arabzadeh, E., R. S. Petersen, and M. E. Diamond (2003). Encoding of whisker vibration by rat barrel cortex neurons: Implications for texture discrimination. *Journal of Neuroscience* 27: 9146–9154.

Arabzadeh, E., E. Zorzin, and M. E. Diamond (2005). Neuronal encoding of texture in the whisker sensory pathway. *Public Library of Science Biology* 3: 155–165.

Barth, D. S. (2003). Submillisecond synchronization of fast electrical oscillations in neocortex. *Journal of Neuroscience* 23: 2502–2510.

Benison, A. M., T. D. Ard, A. M. Crosby, and D. S. Barth (2006). Temporal patterns of field potentials in vibrissa/barrel cortex reveal stimulus orientation and shape. *Journal of Neurophysiology* 95: 2242–2251.

Berg, R. W. and D. Kleinfeld (2003). Rhythmic whisking by rat: Retraction as well as protraction of the vibrissae is under active muscular control. *Journal of Neurophysiology* 89: 104–117.

Bermejo, R. and H. P. Zeigler (2000). "real-time" monitoring of vibrissa contacts during rodent whisking. *Somatosensory and Motor Research* 17: 373–377.

Best, Roland E. (1984). *Phase-Locked Loops: Theory, Design, and Applications*. McGraw-Hill, New York.

Brecht, M., M. S. Fee, O. Garaschuk, F. Helmchen, T. W. Margrie, K. Svoboda, and P. Osten (2004). Novel approaches to monitor and manipulate single neurons in vivo. *Journal of Neuroscience* 24: 9223–9227.

Brecht, M., B. Preilowski, and M. M. Merzenich (1997). Functional architecture of the mystacial vibrissae. *Behavioural Brain Research* 84: 81–97.

Bullock, T. H. and W. Heiligenberg (1987). *Electroreception*. Wiley, New York.

Cacciatore, T. W., P. D. Brodfueher, J. E. Gonzalez, T. Jiang, S. R. Adams, R. Y. Tsien, W. B. Kristan Jr., and D. Kleinfeld (1999). Identification of neural circuits by imaging coherent electrical activity with fret-based dyes. *Neuron* 23: 449–459.

Carvell, George E. and Daniel J. Simons (1990). Biometric analyses of vibrissal tactile discrimination in the rat. *Journal of Neuroscience* 10: 2638–2648.

Carvell, George E. and Daniel J. Simons (1995). Task-and subject-related differences in sensorimotor behavior during active touch. *Somatosensory and Motor Research* 12: 1–9.

Carvell, George E., Daniel J. Simons, Seth H. Lichtenstein, and Patrick Bryant (1991). Electromyographic activity of mystacial pad musculature during whisking behavior in the rat. *Somatosensory and Motor Research* 8: 159–164.

Castro-Alamancos, M. A. (2002). Different temporal processing of sensory inputs in the rat thalamus during quiescent and information processing states in vivo. *Journal of Physiology* 539: 567–578.

Cranch, E. T. and A. A. Adler (1956). Bending vibrations of variable section beams. *Journal of Applied Mechanics* 78: 103–108.

Cullen, K. E. and J. E. Roy (2004). Signal processing in the vestibular system during active versus passive head movements. *Journal of Neurophysiology* 91(5): 1919–33.

Curtis, J. and D. Kleinfeld (2005). Cortical neurons that code vibrissa contact in face-centered coordinates. In *Barrels* (Hartmann, M., editor), Vol. XVIII, Washington, D.C.

Delaney, K. R., A. Gelperin, M. S. Fee, J. A. Flores, R. Gervais, D. W. Tank, and D. Kleinfeld (1994). Waves and stimulus-modulated dynamics in an oscillating olfactory network. *Proc. of the National Academy of Sciences USA* 91: 669–673.

Deliagina, T. G., G. N. Orlovsky, P. V. Zelenin, and I. N. Beloozerova (2006). Neural bases of postural control. *Physiology (Bethesda)* 21: 216–25.

Derdikman, D., R. Hildesheim, E. Ahissar, A. Arieli, and A. Grinvald (2003). Imaging spatiotemporal dynamics of surround inhibition in the barrels somatosensory cortex. *Journal of Neuroscience* 23(8): 3100–3105.

Derdikman, D., M. Szwed, K. Bagdasarian, P. M. Knutsen, M. Pietr, C. Yu, A. Arieli, and E. Ahissar (2006a). Active construction of percepts about object location. *Novartis Found Symp* 270: 4–14; discussion 14–7, 51–8.

Derdikman, D., C. Yu, S. Haidarliu, K. Bagdasarian, A. Arieli, and E. Ahissar (2006b). Layer-specific touch-dependent depression and facilitation in the

somatosensory cortex during artificial active whisking. *Journal of Neuroscience* Under final review.

Deschenes, M., E. Timofeeva, and P. Lavallee (2003). The relay of high frequency sensory signals in the whisker-to-barreloid pathway. *Journal of Neuroscience* 23: 6778–6787.

Diamond, M. L. (2000). Neurobiology: Parallel processing. *Nature* 406: 245–247.

Ego-Stengel, V., T. M. E. Souza, V. Jacob, and D. E. Shulz (2005). Spatiotemporal characteristics of neuronal sensory integration in the barrel cortex of the rat. *Journal of Neurophysiology* 93: 1450–1467.

Engel, J., H. A. Schultens, and D. Schild (1999). Small conductance potassium channels cause an activity-dependent spike frequency adaptation and make the transfer function of neurons logarithmic. *Biophysical Journal* 76: 1310–1319.

Ermentrout, B. (1994). Reduction of conductance based model with slow synapses to neural nets. *Neural Computation* 6: 679–695.

Ermentrout, G. B., J Flores, and A Gelperin (1998). Minimal model of oscillations and waves in the limax olfactory lobe with tests of the model's predictive power. *Journal of Neurophysiology* 79: 2677–2689.

Ermentrout, G. B. and D. Kleinfeld (2001). Traveling electrical waves in cortex: Insights from phase dynamics and speculation on a computational role. *Neuron* 29: 1–12.

Ermentrout, G. B. and J. Rinzel (1984). Beyond a pacemaker's entrainment limit: Phase walk-through. *American Journal of Physiology* 246(R102-106).

Fee, Michale S., Partha P. Mitra, and David Kleinfeld (1997). Central versus peripheral determinates of patterned spike activity in rat vibrissa cortex during whisking. *Journal of Neurophysiology* 78: 1144–1149.

Feldman, D. E. and M. Brecht (2005). Map plasticity in somatosensory cortex. *Science* 310(5749): 810–5.

Felleman, D. J. and D. C. Van Essen (1991). Distributed hierarchical processing in the primate cerebral cortex. *Cerebral Cortex* 1(1): 1–47.

Fend, M., S. Bovet, H. Yokoi, and R. Pfeifer (2003). An artificial whisker array for texture discrimination. In *IEEE/RSJ International Conference on Intelligent*

Robots and Systems, Vol. II, pp. 1044–1049, La Vegas, NV.

Ferezou, I., S. Bolea, and C. C. H. Petersen (2006). Visualizing the cortical representation of whisker touch: Voltage-sensitive dye imaging in freely moving mice. *Neuron* in press.

Friedrich, R. W., C. J. Habermann, and G. Laurent (2004). Multiplexing using synchrony in the zebrafish olfactory bulb. *Nature Neuroscience* 7: 862–871.

Gabbiani, F., H. G. Krapp, N. Hatsopoulos, C. H. Mo, C. Koch, and G. Laurent (2004). Multiplication and stimulus invariance in a looming-sensitive neuron. *Journal of Physiology (Paris)* 98: 19–34.

Ganguly, K. and D. Kleinfeld (2004). Goal-directed whisking behavior increases phase-locking between vibrissa movement and electrical activity in primary sensory cortex in rat. *Proc. of the National Academy of Sciences USA* 101: 12348–12353.

Gibson, J. J. (1966). *The Senses Considered as Perceptual Systems*. Houghton Mifflin Company, Boston.

Gibson, J. R., M. Beierlein, and B. W. Connors (2005). Functional properties of electrical synapses between inhibitory interneurons of neocortical layer 4. *Journal of Neurophysiology* 93: 467–580.

Gottschaldt, K. M. and C. Vahle-Hinz (1981). Merkel cell receptors: Structure and transducer function. *Science* 214: 143–186.

Grannan, E. R., D. Kleinfeld, and H. Sompolinsky (1993). Stimulus dependent synchronization of neuronal assemblies. *Neural Computation* 5: 550–569.

Gray, C. M., P. Konig, A. K. Engel, and W. Singer (1989). Oscillatory responses in cat visual cortex exhibit inter-columnar synchronization which reflects global stimulus properties. *Nature* 338: 334–337.

Green, D and J Swets (1966). *Signal detection theory and psychophysics*. Wiley, New York.

Griffiths, W.J. (1960). Responses of wild and domestic rats to forced swimming. *Psychological Reports* 6: 39–49.

Guic-Robles, Eliana, C. Valdivieso, and G. Guajardo (1989). Rats can learn a roughness discrimination using only their vibrissal system. *Behavioural Brain Research* 31: 285–289.

Gustafson, J. W. and S. L. Felbain-Keramidas (1977). Behavioral and neural approaches to the function of the mystacial vibrissae. *Psychological Bulletin* 84: 477–488.

Hansel, D., G. Mato, and C. Meunier (1993). Phase dynamics for weakly coupled hodgkin-huxley neurons. *Europhysics Letters* 23: 367–372.

Hartmann, M. J., N. J. Johnson, R. B. Towal, and C. Assad (2003). Mechanical characteristics of rat vibrissae: Resonant frequencies and damping in isolated whiskers and in the awake behaving animal. *Journal of Neuroscience* 23: 6510–6519.

Hartmann, William M. (1997). *Signals, Sound, and Sensation*. American Institute of Physics, Woodbury.

Harvey, M. A., R. Bermejo, and H. P. Zeigler (2001). Discriminative whisking in the head-fixed rat: Optoelectronic monitoring during tactile detection and discrimination tasks. *Somatosensory and Motor Research* 18: 211–222.

Heiligenberg, W. and G. Rose (1985). Phase and amplitude computations in the midbrain of an electric fish. intracellular studies of neurons participating in the jamming avoidance-response of eigenmannia. *Journal of Neuroscience* 5: 515–531.

Hipp, J., E. Arabzadeh, E. Zorzin, J. Conradt, C. Kayser, M. E. Diamond, and P. Konig (2006). Texture signals in whisker vibrations. *Journal of Neurophysiology* 95: 1792–1799.

Holtmaat, A. J., J. T. Trachtenberg, Wilbrecht L., G. M. Shepherd, X. Zhang, G. W. Knott, and K. Svoboda (2005). Transient and persistent dendritic spines in the neocortex in vivo. *Neuron* 45(2): 279–91.

Hopfield, J. J. (1982). Neural networks and physical systems with emergent collective computational abilities. *Proc. of the National Academy of Sciences USA* 79: 2554–2558.

Hoppensteadt, F. C. (1997). *An Introduction to the Mathematics of Neurons. Modeling in the Frequency Domain*. Cambridge University Press, Cambridge.

Horowitz, Paul and Winfield Hill (1989). *The Art of Electronics*. Cambridge University Press, Cambridge.

Horton, J. C. and D. L. Adams (2005). The cortical column: a structure without a function. *Philosophical Transactions of the Royal Society London B Biological*

Sciences 360(1456): 837–62.

Huang, X., W. C. Troy, Q. Yang, H. Ma, C. R. Laing, S. J. Schiff, and J. Y. Wu (2004). Spiral waves in disinhibited mammalian neocortex. *Journal of Neuroscience* 24: 9897–9902.

Hutson, K. A. and R. B. Masterton (1986). The sensory contribution of a single vibrissa's cortical barrel. *Journal of Neurophysiology* 56(4): 1196–1223.

Jacobs, G. H., J. A. Fenwick, and G. A. Williams (2001). Cone-based vision of rats for ultraviolet and visible lights. *Journal of Experimental Biology* 204(Pt 14): 2439–46.

Kleinfeld, D., R. W. Berg, and S. M. O'Connor (1999). Anatomical loops and their electrical dynamics in relation to whisking by rat. *Somatosensory and Motor Research* 16: 69–88.

Kleinfeld, D. and S. B. Mehta (2006). Spectral mixing in nervous systems: Experimental evidence and biologically plausible circuits. *Progress of Theoretical Physics Supplement* 161: 86–98.

Kleinfeld, D., R. N. S. Sachdev, L. M. Merchant, M. R. Jarvis, and F. F. Ebner (2002). Adaptive filtering of vibrissa input in motor cortex of rat. *Neuron* 34: 1021–1034.

Koch, C. and T. Poggio (1992). Multiplying with synapses and neurons. In *Single Neuron Computation* (McKenna, T., J. Davis, and S. F. Zornetzer, editors), pp. 315–345. Academic Press, Boston.

Krupa, David J., Matthew S. Matell, Amy J. Brisben, Laura M. Oliveira, and Miguel A. L. Nicolelis (2001). Behavioral properties of the trigeminal somatosensory system in rats performing whisker-dependent tactile discriminations. *Journal of Neuroscience* 21: 5752–5763.

Kuramoto, Y. (1984). *Chemical Oscillations, Waves and Turbulence*. Springer Verlag, New York.

Levitin, D. J. and S. E. Rogers (2005). Absolute pitch: Perception, coding, and controversies. *Trends in Cognitive Science* 9: 26–33.

Ling, J.K. (1966). The skin and hair of the southern elephant seal, mirounga leonina (linn.). *Australian Journal of Zoology* 14: 855–866.

Margrie, T. W., A. H. Meyer, A. Caputi, H. Monyer, M. T. Hasan, A. T. Schae-

fer, W. Denk, and M. Brecht (2003). Targeted whole-cell recordings in the mammalian brain in vivo. *Neuron* 39: 911–918.

Mehta, S. B. and D. Kleinfeld (2004). Frisking the whiskers: Patterned sensory input in the rat vibrissa system. *Neuron* 41: 181–184.

Mitra, P. P. and B. Pesaran (1999). Analysis of dynamic brain imaging data. *Biophysical Journal* 76: 691–708.

Moore, C. and M. L. Andermann (2005). The vibrissa resonance hypothesis. In *Neural Plasticity in Adult Somatic Sensory-Motor Systems* (Ebner, F. F., editor). CRC Press.

Moore, C. I. (2004). Frequency-dependent processing in the vibrissa sensory system. *Journal of Neurophysiology* 91: 2390–2399.

Moore, C. I., S. B. Nelson, and M. Sur (1999). Dynamics of neuronal processing in rat somatosensory cortex. *Trends Neurosci* 22(11): 513–20.

Moss, C. F., K. Bohn, H. Gilkenson, and A. Surlykke (2006). Active listening for spatial orientation in a complex auditory scene. *Public Library of Science Biology* 4(4): e79.

Neiman, A. B. and D. F. Russell (2004). Two distinct types of noisy oscillators in electroreceptors of paddlefish. *Journal of Neurophysiology* 92: 492–509.

Neimark, M. A., M. L. Andermann, J. J. Hopfield, and C. I. Moore (2003). Vibrissa resonance as a transduction mechanism for tactile encoding. *Journal of Neuroscience* 23: 6499–6509.

Nguyen, Q.-T. and D. Kleinfeld (2005). Positive feedback in a brainstem tactile sensorimotor loop. *Neuron* 45: 1–11.

Nishimura, N., C. B. Schaffer, B. Friedman, P. S. Tsai, P. D. Lyden, and D. Kleinfeld (2006). Targeted insult to individual subsurface cortical blood vessels using ultrashort laser pulses: Three models of stroke. *Nature Methods* 3: 99–108.

Oster, G. (1973). Auditory beats in the brain. *Scientific American* 229: 94–102.

Paxinos, G., editor (1995). *The Rat Nervous System*. Academic Press, Sydney, second edition.

Paxinos, G. and C. Watson (1986). *The Rat Brain in Stereotaxic Coordinates*. Academic Press, San Diego, 4th ed. edition.

Pena, J. L. and M. Konishi (2001). Auditory spatial receptive fields created by multiplication. *Science* 292: 249–252.

Pena, J. L. and M. Konishi (2004). Robustness of multiplicative processes in auditory spatial tuning. *Journal of Neuroscience* 24: 8907–8910.

Perkel, D.H. and T.H. Bullock, editors (1968). *Neural Coding*, Vol. 6 of *Neurosciences Research Program Bulletin*.

Peterka, R. J. (2002). Sensorimotor integration in human postural control. *Journal of Neurophysiology* 88(3): 1097–118.

Petersen, C. C. (2003). The barrel cortex–integrating molecular, cellular and systems physiology. *Pflugers Arch* 447(2): 126–34.

Petersen, C. C., T. T. Hahn, M. Mehta, A. Grinvald, and B. Sakmann (2003). Interaction of sensory responses with spontaneous depolarization in layer 2/3 barrel cortex. *Proc. of the National Academy of Sciences USA* 100: 13638–43.

Petersen, R. S. and M. E. Diamond (2000). Spatial-temporal distribution of whisker-evoked activity in rat somatosensory cortex and the coding of stimulus location. *Journal of Neuroscience* 20: 6135–6143.

Polley, D. B., J. L. Rickert, and R. D. Frostig (2005). Whisker-based discrimination of object orientation determined with a rapid training paradigm. *Neurobiol Learn Mem* 83(2): 134–42.

Prechtl, J. C., L. B. Cohen, P. P. Mitra, B. Pesaran, and D. Kleinfeld (1997). Visual stimuli induce waves of electrical activity in turtle cortex. *Proc. of the National Academy of Sciences USA* 94: 7621–7626.

Regan, D. and M. P. Regan (1987). Nonlinearity in human visual responses to two-dimensional patterns, and a limitation of transform methods. *Vision Reserach* 27: 2181–2183.

Reynolds, G.S. (1968). *A Primer of Operant Conditioning*. Scott, Foresman and Company, Glenview, IL.

Rice, F. L. and J. Arvidsson (1991). Central projections of primary sensory neurons innervating different parts of the vibrissae follicles and intervibrissal skin on the mystacial pad of the rat. *Journal of Comparative Neurology* 309: 1–16.

Rice, F. L., B. T. Fundin, K. Pfaller, and J. Arvidsson (1994). The innervation of the mystacial pad in the adult rat studied by anterograde transport of hrp

conjugates. *Experimental Brain Research* 99: 233–246.

Rousche, P.J., R. S. Petersen, S. Battiston, S. Giannotta, and M. E. Diamond (1999). Examination of the spatial and temporal distribution of sensory cortical activity using a 100-electrode array. *Journal of Neuroscience Methods* 90: 57–66.

Schiffman, H. R., R. Lore, and J. Passafiume (1970). Role of vibrissae for depth perception in the rat (rattus norvegicus). *Animal Behavior* 18: 290–292.

Schuster, H. G. and P. Wagner (1990a). A model for neuronal oscillations in the visual cortex i. mean field theory and the derivation of the phase equations. *Biological Cybernetics* 64: 77–82.

Schuster, H. G. and P. Wagner (1990b). A model for neuronal oscillations in the visual cortex. ii. phase description of the feature dependent synchronization. *Biological Cybernetics* 64: 83–85.

Shriki, O., D. Hansel, and H. Sompolinsky (2003). Rate models for conductance-based cortical neuronal networks. *Neural Computation* 15: 1809–1841.

Shuler, M. G., D. J. Krupa, and M. A. Nicolelis (2001). Bilateral integration of whisker information in the primary somatosensory cortex of rats. *Journal of Neuroscience* 21: 5251–5261.

Shuler, M. G., D. J. Krupa, and M. A. Nicolelis (2002). Integration of bilateral whisker stimuli in rats: Role of the whisker barrel cortices. *Cerebral Cortex* 12: 86–97.

Simons, D. J. (1978). Response properties of vibrissal units in rat s1 somatosensory neocortex. *Journal of Neurophysiology* 41: 798–820.

Sompolinsky, Haim, David Golomb, and David Kleinfeld (1991). Cooperative dynamics in visual processing. *Physical Review A* 43: 6990–7011.

Suga, N., Y. Zhang, and J. Yan (1997). Sharpening of frequency tuning by inhibition in the thalamic auditory nucleus of the mustached bat. *Journal of Neurophysiology* 77: 2098–2114.

Szwed, M., K. Bagdasarian, and E. Ahissar (2003). Coding of vibrissal active touch. *Neuron* 40: 621–630.

Szwed, M., K. Bagdasarian, B. Blumenfeld, O. Barak, D. Derdikman, and E. Ahissar (2006). Responses of trigeminal ganglion neurons to the radial

distance of contact during active vibrissal touch. *Journal of Neurophysiology* 95: 791–802.

Thajchayapong, M. and M. Hartmann (2004). How do rat whiskers perform radial distance detection? In *Society for Neuroscience*, Washington, D.C.

Thor, D.H. and W.B Ghiselli (1975). Vibrissal anesthesia and suppression of irritable fighting in rats: A temporary duration of effect in experienced fighters. *Physiological Psychology* 3: 1–3.

van Beers, R. J., D. M. Wolpert, and P. Haggard (2001). Sensorimotor integration compensates for visual localization errors during smooth pursuit eye movements. *Journal of Neurophysiology* 85(5): 1914–22.

Vincent, Stella Burnham (1912). The function of the vibrissae in the behavior of the white rat. *Behavior Monographs* 1: 7–81.

von der Vreeswijk, C., L. F. Abbott, and G. B. Ermentrout (1994). When inhibition not excitation synchronizes neural firing. *Journal of Computational Neuroscience* 4: 313–321.

Waters, J. and F. Helmchen (2004). Boosting of action potential backpropagation by neocortical network activity in vivo. *Journal of Neuroscience* 24(49): 11127–11136.

Webber, R. M. and G. B. Stanley (2004). Nonlinear encoding of tactile patterns in the barrel cortex. *Journal of Neurophysiology* 91: 2010–2022.

Wilson, H. R. and J. D. Cowan (1973). Excitatory and inhibitory interactions in localized populations of model neurons. *Biophysical Journal* 12: 1–24.

Wirth, C. and H.-R. Luscher (2004). Spatiotemporal evolution of excitation and inhibition in the rat barrel cortex investigated with multielectrode arrays. *Journal of Neurophysiology* 91: 1635–1647.

Yu, C., D. Derdikman, S. Haidarliu, and E. Ahissar (2006). Parallel thalamic pathways for whisking and touch signals in the rat. *Public Library of Science Biology* 4: e124.

Zucker, E. and W. I. Welker (1969). Coding of somatic sensory input by vibrissae neurons in the rat's trigeminal ganglion. *Brain Research* 12: 134–156.